Mass transport in inorganic meso- and microporous membranes

Farsi, Ali

DOI (link to publication from Publisher):
10.5278/vbn.phd.engsci.00005

Publication date:
2015

Document Version
Publisher's PDF, also known as Version of record

MASS TRANSPORT IN INORGANIC MESO- AND MICROPOROUS MEMBRANES

BY
ALI FARSI

DISSERTATION SUBMITTED 2015

AALBORG UNIVERSITY
DENMARK

Mass transport in inorganic meso- and microporous membranes

by

Ali Farsi

AALBORG UNIVERSITY
DENMARK

Department of Chemistry and Bioscience

Aalborg University, Denmark

Date of Defense: June 16, 2015

Thesis submitted:	April, 2015
PhD supervisor:	Assoc. Prof. Morten Lykkegaard Christensen, Aalborg University
PhD co-supervisor:	Associate Professor Vittorio Boffa, Aalborg University
PhD committee:	Assoc. Prof. Lars Haastrup Pedersen, Aalborg University, Denmark
	Prof. Aleksander Gurlo, TU-Berlin, Germany
	Prof. Mika Mänttäri, Lappeenranta University of Technology, Finland
PhD Series:	Faculty of Engineering and Science, Aalborg University

The research described in this thesis was performed under the auspices of the Danish National Advanced Technology Foundation. Financial support under project 0-59-11-1 is gratefully acknowledged.

ISSN (online): 2246-1248
ISBN (online): 978-87-7112-279-4

Published by:
Aalborg University Press
Skjernvej 4A, 2nd floor
DK – 9220 Aalborg Ø
Phone: +45 99407140
aauf@forlag.aau.dk
forlag.aau.dk

Printed in Denmark by Rosendahls, 2015

CV

Ali Farsi was born on September 22, 1985 in Rafsanjan (Iran). He moved with his family to the Kerman (Iran) and passed the primary, secondary and high school in Iranian National Organization for Development of Exceptional Talents. After graduation in 2003, he started the Chemical and Process Engineering in Iran University Science and Technology (Tehran, Iran). He was graduated with degree of M.Sc. in Chemical Engineering from the University of Kerman (Kerman, Iran) in 2011. The internship in the Center of Chemical and Process Engineering at University of Technology Malaysia (UTM) and working on chemical reactor engineering were main study components.

On 6th of February 2012, Ali started his PhD research at the Department of Chemistry and Bioscience at the Aalborg University (Aalborg, Denmark). The Project was founded by the the Danish National Advanced Technology Foundation and in a close collaboration with Liqtech International A/S. The main results of this research described in this thesis. As a PhD student, he was always involved in teaching and mentoring undergraduate and graduate students. He has taught undergraduate students Matlab programing for numerical modeling and process simulation.

Up to now, he has published and submitted 18 articles in peer-reviewed Journals. His favorite quote is “There's Plenty of Room at the Bottom” which was a lecture given by Richard Feynman at an American Physical Society meeting at Caltech on December 29, 1959.

English summary

In this thesis, the solvent and ion transports through inorganic meso- and microporous membrane are investigated. In order to simulate solvent flux and ion rejection a mathematical model was developed based on understanding the interactions occurring between solution and membrane. It is thereby possible to predict separation characteristics of meso- and microporous membrane without any adjustable parameters. Due to high ζ-potential observed for inorganic membranes, the permeate flux was modeled by a modified Hagen–Poiseuille equation by inserting the electroviscosity instead of the bulk viscosity. This is important especially for pores smaller than 5 nm and solutions with low ionic strength i.e. $I < 0.1$ M. The ion transport was described with the Donnan-steric pore model, in which the extended Nernst-Planck equation model predicts the ion transport through the membranes pores and the combination of steric, electric and dielectric exclusions defines the equilibrium partitioning at the membrane-solution interfaces.

The model was firstly verified using two different membranes, the mesoporous γ-alumina and the microporous organosilica membranes with solutions contain either monovalent ions (e.g. Na^+) or divalent ions (e.g. Mg^{2+}). The results suggested that the electroviscosity effect should be included when modelling membranes with an absolute surface charge higher than 20 mV and a pore size below 2-5 times the electroviscous double layer thickness.

The model was also tested using mesoporous nanofiltration γ-alumina membrane over a broad pH range for four different salt solutions (NaCl, Na_2SO_4, $CaCl_2$ and $CaSO_4$) with the same ionic strength (0.01 M). The selected ionic strength of 0.01 M was sufficiently low to permit the development of the electrical double layer in the nanopores, and the ionic strength was sufficiently high to not be governed solely by the effective charge density. ζ-potential measurements showed that monovalent ions, such as Na^+ and Cl^-, did not adsorb on the γ-alumina surface, whereas divalent ions, such as SO_4^{2-} and Ca^{2+}, were highly adsorbed on the γ-alumina surface. The model was modified due to pore shrinkage caused by ion adsorption (Ca^{2+} and SO_4^{2-}). The rejection model showed that for a membrane with mean pore radious (r_p) ≤ 3 nm and a solution with ionic strength ≤ 0.01 M, there is an optimum ζ-potential for rejection because of the concurrent effects of the electromigration and convection terms.

Different commercial inorganic membranes, namely, a microfiltration α-alumina membrane, an ultrafiltration titania membrane, a nanofiltration γ-alumina membrane, a nanofiltration titania membrane, and a Hybsi membrane, were studied to test their ability to remove toxic compounds, including aromatic components, humic-like substances, organic micro-pollutants, dissolved inorganic nitrogen compounds and heavy metal ions, from wastewater treatment plant effluent. Among them, the nanofiltration γ-alumina membrane was the most promising membrane for the recovery of wastewater treatment plant effluent with regard to its permeate flux and selectivity. The removal of the indicator bacteria and toxic compounds by the nanofiltration γ-alumina membrane were tested using bioassays which indicated that the treatment with the nanofiltration γ-alumina membrane reduced the overall bacterial load and environmental toxicity of the treated water.

The mathematical model was used to design a pressure-derived inorganic membrane for reducing water hardness in low transmembrane pressure (< 7 bars). The model clearly showed

that a microporous membrane can remove more than 50% NaCl and highly retain divalent ions. The model suggested that the best membrane performance for this purpose should have a mean pore size (diameter) between 1 and 2 nm with 5 mV < |ζ| < 20 mV. A microporous TiO_2-doped SiO_2 membrane was fabricated with a mean pore size (diameter) of 1.44 nm and a ζ-potential of approximately -9 mV at pH = 6. The membrane removed approximately 73% of NaCl. This retention value was significantly higher than reported results for mesoporous inorganic membranes in these operation conditions and was also comparable with commercial polymeric nanofiltration membranes. The TiO_2-doped SiO_2 membrane permeability was tenfold more than modified silica membrane such as silicates and organosilica membranes but still three to six fold less than commercial polymeric NF membranes. Further work is needed to decrease the membrane thickness to provide higher permeability.

Dansk resume

Der er i dette projekt udviklet en ny matematisk model til at simulere stoftransporten (væske og ioner) gennem uorganisk meso- og mikroporøs membraner. Modellen er udviklet for uorganiske membraner. Uorganiske membraner er ofte ladede og har dermed et højt ζ-potentiale i forhold til polymermembraner. Det har derfor været nødvendig at modificere de eksisterende modeller, så modellerne tager højde for membranernes høje ladning. Det er gjort ved ar korrigere den viskositet, der anvendes til beregning af stoftransporten. Simuleringer viser, at korrektionen er vigtig, hvis radius på membranernes porer er mindre end 5 nm og hvis der filtreres på opløsninger med lavt saltindhold (ionstyrke mindre end 0,1 M).

For at validere modellen er der udført eksperimenter på to forskellige membraner, nemlig en mesoporøs γ-aluminiumoxid memban og en mikroporøs organosilica membran. Der er anvendt forskellige opløsninger til filtreringerne. Disse opløsninger indeholder enten monovalente ioner (f.eks Na^{+}) eller divalente ioner (f.eks Mg^{2+}). Resultaterne viser, at membranernes ladning er vigtig for stoftransporten og den modificerede model bør anvendes, hvis der anvendes membraner med et ζ-potentiale større end 20 mV eller mindre en – 20 mV, og hvis membranens porestørrelse er mindre end 2-5 gange Derbylængden (tykkelsen af det elektriske dobbeltlag). Derbylændgen afhænger af fødestrømmens saltkoncentration.

Modellen er desuden testet ved at filtrere fire forskellige saltopløsninger (NaCl, Na_2SO_4, $CaCl_2$ og $CaSO_4$) med en ionstyrke på 0,01 M gennem en mesoporøs nanofiltrering γ-aluminiumoxid membran. Filtreringerne er udført i et bredt pH interval. Målinger af membranernes ζ-potentialet viser, at monovalente ioner, såsom Na^{+} og Cl^{-}, ikke adsorberes til membranoverfladen eller porerne, hvorimod divalente ioner, såsom SO_4^{2-} og Ca^{2+}, adsorberes til γ-aluminiumoxid overfladen. Modellen er efterfølgende blevet modificeret så der tages hensyn til at membranens porer indsnævres på grund af ionadsorptionen. De matematiske simuleringer viser, at en membran med en gennemsnitlig poreradius mindre en 3 nm, hvis membranen skal bruges til at afsalte og reducere væskers hårdhed. Derudover opnås den bedste separation, hvis fødestrømmens ionstyrke er mindre en 0,01 M dvs. fødestrømme med relativt lav saltindhold.

Vi har undersøgt fire kommercielle uorganiske membraners evne til at fjerne giftige stoffer fra renset spildevand. Det er en mikrofiltrering α-aluminiumoxid membran, en ultrafiltrering titania membran, en nanofiltrering γ-aluminiumoxid membran, en nanofiltrering titania membran og en Hybsi membran. Den mest lovende membran til rensningen er nanofiltreringen γ-aluminiumoxid membranen, der fjerne de giftige stoffer, men samtidig har et relativt høj vandgennemtrængelighed.

Udfra de ovenstående erfaringer og simuleringer ved brug af den modificerede matematiske model har vi produceret en ny uorganisk membran til at reducere vandhårdhed ved lavt transmembrane tryk (<7 bar). Simuleringer viser at den bedste membran til formålet, bør have en gennemsnitlig porestørrelse (diameter) mellem 1 og 2 nm og med $5 < |\zeta| < 20$ mV. Det burde herved være muligt at fjerne mere end 50 % NaCl og næsten alle divalente ioner. Baseret på disse simuleringer, har vi fremstillet en mikroporøs TiO_2-dopede SiO_2 membran med en gennemsnitlig porestørrelse (diameter) på 1,44 nm og et ζ-potentiale på ca. -9 mV (pH = 6). Efterfølgende test viser at membranen fjernede ca. 73% NaCl, hvilket er højere en tidligere data

for mesoporøse uorganiske membraner. Derudover var den TiO_2-dopedede SiO_2 membrans vandgennemtrængelighed 10 gange højere end eksisterende modificerede silica membraner, såsom silicat og organosilica membraner, men stadig 3-6 gange mindre end kommercielle polymere NF-membraner. Der er derfor behov for en yderligere optimering af den producerede membran for at sikre en højere vandgennemtrængelighed, for eksempel ved at mindske membrantykkelsen.

Preface and acknowledgements

This thesis has been developed between February 2012 and March 2015 at the Department of Chemistry and Bioscience, Aalborg University, Denmark.

I wish to express my gratitude to everyone who contributed to making this research work a reality. First and foremost I must single out my kind supervisor, Morten L Christensen, who gave me the opportunity to embrace this project and lead it with as much entrepreneurialism as no researcher could ever wish for. I have been extremely lucky to have a supervisor who cared so much about my work, and who responded to my questions and queries so promptly. Thank you for your constant attention and criticism which has allowed this work to grow solid.

Special thanks also go to Vittorio Boffa, my co-supervisor and more importantly my daily supervisor. Thank you for your time, consideration and suggestions throughout this research work. Thank you for your patience and all the time we spent together in the lab and in front of your computer screen. I am grateful for your support especially during those hard times of mine.

My appreciation also goes to Peter Roslev with whom I friendly shared interesting discussion and ideas on using bioassays for nanofiltration of waste water treatment. The results of such a fruitful cooperation are shown in Chapter Five of this thesis. I would also like to acknowledge Peter K Kristensen (Department of Physics and Nanotechnology, AAU) for his valuable help for cross-section SEM analysis. The results of this productive collaboration are presented in Chapter Six of this thesis.

Special thanks go to Hanne S Bengaard from the Danish National Advanced Technology Foundation and Johnny Marcher, Haris Kadrispahic and Jesper D Freisleben from Liqtech International A/S for our enjoyable and fruitful scientific discussions during the Low-Energy, High-Stability, Ceramic Reverse Osmosis Nano Membrane project meetings.

I am indebted to AAU staff members from whom I have always benefited scientifically and personally: Henriette Giese (Head of the Department), Kim L Larsen (Section Leader), Witold Szwebs (Special Consultant), Annemarie Davidsen (PhD administration), Lea Otte (Senior Clerk), Camilla Kristensen (Academic Officer) and Iris Jakobsen (Senior Secretary). A special thank also goes to the lab technicians, Lisbeth Wybrandt, Anne Flensborg and Helle Blendstrup.

My kind acknowledgments go to my Colleagues at Aalborg University, especially member of the separation science group have provided me an ambitious, supportive and fun working environment: Rasmus R. Petersen, Jakob and Katja König, Eskandar Poorasgari, Mads K Jørgensen, Søren Lorenzen and Thomas V Bugge. I would also like to acknowledge my friends in other institutes because of their helps and supports during these three years: Soheil Mansouri and Saeed Masoud M Malek-Shah (Technical University of Denmark), Waruna Wijesekara (Deaprtment of Energy Engineering, AAU), Onofrio De Bartolis (Universita' Degli Studi di Torino) and Marco Facciotti (University of Southampton).

I finish with Iran, where the most basic source of my life energy resides: my family. Their support has been unconditional all these years; they have given up many things for me to be at

Aalborg University; they have cherished with me every great moment and supported me whenever I needed it. This thesis, like always, is dedicated to my parents, Mohammad Ali Farsi and Batool Amiri, with warmest regards.

Table of Contents

1. Introduction 1
1.1 Background 1
1.2 Objectives 6
1.3 Thesis content 7

2. Theoretical aspects 9
2.1 Electroviscous effect 10
2.2 Boundary conditions 13
2.3 Numerical simulation 15

3. Materials and Methods 17
3.1 Membranes 17
3.1.1 Commercial membranes 17
3.1.3 TiO_2-doped silica membrane 19
3.2 Filtration protocol 21
3.2.1 Setup 21
3.2.2 Electrolytes 21
3.2.3 Active layer permeability 22
3.2.4 Concentration polarization 23
3.3 Analysis 24
3.3.1 ζ-potential 24
3.3.2 Colloidal titration 25
3.3.3 Wastewater sample characterization 26

4. Model verification 29
4.1 Mass transport in mesoporous γ-alumina and microporous organosilica membranes 29
4.2 Influence of pH on mass transport in mesoporous NF γ-alumina membrane 33

5. Inorganic membranes for recovery of effluent from wastewater treatment plants 41
5.1 Membrane permeability 42
5.2 Fouling resistance 44
5.3 Membrane selectivity 45
5.4 Membrane selection 47

6. Designing new materials for nanoporous inorganic membranes for water desalination 51
6.2 TiO_2 doped silica membrane for water desalination 54
6.3 TiO_2-doped silica Membrane performance 55

7. Conclusions and perspectives 59

8. Nomenclature 61

9. Bibliography 65

1. Introduction

1.1 Background

Nanofiltration (NF) is a rapidly developing area with great potential for separation and purification of aqueous solutions. As a relatively recent pressure-driven membrane separation technique, NF offers better ion rejection than ultrafiltration and higher flux than reverse osmosis. A fairly high retention of multivalent ions and a moderate retention of monovalent ions can be achieved with NF membranes, although their pores are larger than the diameter of the ions [1, 2]. Ion sieving, ion-surface electrostatic interaction, ion adsorption on the surface, and differences in ion diffusivity and solubility simultaneously affect the separation and retention of ions [3-5]. Thus, understanding the ion transport mechanism through a NF membrane is challenging but essential for further optimising membrane processes [6,7]. Table 1 summaries the possible applications of NF in various industries.

Table 1: Industrial applications for nanofiltration.

Industry	Application
Water Purification	Hardness removal [8] Removal of natural organic and color matters [9-11] Removal of heavy metals [12,13] Removal of phosphate, sulphate, nitrate and fluoride [14,15] Brackish water desalination [16,17] Recovery of water from waste water or waste water treatment effluent [18]
Chemical and petrochemical	Sulfate removal preceding chlorine and NaOH production [19,20] Solvent recovery in lube oil dewaxing [21,22] Desulfurization of gasoline [23,24]
Pharmaceutical	Recovery of 6-aminopenicillanic acid (216 Da) in the enzymatic manufacturing of synthetic penicillin [25] Microfluidic purification [26] Solvent exchange [27]
Electronic and optical	Recovery of LiOH during treatment of battery waste [28]
Food	Demineralization of whey [29,30] Separation of sunflower oil from solvent [31] Demineralization of sugar solutions [32]

Up to now, NF has been mainly performed with polymeric membranes, which still have chemical, thermal and mechanical stability problems. These stability problems increase the membrane replacement costs and pose operation limitations for pressure, temperature and pH. One alternative to the use of polymeric membranes is inorganic membranes [33-40].

1. Introduction

Due to their high stability, inorganic membranes have high potential in the treatment and filtration of foods and beverages, since they can be easily cleaned and sterilized. Most of them have been used for microfiltration of milk as well as (pre-) filtration of wines and juices. Moreover inorganic ultrafiltration (UF) membranes have been used where the applications of polymeric membranes were limited, for example oil and petrochemical industry [41]. Recently, inorganic NF membrane has been commercially developed for water purification [42-50]. Inorganic NF membranes are more expensive than polymeric membranes and have low loading density, but they are resistant to severe chemical environments and are structurally stable over a broad range of pH values; hence, they can be used for longer periods and allow for easy cleaning and sterilisation. Inorganic membranes have demonstrated high hydrothermal stabilities and low tendencies for fouling. Therefore, increasing interest has been directed toward the development and application of inorganic NF membranes. Compare to polymeric membranes, research on inorganic membrane materials is however in relatively early stage of development, especially in the area of NF. This is mainly due to technical difficulties of synthesizing a defect-free-thin-layer with pore size less than 5 nm with commonly used methods like slip casting, tape casting, chemical vapor deposition and dip coating [51]. Inorganic membranes mostly consist of metal oxides like silica, alumina, titania, and zirconia [42-50] or mixed oxides. Recently, organosilica and SiC membranes have been produced [35,36,44].

The mechanism of ion separation in NF membranes lies between dense RO membranes and porous ultrafiltration (UF) membranes [3,52]. NF membranes have lower ion rejection than RO membranes, but can offer several advantages such as low operating pressure (ΔP), high permeability (L_p), relatively low investment, and low operation and maintenance costs [1]. Moreover, NF membranes can remove small organics molecules, remove hardness, and reduce the concentration of monovalent ions (sodium, chloride, fluoride and nitrate). Thus, NF membranes can be used as RO pre-treatment [53,54], or for the direct production of drinking water from brackish water [54]. Table 2 summarizes the water desalination performance for some of the commercial low-energy RO and NF polymeric membranes [55-66]

Table 2: Performance of commercial low-energy polymeric RO and NF membranes [55-66].

Membrane/Company	**Type**	**ΔP [bar]**	**T [C]**	**pH**	**c_{NaCl}[1] [M]**	**Rec.[2] [%]**	**L_p [LMHB]**	**R_{NaCl} [%]**	**$R_{d\text{-}ion}$[3]**
XLE-2521 / DOW-FILMTEC[55]	RO	6.90	25	6-7	0.008	15	7.04	99	>99 $MgSO_4$
BW30-2540 / DOW-FILMTEC[55]	RO	10.3	25	6-7	0.03	15	4.98	99.50	>99 $MgSO_4$
4040-ULP / KOCH[56]	RO	8.60	25	7.5	0.03	15	4.17	98.65	>99 $MgSO_4$
TMG10 / TORAY[57]	RO	7.60	25	7	0.01	15	5.2-6.2	99	>99 $MgSO_4$
ESPA4-4040 / HYDRANAUTICS[58]	RO	7.00	25	6.5-7	0.01	15	7.13	99.2	>99 $MgSO_4$

1. Introduction

AK8040N 400 / GE-DESAL[59]	RO	7.93	25	7.5	0.01	15	5.61	98	>99 $MgSO_4$
NF270/ DOW-FILMTEC[60,61]	NF	4.8	25	6.5-7	0.016	15	10.5-10.85	>50	97 $MgSO_4$
NF90/ DOW-FILMTEC [58,62]	NF	4.8	25	6.5-7	0.016-0.034	15	6.66-8.68	>85	97 $MgSO_4$
CK2540FM 30D/ GE-DESAL[63]	NF	15.5	25	6.5	0.016	15	2.47	>50	94 $MgSO_4$
ESNA1-LF-LD/ HYDRANAUTICS[64]	NF	5.2	25	6.5-7	0.004	15	6.70	>50	86-89 $CaCl_2$
8040-TS80-UWA/ TRISEP[65]	NF	7.6	25	7-8	0.016	15	5.45	>50	97-99 $MgSO_4$
NE 8040-90/ CSM[66]	NF	5	25	6.5-7	0.004-0.034	15	6.36	85-95	90-95 $CaCl_2$
NE 8040-70/ CSM[66]	NF	5	25	6.5-7	0.004-0.034	15	5.9	40-70	45-70 $CaCl_2$

[1] *Concentration of NaCl in the feed.*
[2] *Recovery.*
[3] *Retention of divalent ions.*

Transport in pressure-derived membranes has been studied by several models as shown in Table 3.

Table 3: Mathematical models for pressure-derived membranes.

Model		Advantages	Disadvantages
Irreversible thermodynamics	Kedem and Katchalsky [69]	Phenomenological relationships representing fluxes for water and solute calculation	Model coefficients are not concentration dependent
	Spiegler and Kedem [70]	Phenomenological relationships representing fluxes for water and solute calculation, widely applicable	Do not describe the membrane transport mechanism in detail (black box model)
Solution-diffusion	Lonsdale et al. [71]	The model is based on diffusion of the solute and solvent through the membrane	Membrane characteristics are not included in the model
	Bhattacharyya and Willians [72]	Calculates solvent and solute flux as the two parameters characterizes the membrane system in the model for inorganic and organic solutes	The model is limited to membranes with low water content

Maxwell–Stefan	Krishna and Wesselingh [73]	The Maxwell–Stefan method relates the driving forces to the Friction forces acting on the species in a system. The non-ideality of the mixture is not incorporated in the diffusivities (like in Fick's law).	This method is not sufficient to capture the Complex adsorption and diffusion behavior.
Donnan-steric pore	Bowen et al. [3,4]	This model considered diffusion, convection and electromigration terms and it useful for transport through porous membranes.	This model is limited to the porous membrane and not useful for dense membrane. Electroviscous effect was not considered.

Phenomenological relationships representing fluxes incorporating irreversible thermodynamic characteristic can be developed assuming that the membrane is not far from equilibrium. The difficulty in irreversible thermodynamic model [69] due to presence of concentration dependent coefficient were simplified by Spiegler and Kedem [70] and thereby got wide applicability. However, these black box type models do not describe the membrane transport mechanism in detail. Lonsdale et al. [71] removed these difficulties by proposing solution-diffusion which has emerged over the past decades as the most widely accepted explanation of transport in RO membranes in which separation is a result of differences in solubility and diffusivity of permeates [68]. The water and solute fluxes are given by the solution-diffusion model that was proposed based on four assumptions; (I) the membrane morphology is homogeneous and dense, (II) the solvent and solute dissolve in the membrane dense layer and then each diffuses across it down their respective concentration gradient, (III) the solute and solvent diffuse across the membrane independently, each due to its own chemical potential and (IV) the chemical gradients are the result of concentration and pressure gradients across the membrane. The water flux in dense membrane ($J_v = \frac{k_w D_w v_w}{RTl}(\Delta P - \Delta\pi)$) is a function of the water–membrane partition coefficient (k_w), water diffusion coefficient in membrane (D_w), molar volume of water (v_m), membrane thickness (l) and applied pressure (ΔP) and osmotic pressure differences ($\Delta\pi$). The ion flux is derived Fick's law ($J_i = \frac{k_i D_i}{l}(c_f - c_p)$) where D_i is solute diffusion coefficient in the membrane, k_i is solute–membrane partition coefficient, c_f is ion concentration in feed side and c_p is ion concentration in permeate side. Figure 1 shows schematic of the solution-diffusion process in a dense membrane.

1. Introduction

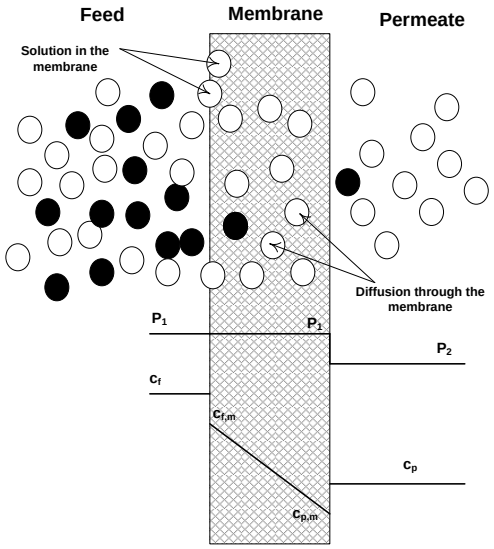

Figure 1: Schematic of the solution-diffusion model in a dense membrane.

NF with polymeric membranes can be described by modified solution–diffusion models which are suitable for tight membranes; but the ion transport through NF inorganic porous membranes is substantially different from the dense membranes even if they are in a range of a NF membrane [75, 76]. Therefore, the solution-diffusion model that is used in the case of dense diffusion membranes cannot be modified for inorganic membrane. The substance transport for inorganic NF membranes can alternative be described using the Donnan-steric pore model (DSPM) proposed by Bowen et al. [3,4], in which the Hagen–Poiseuille equation predicts solvent flux and the extended Nernst-Planck equation model predicts the ion transport through the NF pores. Ion rejection depends on the diffusion, convection and electromigration (potential gradient) terms. Further, the combination of steric, electric and dielectric exclusions defines the equilibrium partitioning at the interfaces. Water flux and effective charge density often increase ion rejection. The DSPM has been used by several authors [5,76-78] with fairly good results, but most studies ignored the electroviscous effect in the pore and ion adsorption. Ions moving along the electric field generated by the streaming potential will drag solvent molecules within membrane pores, thus increasing the apparent viscosity of the liquid. This phenomenon is commonly named electroviscous effect [79].

Electroviscous effect influences not only permeation of the solvent through the membrane but also the rejection of ions. The Hagen–Poiseuille and extended Nernst-Planck equations indicate that viscosity in the membrane pores decreases the water flux and subsequently the convection term, which may govern the ion transport through the membrane pore. The electroviscous effect has been previously introduced for microfiltration and ultrafiltration inorganic membranes [80,81]. However, in these cases the ion rejection effect on the electroviscous term was not considered. Furthermore, electroviscous effect can be neglected for polymeric NF membranes because of low surface potential.

The aim of this dissertation is to derive a mathematical model, based on understanding the interactions occurring between solution and membrane, for simulating flux and rejection in inorganic NF membranes in order to reduce the number of required experiments to develop new

membranes and optimize filtration parameters for a specific application; Therefore, these assumptions, i.e. no ion rejection and low surface potential, may not be acceptable for inorganic NF membranes, due to their small pore size and high surface potential. In this study, a mass transport model based on DSPM model, including the electroviscous effect, is proposed to understand the ion transport mechanism through meso- and microporous inorganic membranes. The model is verified by different inorganic membranes and in a broad pH range, which can be useful to optimize operation conditions of filtration system for a specific application. The model is also used for material design to fabricate an inorganic membrane for water desalination to have a value in the market compare to NF polymeric membrane.

1.2 Objectives

The overall objective is to study mass transport through inorganic meso- and microporous inorganic membranes for developing a theoretical model that can be used to predict the performance of membrane, i.e. calculate solvent flux and solute selectivity. The major issues are the investigation of electroviscous effect and charge density in the membrane pores, and using this knowledge to modify the Hagen–Poiseuille equation and subsequently the DSPM model.

The specified objectives of the Ph.D. thesis are summarized as follow:

1- Determine the influence of solution concentration, pH, ζ-potential and pore size on the electroviscous effect in inorganic meso- and microporous membrane.

2- Determine the influence of ion adsorption on mesoporous inorganic membrane performance.

3. Modify the existing mathematical model for simulating membrane filtration, so it can be used for inorganic NF membranes.

4. Study the performance of commercial inorganic meso- and microporous membrane in real life (e.g. treatment of municipal wastewater treatment plant, WWTP, effluent to reduce its toxicity).

5. Fabricate an inorganic membrane with optimized performance that have a value on the market compare to NF polymeric membrane.

1.3 Thesis content

This thesis presented as an introduction to mass transport in meso- and microporous inorganic membranes followed by an overview of journal papers which I act as the first author. These papers constitute the main body of the thesis, and are appended after the bibliography.

Papers include

I. **A. Farsi**, V. Boffa, H .F. Qureshi, A. Nijmeijer, L. Winnubst, M. L. Christensen, Modelling water flux and salt rejection of mesoporous γ-alumina and microporous organosilica membranes, *Journal of Membrane Science , 2014, 470, 307-315.*

II. **A. Farsi**, V. Boffa, M. L. Christensen, Modeling water permeability and salt rejection of mesoporous γ-alumina nanofiltration membrane: contribution of electroviscous effect and surface charge density. *Journal of Membrane Science, 2015, under review.*

III. **A. Farsi**, S. H. Jensen, P. Roslev, V. Boffa, M. L. Christensen , Inorganic membranes for the recovery of effluent from municipal wastewater treatment plants, *Industrial & Engineering Chemistry Research, 2015, 54, 3462-3472.*

IV. **A. Farsi**, M. L. Christensen, V. Boffa, A titania-doped silica nanofiltration membrane for water purification. *Journal of Membrane Science, 2015, submitted.*

Papers not included

V. K. Koning, V. Boffa, B. Buchbjerg, **A. Farsi**, M. L. Christensen, G. Magnacca, Y. Yue, One-step deposition of ultrafiltration SiC membranes on macroporous SiC supports, *Journal of Membrane Science, 2014, 472, 232–240.*

VI. M. Facciotti, V. Boffa, G. Magnacca, L. B. Jørgensen, P. K. Kristensen, **A. Farsi**, K. König, M. L. Christensen, Y. Yue, Deposition of thin ultrafiltration membranes on commercial SiC microfiltration tubes, *Ceramics International, 2014, 40, 3277-3285.*

VII. **E. Poorasgari**, A. Farsi, K. König, M. L. Christensen, A mathematical approach to modelling retention of humic-like substances by a microfiltration membrane, *Industrial & Engineering Chemistry Research, 2015, Submitted.*

Conference Presentations

VIII. **A. Farsi**, S. H. Jensen, P. Roslev, V. Boffa, M. L. Christensen, "Cross-flow filtration with different ceramic membranes for polishing wastewater treatment plant effluent", *Oral presentation*, 13th International Conference on Inorganic Membranes, Brisbane, Australia, July 2014.

IX. **A. Farsi**, V. Boffa, M. L. Christensen "Filtration of several uncharged solutes on reverse osmosis membrane: theory modification based on slip boundary", *Poster presentation*, 14th Nordic Filtration Symposium, Aalborg, Denmark, August 2012.

X. **A. Farsi**, K. König, V. Boffa, M. L. Christensen "Nanofiltration ceramic membrane: Interlayer preparation by polymer derived SiC dip-coating on silicon carbide supports", *Oral presentation*, Network Young Membrains 14, Imperial College London, UK, September 2012.

2. Theoretical aspects

A mathematical model has been derived for simulating mass transport through inorganic membranes modifying the existing Nernst-Planck equation. The existing model will be described as well as the required modification for simulating transport of solvent and solutes through inorganic NF membranes.

The transport of ions through NF membranes can be calculated using the extended Nernst–Planck equation and an equilibrium partitioning at the membrane-solution interface based on the DSPM [3-5]. The flux of ion *i* in the membrane (J_i) is controlled by convection, diffusion and electromigration. The effective pressure gradient ($\Delta P_{eff}/\Delta x$) causes the convection term i.e. solvent flux (J_p), while ion diffusion is caused by the concentration gradient (dc_i/dx) and electrical immigration is caused by the electrical potential gradient ($d\psi/dx$). By considering steric and hydrodynamic interactions between the permeating solute and the pore wall, Eq. (1) describes J_i as follow:

$$J_i(x) = K_{i,c}\, c_i(x) J_p + \left(-K_{i,d} D_{i,\infty} \frac{dc_i(x)}{dx}\right) + \left(-\frac{z_i D_{i,\infty} F c_i(x)}{RT} \frac{d\psi(x)}{dx}\right) \qquad (1)$$

Where $D_{i,\infty}$ represents the diffusivity of the ion *i* in a dilute bulk solution, z_i is its valence, *R* is the universal gas constant, *T* is the absolute temperature, *F* is the Faraday constant. $K_{i,c}$ and $K_{i,d}$, are the hindrance factors for convection and diffusion of virtually spherical and rigid ions in cylindrical pores, respectively. These factors are functions of the ratio between ion and pore radii ($\lambda_i = r_i/r_p$) and the hydrodynamic coefficients and were first introduced by Deen [82]. The equations were later recalculated for a limited range ($\lambda_i \leq 0.95$) by Dechadilok and Deen [83].

$$K_{i,d}(\lambda_i) = 1 - 2.3\lambda_i + 1.154\lambda_i^2 + 0.224\lambda_i^3 \quad (2)$$

$$K_{i,c}(\lambda_i) = (2 - (1-\lambda_i)^2)(1 + 0.054\lambda_i - 0.988\lambda_i^2 + 0.441\lambda_i^3 \quad (3)$$

At steady state conditions, $J_i(x) = J_i = c_{i,p} J_p$, and the concentration gradient of ion *i* along the pore is:

$$\frac{dc_i(x)}{dx} = \frac{J_p}{K_{i,d} D_{i,\infty}} (K_{i,c}\, c_i(x) - c_{i,p}) - \frac{z_i F c_i(x)}{RT} \frac{d\psi(x)}{dx} \qquad (4)$$

In order to calculate the electrical potential gradient ($d\psi/dx$) in the pore, a balance for electrical charge neutrality is set up:

$$\sum_{i=1}^{n} z_i c_i(x) + X_d = 0 \qquad (5)$$

where X_d is the effective membrane pore charge density in diffuse layer (charge per pore volume). With respect to Eq. (4) and (5), the electrical potential gradient can be expressed by:

$$\frac{d\psi(x)}{dx} = \frac{\sum_{i=1}^{n} \frac{z_i J_p}{K_{i,d} D_{i,\infty}} \left(K_{i,c}\, c_i(x) - c_{i,p}\right)}{\frac{F}{RT} \sum_{i=1}^{n} z_i{}^2 c_i(x)} \qquad (6)$$

Thus, the concentration gradient along the pore can be defined by a set of ordinary differential equations:

$$\frac{dc_i(x)}{dx} = \frac{J_p}{K_{i,d} D_{i,\infty}} \left(K_{i,c}\, c_i(x) - c_{i,p}\right) - \frac{z_i c_i(x)}{RT} F \frac{\sum_{i=1}^{n} \frac{z_i J_p}{K_{i,d} D_{i,\infty}} \left(K_{i,c}\, c_i(x) - c_{i,p}\right)}{\frac{F}{RT} \sum_{i=1}^{n} z_i{}^2 c_i(x)} \qquad (7)$$

To solve the above set of equations, the concentration at the permeate side $c_{i,p}$, the convective flux J_p, as well as the inlet and outlet boundary conditions should be determined. $c_{i,p}$ can be estimated initially and adjusted by several iterations to reach a constant $c_{i,p}$ value for a certain operational condition.

2.1 Electroviscous effect

The Hagen–Poiseuille equation [10,15,22] is used to describe the permeate flux (J_p) in NF membranes:

$$J_p = \frac{r_p^2 \varepsilon}{8\eta\tau} \frac{\Delta P_{\text{eff}}}{\Delta x} \qquad (8)$$

Where η, r_p, Δx, ε, τ and ΔP_{eff} represent viscosity, pore radius, membrane thickness, porosity, tortuosity and effective pressure driving force ($\Delta P - \Delta\pi$), respectively. For dilute solutions (< 0.1 M), the osmotic pressure can be calculated simply by using the Van't Hoff equation for ideal solutions [84].

The viscosity term (η) in the Hagen–Poiseuille equation (Eq. (8)) is often considered as the bulk viscosity (η_b) of the solution. However, this assumption may not be valid for narrow NF pores, because in the presence of small pores and a high ζ-potential (ζ > 20mV), the ionic strength of the solution as well as the surface properties of the membrane pores have to be considered [79, 81]. When an electrolyte solution is in contact with a solid surface, the surface will generally be charged through electrochemical adsorption. As a result, a net countercharge distribution is formed in the solution near charged surfaces, which is referred as electrical double layer. When the electrical double thickness (κ^{-1}), also referred to as the Debye length [79], is comparable with pore size, a pressure-driven flow of an electrolyte solution in a pore will cause a potential against the flow direction and reduce the flow rate. This effect can be interpreted in terms of electroviscosity. In a cylindrical pore filled with an incompressible Newtonian aqueous

2. Theoretical aspects

electrolyte, the apparent viscosity (η_{app}) is related to the bulk solution viscosity (η_b) as follow [79]:

$$\frac{\eta_{app}}{\eta_b} = \left[1 - \frac{8\beta\left(1 - \frac{2I_1(\kappa r_p)}{\kappa r_p I_0(\kappa r_p)}\right)}{(\kappa r_p)^2\left(1 - \beta\left(1 - \frac{2I_1(\kappa r_p)}{\kappa r_p I_0(\kappa r_p)} - \frac{{I_1}^2(\kappa r_p)}{{I_0}^2(\kappa r_p)}\right)\right)}\right]^{-1} \quad (9)$$

I_0 and I_1 are the zero-order and first order modified Bessel functions of the first kind. κr_p is a dimensionless number, which indicates the ratio between pore radius and double layer thickness. The dimensionless parameter β, which merges the characteristic of the pore surface and of the electrolyte, is:

$$\beta = \frac{(\varepsilon_p \varepsilon_0 \zeta \kappa)^2}{16\,\pi^2 \eta_b \sigma_p} \quad (10)$$

The electrical conductivity (σ_p) is calculated from the molar conductivity (Λ_p) [71]

$$\Lambda_p = \Lambda_0 + A\,\frac{{m_p}^{1/2}}{1 + B{m_p}^{1/2}} \quad (11)$$

m_p is the molar concentration in the pore, Λ_0, A, B are constants which are functions of temperature.

Studies [3,86-92] have shown that the dielectric constant of a nanoconfined aqueous solution (ε_p) was significantly smaller than the dielectric constant in the bulk. ε_p depends on both the solution and membrane material properties, such as the ion type, bulk concentration, pore radii and potential profile in the diffuse layer [87-92]. The model suggested by Bowen et al. [3,4] for polymeric NF membrane was used in this study (Eq. 12).

$$\varepsilon_p = \varepsilon_b - 2(\varepsilon_b - \varepsilon^*)\left(\frac{d}{r_p}\right) + (\varepsilon_b - \varepsilon^*)\left(\frac{d}{r_p}\right)^2 \quad (12)$$

where ε_b is the bulk dielectric constant (dielectric constant of water at 25 °C is 79.4 [93]) and ε^* is the reduction coefficient for solvent orientation in the nanoconfined solution, which has been described in detail elsewhere [87-91].

Figure 2 shows the electroviscous effect on the solution viscosity in the nanopore as function of the ζ-potential for different r_p values (a) and ionic strength (b) for 1:1 electrolytes (e.g., NaCl). The electroviscous effect consists of the increase of solution viscosity in membrane nanopores ($\eta_{app}/\eta_b >> 1$) caused by an increase in ζ-potential. The electroviscous effect is more significant for low pore size membranes and dilute solutions. From this simulation, the electroviscous effect appears to be negligible for ζ-potential < 20 mV, r_p > 4 nm or ionic strength < 0.1 M. In presence of dilute solution, as for deionised water, κ^{-1} > 10 nm and the electrical double layer fully

covered the active layer pores ($\kappa^{-1} > r_p$). ζ-potential values larger than 60 mV or lower than -60 mV can increase the solution viscosity (by more than 25%) in pores with $r_p \leq 2$ nm and subsequently lower the membrane permeability.

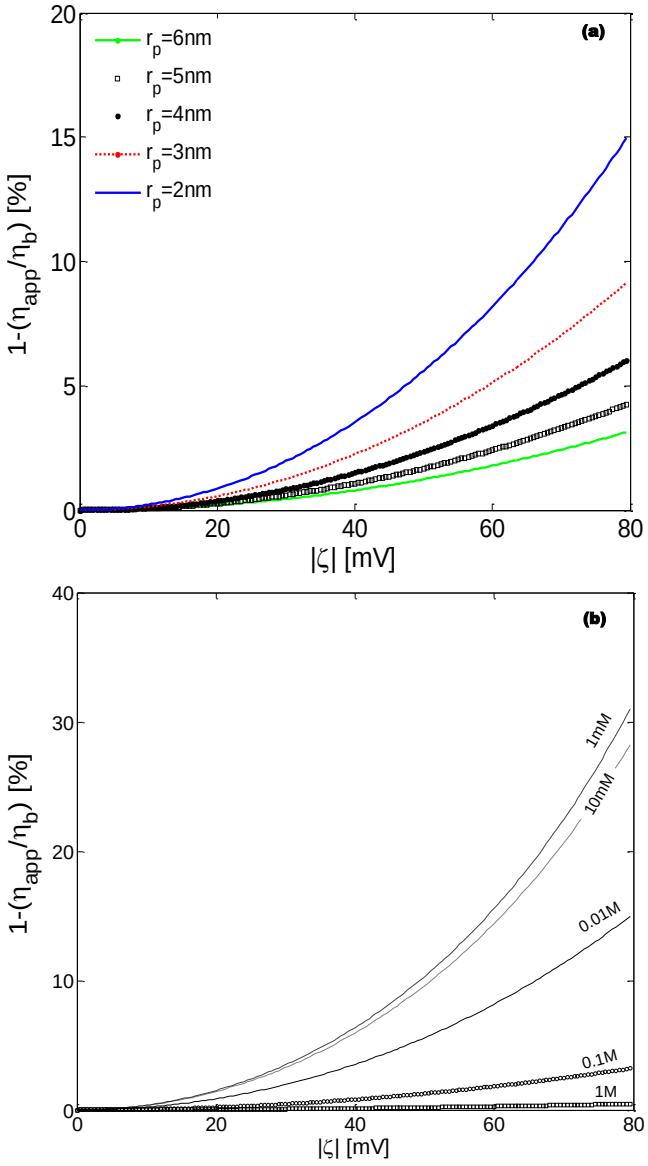

Figure 2: Viscosity increasing as function of ζ for different pore radios at 0.01 M ionic strength of NaCl (a) and different ionic strength in r_p = 2 nm (b).

The permeate flux has been simulated considering electroviscous effect (Eq. (9)) and its relative differences with the Hagen–Poiseuille model are shown in Figure 3 as a function of κr_p (dimensionless number) for different membrane ζ-potentials. It shows that in presence of high ζ-potential (> 20 mV), the Hagen–Poiseuille model may overestimate the flux especially when the Debye length is comparable with the pore size ($\kappa r_p > 5$).

2. Theoretical aspects

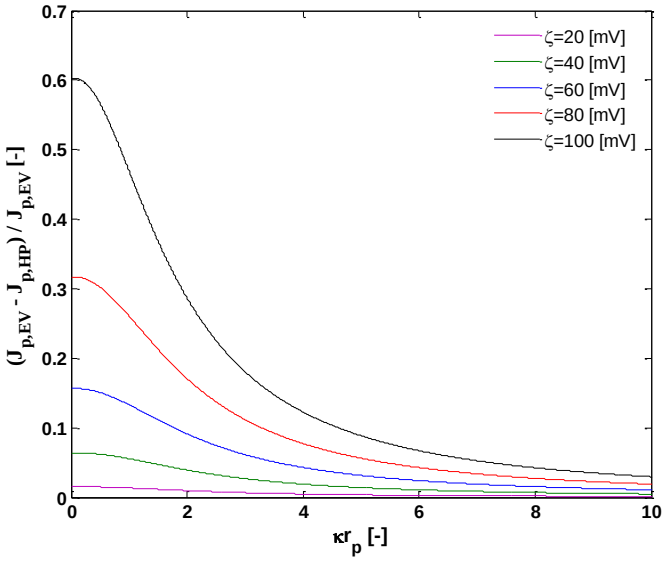

Figure 3. Relative difference of Electroviscous model (EV) and Hagen–Poiseuille (HP) models ($\frac{|J_{p,EV}-J_{p,HP}|}{J_{p,EV}}$) as function of κr_p for different membrane ζ-potentials.

2.2 Boundary conditions

To solve the equation of calculating the concentration gradient along the pore (Eq. (7)), the concentration at the permeate side $c_{i,p}$ and the inlet and outlet boundary conditions should be determined. $c_{i,p}$ can be estimated initially and adjusted by several iterations to reach a constant $c_{i,p}$ value for a certain operational condition. The model algorithm shown in Figure 4 clarifies this iterative calculation.

Donnan, steric, dielectric interfacial exclusion mechanisms (Eq. (13)) and electroneutrality conditions (Eq. (14)) express the ion concentrations at both the feed and permeate boundaries.

$$\left(\frac{\gamma_i(x)}{\gamma_i\phi_i\exp(-\Delta w_i)}\frac{c_i(x)}{C_i}\right)^{\frac{1}{z_i}} = \left(\frac{\gamma_j(x)}{\gamma_j\phi_j\exp(-\Delta w_j)}\frac{c_j(x)}{C_j}\right)^{\frac{1}{z_j}} \quad (13)$$

$$\sum_{i=1}^{n} z_i c_i(x) + X_d = 0 \quad (14)$$

The extended Debye–Huckel equation [80] is used for the activity coefficients (γ_i). The steric partitioning coefficient (ϕ_i) depends on the ratio between the sizes of the ion *i* and that of the pores. The Ferry [94] model is mostly used for this purpose:

$$\phi_i = (1-\lambda_i)^2 = \left(1-\frac{r_i}{r_p}\right)^2 \quad (15)$$

2. Theoretical aspects

Hydrated ion radii (r_i) can be obtained in a variety of ways and can show significant variation. In this study, the hydrodynamic (Stokes) radius is used [95]. Furthermore, ΔW_i is the difference between the excess solvation energies (ΔW_i), which governs the dielectric exclusions [3-5]. ΔW_i can be calculated from the Born equation [96]:

$$\Delta W_i = \frac{z_i^2 e^2}{8\pi\epsilon_0 r_i}\left(\frac{1}{\varepsilon_p} - \frac{1}{\varepsilon_b}\right) \quad (16)$$

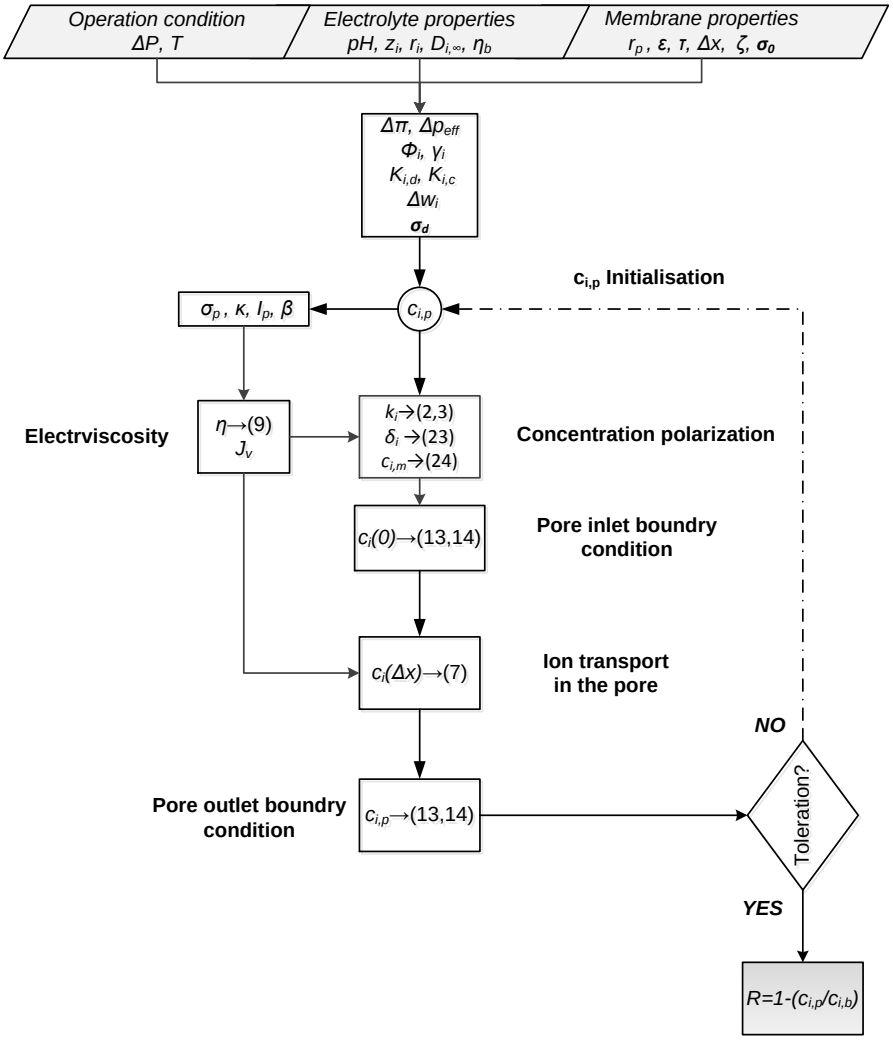

Figure 4: The transport model considering the electroviscous effect and surface charge density in the membrane pores.

2. Theoretical aspects

2.3 Numerical simulation

Figure 5 shows three main domains that should be considered for the transport model, namely feed-membrane interface, membrane-permeate interface and the membrane pore. The membrane pore domain is divided into a set of *N* non-overlapping control volumes where the concentration and electric potential of each ion are simulated using MATLAB® (R2012b). Both solution-membrane interfaces, so at the feed and permeate side, were simulated according to Eq. (13) and Eq. (14) using a nonlinear solving method. For the pore inlet condition, the permeate concentration ($c_{i,p}$) should be initialized first, which would then be modified by an iteration loop as shown in Figure 4.

The loop accuracy has been considered less than 10^{-6} ($\frac{|c_{i,p}(k+1)-c_{i,p}(k)|}{c_{i,p}(k+1)} < 1\times10^{-6}$), where k shows the loop numbers. The concentration profile in the active layer domain was simulated for each ion *i* and for each grid node *j* using equation (7). This set of ordinary differential equations has been solved with the fourth and fifth order Runge–Kutta method. The step size has been controlled for one million points along the pore for both membrane and permeate concentrations ($c_{i,p}$) and adjusted in each loop based on the iteration algorithm. For the electroviscous model (EV model), the solvent flux (J_p) term (Eq. (8)) is calculated based on inserted viscosity term (Eq. (9)) while the bulk viscosity is considered for the Hagen–Poiseuille model.

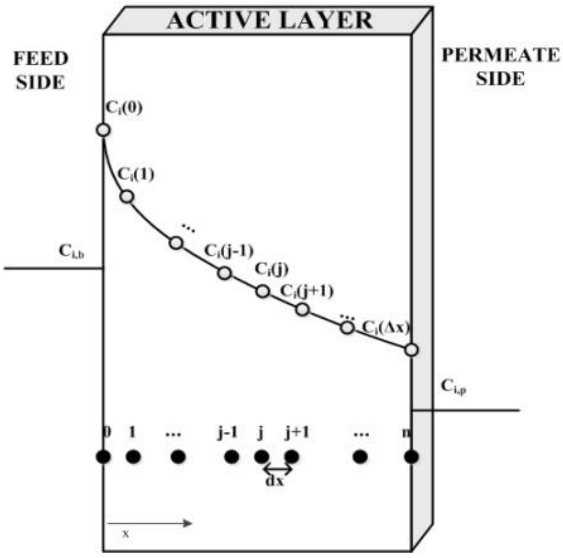

Figure 5: The main domains for mass transport across a NF active layer and the grid nodes.

3. Materials and Methods

3.1 Membranes

3.1.1 Commercial membranes

Five different commercial inorganic membranes were used for testing the mathematical model and compare the performance of different membranes to purify the effluent of wastewater treatment plant. MF α-alumina, UF titania, NF γ-alumina, NF titania and Hybsi monotubular membranes (250×10×7 mm (L×OD×ID)) were purchased from Pervatech B.V., The Netherlands. All five membranes possessed an asymmetric structure that consisted of an active layer and support layer. Table 4 lists the active layer properties for each membrane. For clarity, membranes will now be referenced according to their designation in Table 4.

Table 4: Model parameters used in this study for different active layers.

Parameter	**Membrane**				
	MF α-alumina	UF titania	NF γ-alumina	NF titania	Hybsi
Membrane type	Macroporous	Mesoporous	Mesoporous	Microporous	Microporous
Nominal pore size (r_p) [nm]	110[a]	15[a]	4.4[a]	2[a]	0.4[a]
Active layer thickness (Δx) [μm]	100 (100-300)[b]	3 (0.4-5)[b]	1.2 (1-2)[b]	0.1 (0.1-0.4)[b]	0.2 (0.1-0.5)[b]
Active layer porosity (ε) [-]	0.36 (0.3-0.43)[b]	0.38 (0.35-0.4)[b]	0.55 (0.4-0.55)[b]	0.42 (0.3-0.4)[b]	0.2 (0.2-0.3)
Active layer tortuosity (τ) [-]	(1.5-2.5)[b]	(2-3)[b]	(2.5-15)[b]	(2.5-5)[b]	11
$\lvert\zeta\rvert$[c] [mV]	35	15	60	15	20

[a] *Data Provided by manufacture.*
[b] *Data Provided by literature [97-106].*
[c] *at pH 5.5 for a dilute solution (c<0.001 M).*

3.1.2 Organosilica membrane

In order to verify the model and investigate the electroviscous effect in nanopores, two different membranes have been compared: a mesoporous γ-alumina membrane (NF γ-alumina) and a

3. Materials and Methods

microporous organosilica top-layer coated on a NF γ-alumina membrane. The organosilica membrane was fabricated using dip-coating of a BTESE sol (with dipping speed of 1.7cm/s) on γ-alumina tubes. The dipping procedure was performed only once to deposit a selective organosilica layer on the mesoporous support. This procedure is described in detail in *paper I*. The thickness of the calcined organosilica layer was determined by analyzing the cross-sectional view of the membrane using a high-resolution scanning electron microscope HR-SEM (ZEIS 1550) at an accelerating voltage of 2.0 kV. Single-gas permeation experiments were performed as reported elsewhere [107].Figure 6 shows the microporous organosilica membrane, which is deposited on a mesoporous γ-alumina membrane. A thickness (Δx) 200 nm was measured for the organosilica layer. The determination of the pore size distribution of microporous membranes is challenging due to the fact that some of their pores are not accessible to most of the gas molecules.

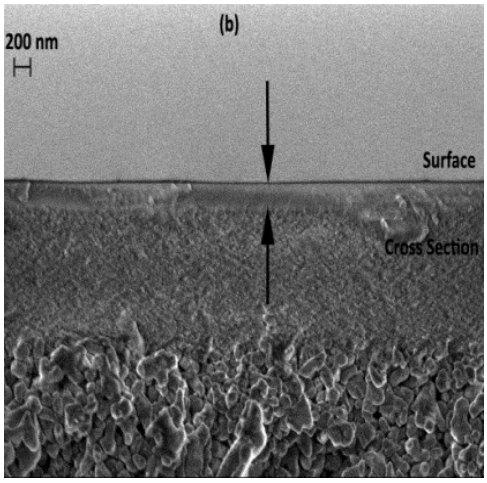

Figure 6: High resolution SEM images the organosilica tubular membrane.

The organosilica membrane is a network of hybrid silica chains, which give an apparent pore-size. In this study, single gas-permeation experiments were performed on the organosilica membrane to assess the presence of defects and to determine its pore size distribution. A permeance of 2×10^{-7} mol (Pa m^2 s)$^{-1}$ was measured for H_2 (kinetic diameter, d_K = 0.289 nm), whereas he permeate flux of SF_6 (d_K = 0.55 nm) was below the detection limit 10^{-10} mol (Pa m^2 s)$^{-1}$. These data indicate that organosilica membrane pores have mean radius (r_p) between 0.15 and 0.275 nm. For this reason numerical flux simulations were performed by considering r_p= 0.275 nm. Simulations with $0.15 < r_p < 0.55$ nm satisfied $\kappa r_p < 1$ condition (i. e. fully covered pore condition). Therefore, rejection simulation could be done for this pore size distribution.

3.1.3 TiO_2-doped silica membrane

The DSPM model was used to design a pressure-derived inorganic membrane for ion separation for dilute solution (<0.1 M) at low transmembrane pressure ($4 < \Delta P_{eff} < 7$ bar). The theoretical model clears that inorganic porous membranes cannot compete with commercial dense polymeric RO membrane for water desalination unless membrane thickness would be technically reduced to be less than 50 nm, which is not possible with current fabrication procedure [51]. The model suggests that in order to design an inorganic porous membrane to be comparable with commercial polymeric NF membrane, the membrane should have a pore size between 1 and 2 nm. In this pore size range the optimum ζ-potential is between 5 to 20 mV (absolute ζ-potential). Further investigation were disused in *Chapter 6*. In this study, the microporous TiO_2-doped silica membrane was fabricated by sol-gel deposition on NF γ-alumina tubular membrane. The procedure is described in detail in *paper IV*.

Specific surface area (*SSA*) and porosity (ε) of materials were determined by means of N_2 adsorption at liquid-nitrogen boiling point in a gas-volumetric apparatus ASAP2020 (Micromeritics, Norcross USA). Samples were outgassed at 300 ºC in vacuum (residual pressure 10^{-2} mbar) for about four hours, that is, until no gaseous species arise from them. Specific surface areas were determined using the Brunauer-Emmett-Teller (BET) model [36] and porosity was obtained applying the Density Functional Theory (DFT) method on the adsorption branch of the isotherms [35,36]. The crystal structure of the materials was determined on a X-ray diffractometer Philips PW1830 working with a Cu-Kα source and was found to be amorphous. High-resolution transmission electron microscopy (HRTEM) images were obtained on a JEOL 3010-UHR instrument (acceleration potential: 300 kV). Samples for TEM investigation were supported onto holed carbon coated copper grid by dry deposition. The membrane composition and thickness of the TiO_2-doped silica active layer was determined by analyzing the cross-sectional view of the membrane on a focused ion beam scanning electron microscopes (FIB-SEM, Zeiss, EDX) at an accelerating voltage of 10 kV.

Figure 7(a) shows a TEM image of the heat-treated unsupported TiO_2-doped silica membrane fabricated in this study. The membrane material appears to be fully amorphous and homogenous with a disorder pore structure. The absence of long-range order in the sample was confirmed by the absence of peak in the X-ray diffractograms, which are not reported here for the sake of briefness. The pore size distribution of the material was measured by low temperature nitrogen adsorption. As shown in the insert of Figure 7 (b), most of the nitrogen is adsorbed at a relative pressure < 0.2 and the sorption curve has a plateau at a higher relative pressure. These sorption isotherms correspond to the Type I to IUPAC classification [108] which is typical of systems with micropores and/or small mesopores. The pore size distribution (Figure 7 (b)) shown indeed that have size smaller than 2.3 nm and mean pore size of 1.44 nm, which is consistent with the use of Cetyltrimethylammonium bromide (CTAB) micelles as structure directing agents.

3. Materials and Methods

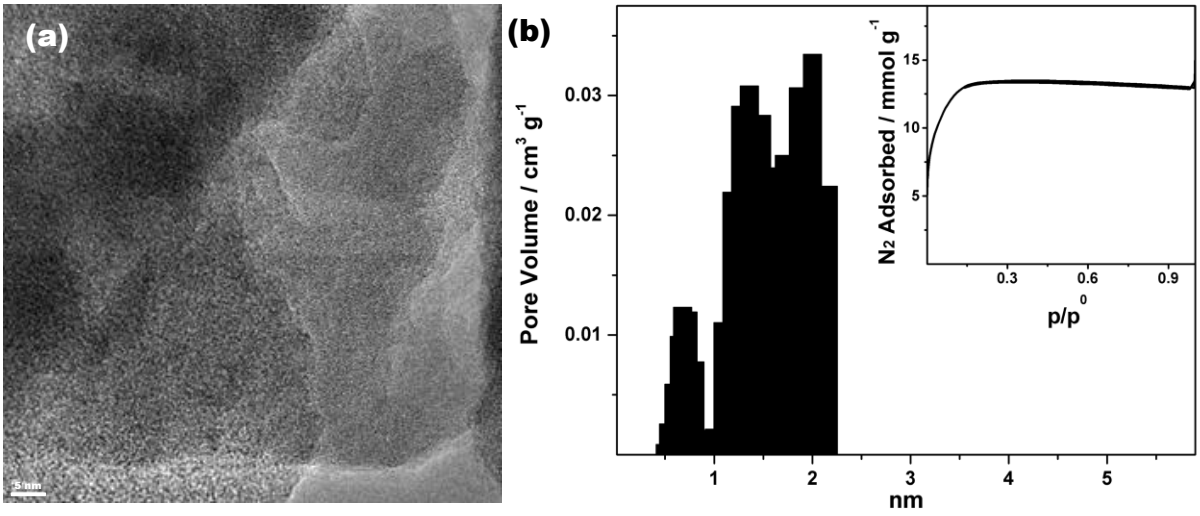

Figure 7: (a) TEM image of unsupported titania-silica membrane and (b) pore size distribution of the titania-silica membrane. (The pore size distribution of the membrane from the sorption isotherm in the insert by the DFT method).

The active layer composition and the thickness of the titania-silica active layer were determined by analyzing the cross-sectional view of the membrane using a focused ion beam scanning electron microscopes (FIB-SEM, Zeiss, EDX) at an accelerating voltage of 10 kV. Figure 8 represents the scanning electron microscope (SEM) cross-section image of titania-silica membrane, which shows a defect free microporous titania-silica layer deposited on the mesoporous NF γ-alumina interlayer. A thickness (Δx) of 1.87 μm was measured for titania-silica layer. EDX measurement showed that $\left(\frac{N_{Ti}}{N_{Ti}+N_{Si}}\right)$ = 5 ± 2 % which is close to our expectation.

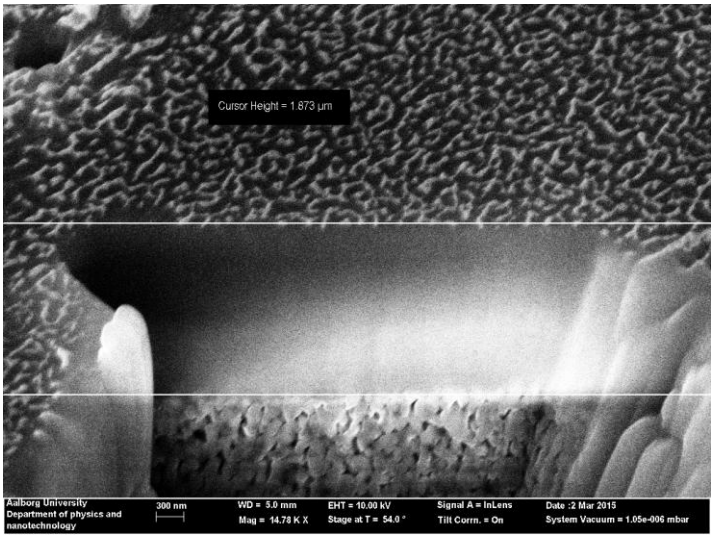

Figure 8. SEM cross-section image of the titania-silica layer deposited on the NF γ- alumina interlayer.

3. Materials and Methods

3.2 Filtration protocol

3.2.1 Setup

The experimental cross-flow filtration set-up is shown in Figure 9. A feed solution was pumped into the membrane by a feed pump (BEVI, IEC 34-1, Sweden) that was capable of providing pressures of up to 1.9 MPa. The mass flow of permeate was measured by a balance (Mettler Toledo, Mono Bloc series, Switzerland) connected to a computer. The feed pressure was measured before and after the membrane by two pressure transmitters (Danfoss, MBS 4010, Denmark), and an electronic heat sensor (Kamstrup A/S, Denmark) was used to measure the temperature in the feed entering the membrane module. The cross-flow stream was provided by a rotary lobe pump (Philipp Hilge Gmbh & Co, Novalobe, Germany) that was capable of generating a cross-flow of 2 L/min. The cross-flow rate was measured by a microprocessor-based flow rate transmitter (Siemens, MAG 50000). The retentate stream was controlled by a manual valve (Nupro ®).

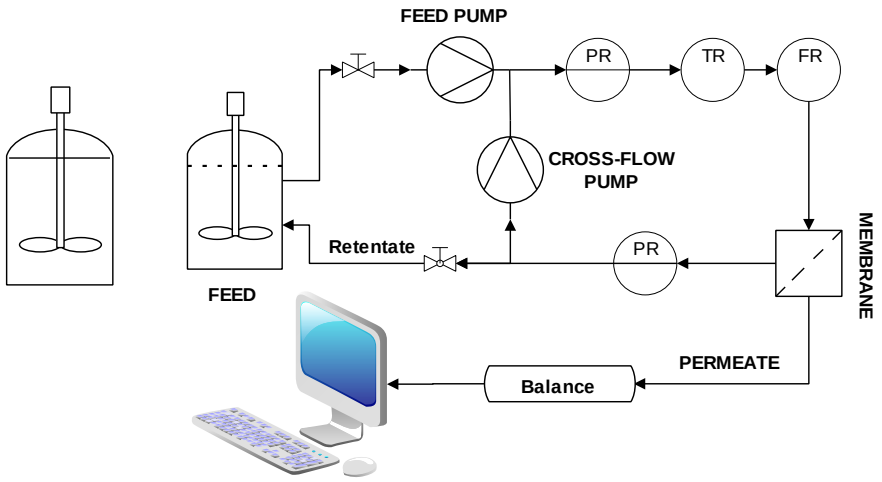

Figure 9. Experimental cross-flow filtration set up (TR, PR and FR are temperature, pressure and flow rate transmitters, respectively).

3.2.2 Electrolytes

De-ionized water (Milli-Q produced by Nanopure Dimond, 18.2 MΩ.cm) was used in all experiments besides NaCl, Na_2SO_4, $CaCl_2$, $CaSO_4$ and $MgCl_2$ in strength. The system was operated for 2 h to ensure that membrane surface was in equilibrium with solution and the system was at the steady state condition. During filtration, 10 samples were collected from each stream (feed, permeate and retentate) at various times to observe system changes during time. Filtration experiments were done at room temperature. The salt rejection was determined by measuring the conductivity of feed (σ_b) and permeate (σ_p). The salt concentration was assumed as a linear function of conductivity for dilute solutions (< 0.1 M) [85].

3. Materials and Methods

Performance of NF γ-alumina membrane was also tested in different pH. Filtration experiments were start from free-base solutions (pH ~ 5.5 for NaCl, pH~ 7.6 for Na_2SO_4 and $CaCl_2$, pH~ 8 for $CaSO_4$) and the pH increased steadily to pH = 11 where the NF γ-alumina is still stable at the room temperature [109]. Feed pH was changed using KOH (less than 1 mM in the feed) and measured by a digital pH meter (Radiometer PHM 92 Lab pH-meter).

3.2.3 Active layer permeability

The modified DSPM model focuses on the performance of the active layer; hence, it was important to eliminate the effect of membrane interlayer and support layer on the permeability and selectivity of membrane active layer. The active layer permeability was calculated using the resistance-in-series theory. Figure 10 represents the schematic of different resistances against the solvent flux. Resistance-in-series theory was used to determine the active layer resistance (R_{ac}) as follows:

$$R_{ac} = R_o - R_{int} - R_{sup} \quad (17)$$

where R_{sup}, R_{int} and R_{ac} are the support, interlayer layer and active layer resistances, respectively.

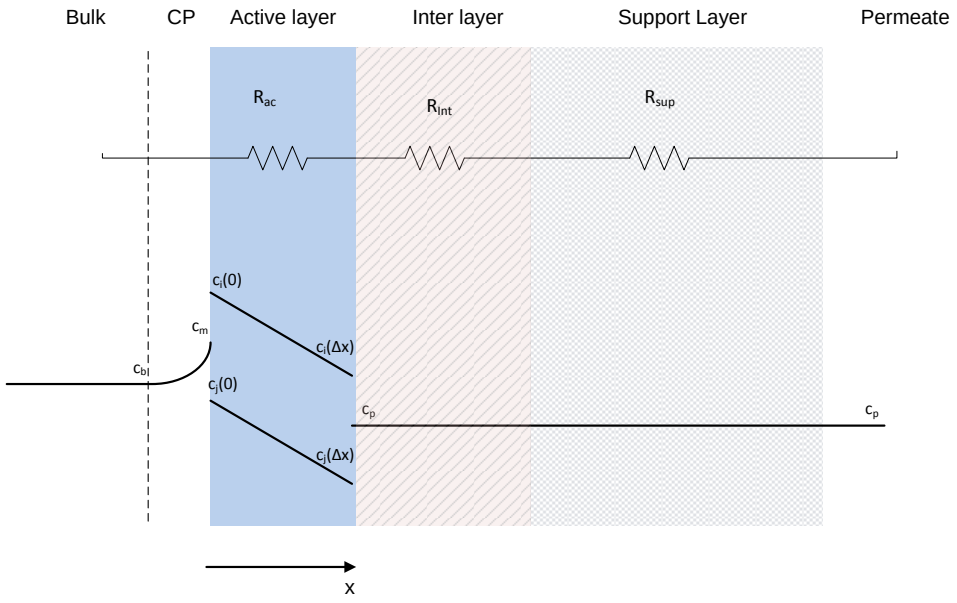

Figure 10: Schematic represents the different layer resistance against solvent flux and the ion concentration profile in different layers.

3. Materials and Methods

The overall resistance (R_o), support layer resistance (R_{sup}) and interlayer resistance (R_{int}) were calculated from Eqs. (18) - (20):

$$R_o = \frac{\Delta P_{\text{eff}}}{\eta_{\text{app}} J_{p,O}} (18)$$

$$R_{sup} = \frac{\Delta P_{\text{eff}}}{\eta_{\text{app}} J_{p,sup}} (19)$$

$$R_{int} = \frac{(J_{p,sup} - J_{p,O})\Delta P_{\text{eff}}}{\eta_{\text{app}} J_{p,O} J_{p,sup}} (20)$$

where $J_{p,o}$ and $J_{p,sup}$ are the measured permeate flux for the membrane and support, respectively. η_{app} is the viscosity in the membrane pore (i.e. electroviscosity), and ΔP_{eff} is the effective pressure driving force ($\Delta P - \Delta \pi$). The difference in osmotic pressure was calculated from the salt concentration in the feed and permeate. Due to concentration polarisation, the osmotic pressures were underestimated, but as argued in the text below, the effect of concentration polarisation was low in the performed experiments. Therefore, the active layer permeability ($L_{p,ac}$) and solvent flux ($J_{p,ac}$) could be calculated as follows:

$$J_{p,ac} = L_{p,ac}\Delta P_{\text{eff}} = \frac{\Delta \text{P}_{\text{eff}}}{\eta_{\text{app}} R_{ac}} (21)$$

3.2.4 Concentration polarization

The concentration polarisation (CP) refers to the rise of concentration gradients at the membrane/solution interface, as a result of ion retention under the effect of transmembrane driving forces. Due to the high cross-flow velocity that was applied in this study (u_{cf} > 20 m/s), the bulk flow was governed by the turbulent regime (Re >> 4,000). Eqs. (22)-(24) were used to calculate the mass transfer coefficient (k_d), the concentration modulus $\left(\frac{c_m}{c_b}\right)$ and the thickness of the CP layer (δ) [111]:

$$k_d = \frac{D}{d_h} Sh = \frac{D}{d_h} (0.04 Re^{0.75} Sc^{0.33}) (22)$$

$$\delta = \frac{D}{k_d} (23)$$

$$\frac{c_m}{c_b} = \left(\frac{\exp\left(\frac{J_p}{k}\right)}{R + (1 - R)\exp\left(\frac{J_p}{k}\right)} \right) (24)$$

where *Sh* and *Sc* are the Sherwood and Schmidt numbers, respectively. d_h is the hydraulic diameter, *D* is the diffusion coefficient of the salt [76,84], c_b is the bulk concentration, c_m is the concentration on the membrane surface and *R* is the salt rejection.

Figure 11 shows that the calculated concentration increased at the active layer surface as function of the active layer permeability and cross-flow velocity (u_{cf}). Figure 11 indicates that the concentration polarization modulus ($\frac{c_m}{c_b}$) was neglected for all of the studied active layers due to the high cross-flow velocity that was applied in this study (u_{cf} > 20 m/s). The thickness of the CP layer (δ) was less than 1 μm. In addition, the cross-flow velocity of 20 m/s is unrealistically high in real life situations (u_{cf} < 2 m/s) and CP can reduce the performance of the membrane. Influence of CP on UF membranes is more significant that NF membranes. As shown in Figure 11, CP can reduce more than 50% of UF titania selectivity in u_{cf} =2 m/s, while selectivity reduction due to CP is less than 15% for NF membranes in u_{cf} =2 m/s.

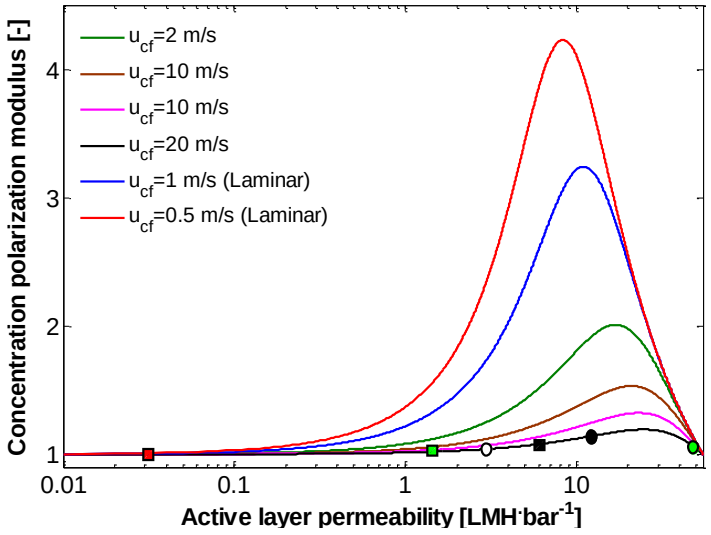

Figure 11: The concentration polarization modulus as function of active layer permeability and cross-flow velocity (u_{cf}) for MF α-alumina (green circle), UF titania (black circle), NF γ-alumina (black rectangle), NF titania (white circle), TiO_2-doped silica (green rectangle) and Hybsi/ organosilica (gray rectangle).

3.3 Analysis

3.3.1 ζ-potential

The ζ-potential was measured as a function of pH using a Zetasizer (Nano NS, Malvern, UK). The suspension was containing 20 ml de-ionized water in which the ionic strength was increased to 0.01 by adding salt. 20 mg of membrane particles (in this study, γ-alumina or TiO_2) doped silica was dispersed by ultrasonic treatment and remained totally 24 hours at room temperature to ensure that adsorption equilibrium has been reached. The particles used were identical to the particles used for coating the membranes.

3.3.2 Colloidal titration

Several techniques have been developed to determine the surface charge (δ_0) but due to large surface area of NF material, the different results might be obtained from various independent experimental techniques [111-114]. Mikkelsen [115] has developed a method to determine the surface charge density of suspended materials in the biological sludge which was recently used for charge density of organic macromolecules in manure [116]. The method was used here to determine the surface charge density of γ-alumina particles in the electrolyte solution. 20 mg γ-alumina particles were suspended into electrolyte (ionic strength 0.01 M), 0.1 µl of cationic/ anionic polymer was added stepwise by an auto-titrator (Malvern MPT-2) and the ζ-potential of the suspension was measured. The ζ-potential was plotted as a function of added cationic/anionic polymer (Figure 12) and the mass of added cationic polymer at ζ-potential = 0 was determined. The charge density of γ-alumina therefore was calculated using Eq. 25.

$$\sigma_0 = \frac{Fc_{ploy}v_{poly}\sigma_{0,poly}}{SSA\ v_{sample}\ c_{sample}} \quad (25)$$

Where c_{poly} is the mass concentration of cationic/anionic polymer, v_{poly} is the added volume of cationic/anionc polymer at ζ = 0, v_{sample} is the sample volume, c_{sample} is the electrolyte concentration of measured sample and $\sigma_{0,poly}$ is the surface charge of cationic/anionic polymer. In this study poly acrylic acid (Aldrich, MW~18 kDa and $\sigma_{0,poly}$ = 13.9 eq kg^{-1} [117]) was used as anionic polymer and poly diallyl dimethyl ammonium chloride (Aldrich, MW< 100 kDa and $\sigma_{0,poly}$=6.19 eq kg^{-1} [116]) was used as cationic one. Furthermore, sample pH was increased using KOH (less than 1 mM in the feed).

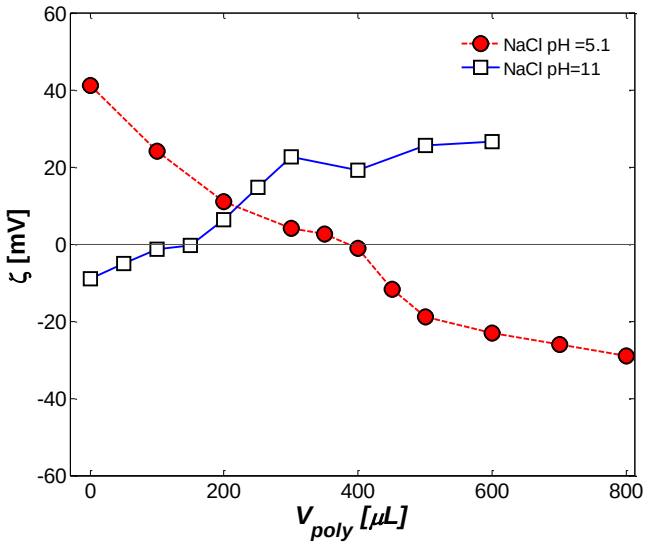

Figure 12: ζ-potential of γ-alumina vs. volume of the cationic/anionic polymer.

The volumetric charge density (X_d) at the liquid-solid interface was derived from the charge density in the diffuse layer (σ_d) as follows:

$$X_d = \frac{\alpha \sigma_d}{F r_p} \quad (25)$$

where α depends on the pore geometry, which is 2 for a cylindrical pore [118]. The Gouy–Chapman equation was used to determine the charge density in the diffuse layer (σ_d) as a function of the charge density profile in the electrical double layer (σ(y)) as follows:

$$\tanh\left(\frac{ze\sigma_d}{4kT}\right) = \frac{\tanh\left(\frac{ze\sigma(y)}{4kT}\right)}{\exp[-\kappa(y-d)]} \quad (27)$$

where y is distance from the stern layer. The diffuse layer starts at $y = d$ with an electrical potential equal to the ζ-potential and charge density σ_d. The potential and charge density at $y = 0$ were assumed to be the surface potential and surface charge density (σ_0), respectively. The Grahame equation can be used to calculate the charge density in the diffuse layer (σ_d) as a function of the ζ-potential:

$$\sigma_d = \left(8RT\varepsilon_p\varepsilon_0 c_b\right)^{\frac{1}{2}} \sinh\left(\frac{ze\zeta}{2kT}\right) (28)$$

3.3.3 Wastewater sample characterization

Samples of the effluent from the secondary wastewater treatment were collected from a municipal WWTP (250,000 PE, Aalborg West, Denmark, Figure 13) in sterilized 4 L glass bottles. All samples were immediately filtered by glass fiber filters (0.45 μm) to eliminate the suspended solids and subsequently stored at 4 °C to minimize changes in the constituents in the water. The Aalborg West WWTP effluent contained approximately 2.8 mg/l organic matters, 5 mg/l inorganic nitrogen compounds and it conductivity was measured to be 1120 μS/cm. Because sodium and chloride were the main inorganic ions in the water, we assumed it as a dilute NaCl solution (concentration below 0.1 M).

3. Materials and Methods

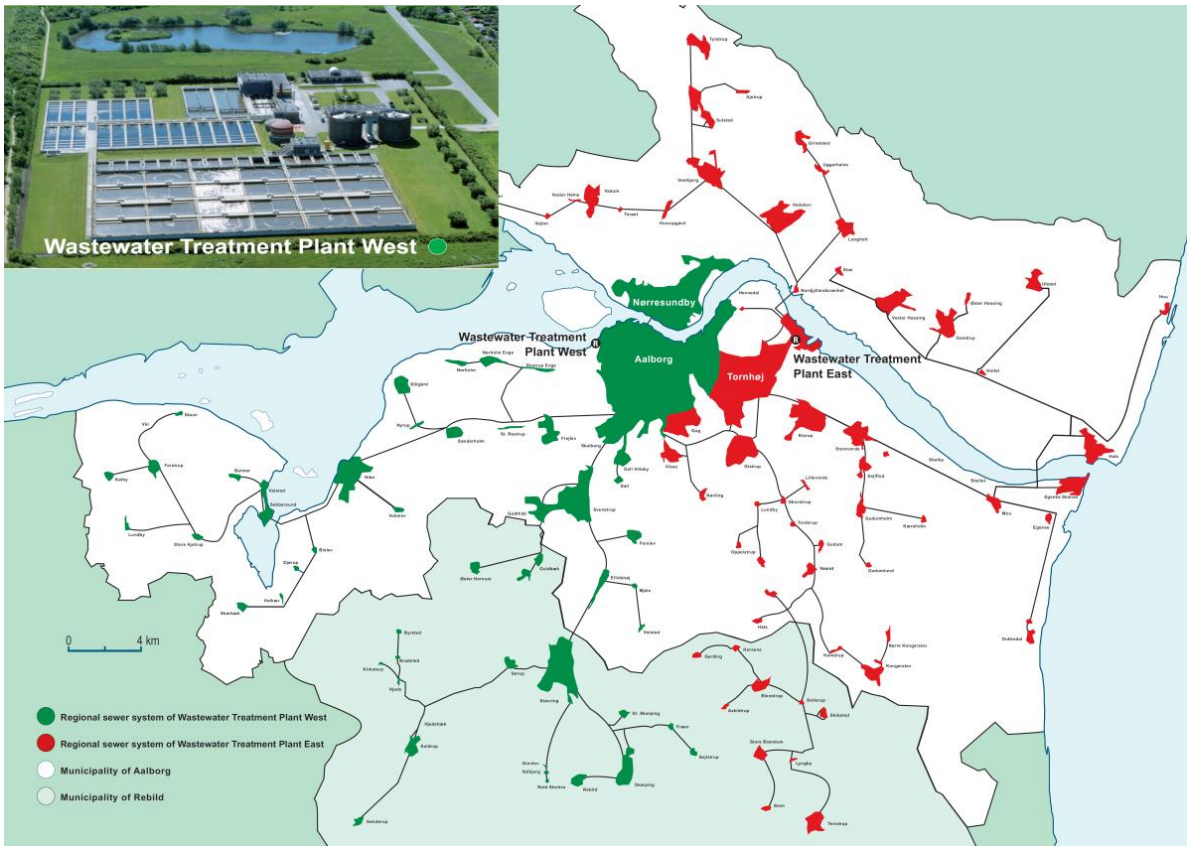

Figure13: Aalborg WWTP (plant west).

A UV–Vis spectrophotometer (Varian, Palo Alto, CA, USA) was used to calculate the retention of the UVAs at a wavelength of 254 nm and the color retention at a wavelength of 436 nm. The reduction of the conductivity was determined from the conductivity measurements (SevenMulti^{TM} S70-K benchtop, Switzerland) performed in both the feed and permeate streams. The ion concentration was assumed to be proportional to the conductivity due to the relatively low ion concentrations (<0.1 M). The concentrations of the $NH4^{+}$, NO_2^{-}, and NO_3^{-} species in the WWTP effluent and membrane permeate were determined colorimetrically according to standard methods for water and wastewater analysis using a nitrogen-autoanalyzer (Technicon TRAACS 800, Bran+Luebbe GmbH, Norderstedt, Germany). The concentration of the copper ions in the WWTP effluent and membrane permeate streams were determined using an atomic absorption spectrophotometer (AAS, Perkin Elmer, Analyst 100). Wastewater samples were spiked with additional copper (1 ± 0.1 mg L^{-1}) of Cu(I) or Cu(II) using CuCl and $CuSO_4$, respectively, to further investigate the abatement of these ions by membrane filtration.

Furthermore, the toxicity of the samples was measured by several bioassays. The acute and long-term toxicities of the WWTP effluent and NF γ-alumina membrane permeate to *Daphnia magna* were determined according to ISO 6341 [119] and ISO 10706 [120]. The acute toxicities of the WWTP effluent and NF γ-alumina membrane permeate to the luminescent bacterium *Aliivibrio fischeri* were determined as described in ISO 11348 [121]. The concentrations of the fecal

indicator bacteria *E. coli* and *Enterococci* in the WWTP effluent and NF γ-alumina membrane permeate were enumerated by a 96-well most probable number (MPN) method with a detection limit of 1 MPN per 100 mL [122]. A schematic of the process is shown in Figure 14.

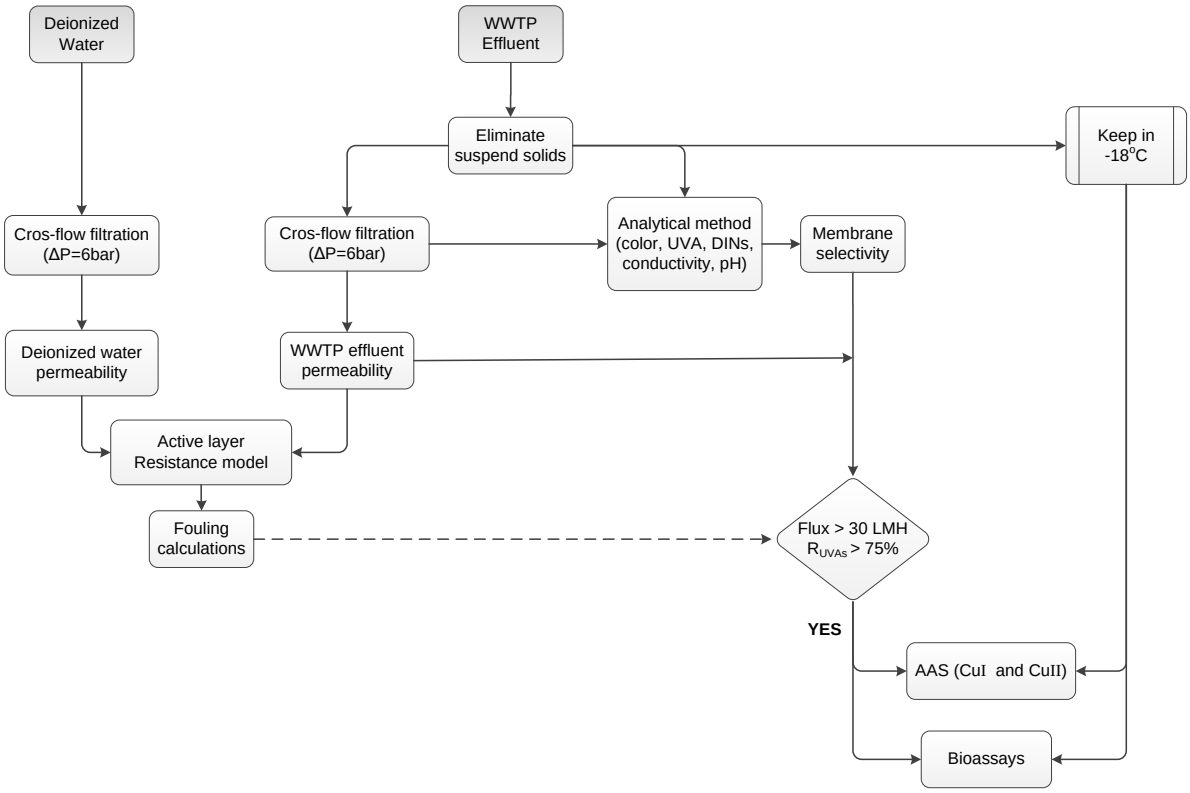

Figure 14. Schematic diagram of the process for recovery of effluent from wastewater treatment plant.

4. Model verification

4.1 Mass transport in mesoporous γ-alumina and microporous organosilica membranes

A DSPM model has been developed for simulating mass transport in inorganic NF membranes by incorporating the electroviscous effect. The electroviscosity is extended to pores smaller than 5 nm, and the permeate flux modeled by a modified Hagen–Poiseuille equation in which the electroviscosity are used instead of the bulk viscosity (electroviscous model). To verify the model, two different membranes have been used: mesoporous γ-alumina and microporous organosilica membranes. The permeate flux and salt rejection of these two membranes has been measured filtering NaCl and $MgCl_2$ solutions. The results compared with model predictions and with literature data [44].

As shown in Figure 3, the Hagen–Poiseuille model may overestimate the flux especially when κr_p <5. Experimental data support the model as Figure 15 shows the volumetric fluxes (J_p) for the NF γ-alumina membrane as a function of κr_p for NaCl (Figure 15a) and $MgCl_2$ (Figure 15b) solutions.

In order to show the importance of the electroviscous effect, simulation has been done using the electroviscous model. The flux behavior through γ-alumina membrane can be split into three cases:

1) The ionic strength in the pore (I_p) is very low (e.g. deionized water I_p < 0.01 mM), so, $\kappa r_p < 1$ and the double layers overlap in the pore. The viscosity in the pore is much higher than the bulk viscosity and its value depends on the absolute ζ-potential monotonically. As already expected from Figure 2, the unmodified Hagen–Poiseuille model overestimates the flux, while the electroviscous model shows good agreement with the experimental results;

2) The ionic strength is moderate (like 0.034 M NaCl and 0.021 M $MgCl_2$ as feeds), thus, $1< \kappa r_p < 5$ and the double layer is comparable with the pore radius and covers the pore partially. Although the viscosity in the pore is higher than the bulk viscosity, the unmodified Hagen–Poiseuille model can roughly predict it. The electroviscous model predicts the experimental results well.

3) The ionic strength is high (like 0.068 M NaCl and 0.042 M $MgCl_2$ as feeds), therefore $\kappa r_p > 5$ and electroviscous effect in the pore are negligible. The solvent flux in the pores is controlled mostly by bulk convection and the viscosity in the pore is equal to the bulk viscosity. Because of that, the unmodified Hagen–Poiseuille model, and the electroviscous model shows the same trend.

Figure 15 (c and d) presents the solvent flux for organosilica membrane at different pressures filtering a solutions of NaCl (Figure 15c) and $MgCl_2$ (Figure 15d). Although the Debye length is the same as for the NF γ-alumina membrane, the smaller pore radius of organosilica membrane caused diffuse layer overlapping (i.e. $\kappa r_p < 1$) at all salt concentrations, meaning that the solvent flux in the pore is controlled by the electroviscous effects for all conditions. However, as shown

4. Model verification

in Table 4, the absolute ζ-potential for organosilica is lower than for γ-alumina. Therefore, the viscosity in the pore is not far from the bulk viscosity and both the unmodified Hagen–Poiseuille and the electroviscous models show a close agreement with experimental data. Both the Hagen–Poiseuille and the electroviscous models show a flux decline with salt concentration, which is caused by the osmotic pressure.

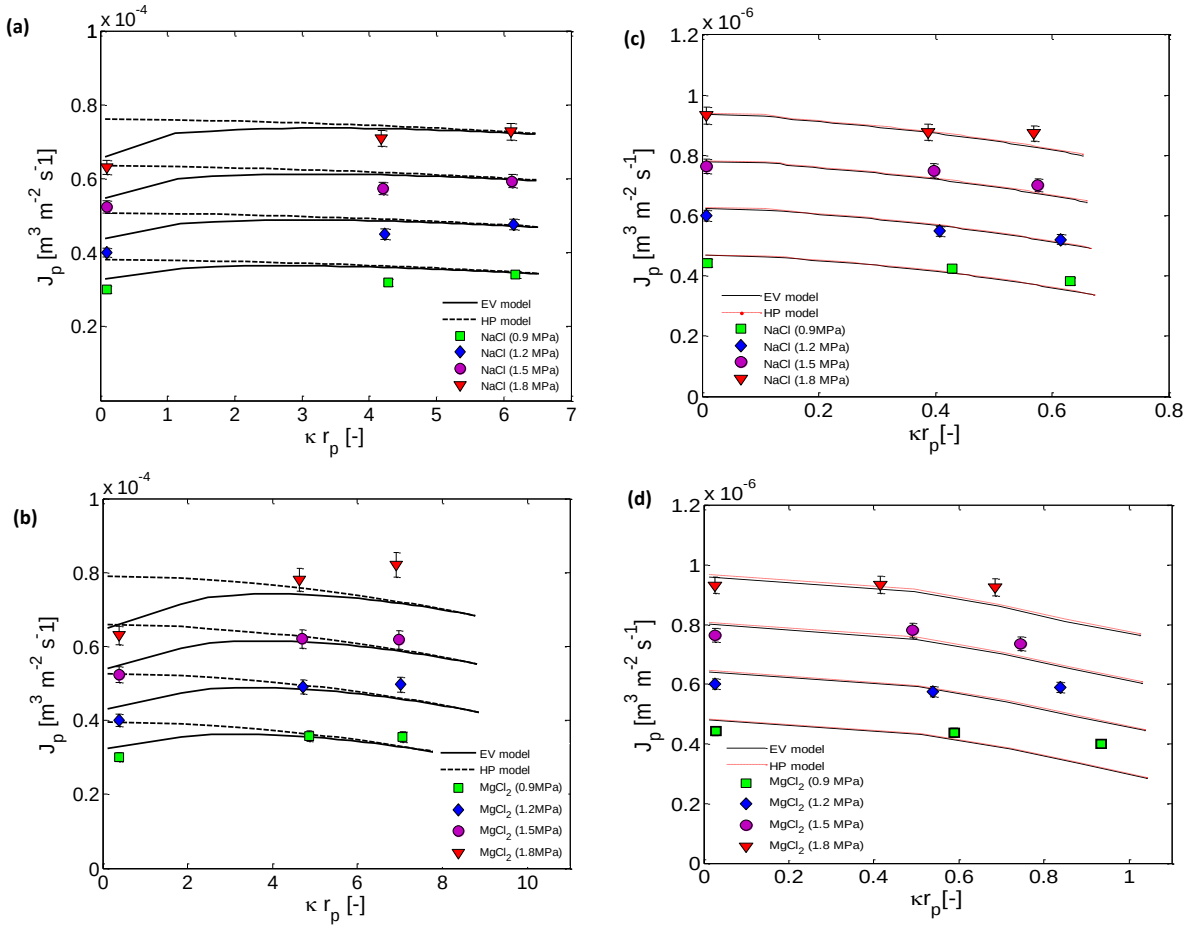

Figure 15: Solvent volumetric flux (J_p) versus dimensionless number (κr_p) in different applied pressures (ΔP= 0.9 ■, 1.2 ♦, 1.5 ●, 1.8 MPa▼) for γ-alumina (a) NaCl and (b) $MgCl_2$ and for organosilica (c) NaCl and (d) $MgCl_2$ in order to validate the electroviscous models model in this study (EV model, solid lines) and compare with the Hagen–Poiseuille model (HP model, dash lines).

Furthermore, the permeate flux is highly different for the two membranes. NF γ-alumina has larger pores and higher porosity than organosilica membrane; therefore the permeate flux of the organosilica membrane is approximately 70 times lower for deionized water and around 100 times lower for salt solutions than for the NF γ-alumina membrane.

Figure 16 shows experimental and simulated rejection curves as a function of effective applied pressure filtering different salt solutions. The rejection of $MgCl_2$ is higher than the rejection of NaCl because of the higher steric-partitioning coefficient (i.e. $\phi_i = (1-\lambda_i)^2$). Rejection of Mg^{2+} ions

(r_s=0.345 nm) is more pronounced that Na^+ ions (r_s=0.17 nm) in the boundaries (in both bulk and permeate sides) because of its larger hydrated ion radius (r_s) of Mg^{2+} ions [3,4]. Due to electroneutrality conditions the same occurs for their anions.

Figure 16 (a) shows that the electroviscous model fits experimental data fairly well. The largest error is around 5% and is observed for the $MgCl_2$ solution. This may be caused by ion adsorption in the pore, thereby changing the pore surface charge and to some extent reducing the pore radius. De Lint et al. [123] reported that Mg^{2+} ions are more strongly adsorbed on a γ-alumina surface than Na^+ ions. Deon et al. [92] employed an adjusted Freundlich adsorption isotherm and applied a profile for the surface charge X_d along the pore for taking into account adsorption phenomena.

The ion rejection and water flux can influence each other mutually because of the electroviscous term. Generally, ion rejection increases with solvent flux. This lowers the ionic strength in the pore resulting simultaneously larger Debye length and higher electroviscosity. The ion rejection increases slightly with permeate flux because the convection term becomes more important than the electromigration term (Eq. (1)). This opposite performance can be derived from the algorithm in Figure 14.

Figure 16 (b) shows the modeled and experimental rejections as a function of the effective applied pressure for the organosilica membrane in the presence of electrolyte solutions (i.e. NaCl and $MgCl_2$). It shows that the controlling terms for transport in the pore and at the interfaces behave similar to those for NF γ-alumina membrane. The rejection, caused by steric exclusion in the pore entrance, is higher for the organosilica top layer than for NF γ-alumina layer because of the smaller pore size of the organosilica membrane. The relative error between experimental and simulated rejections data is more pronounced for organosilica membrane than NF γ-alumina. There might be two reasons for this higher relative error, namely ignoring the intermediate layer (i.e. the γ-alumina layer) for the organosilica membrane and the sensitivity of the model to the pore size estimation.

4. Model verification

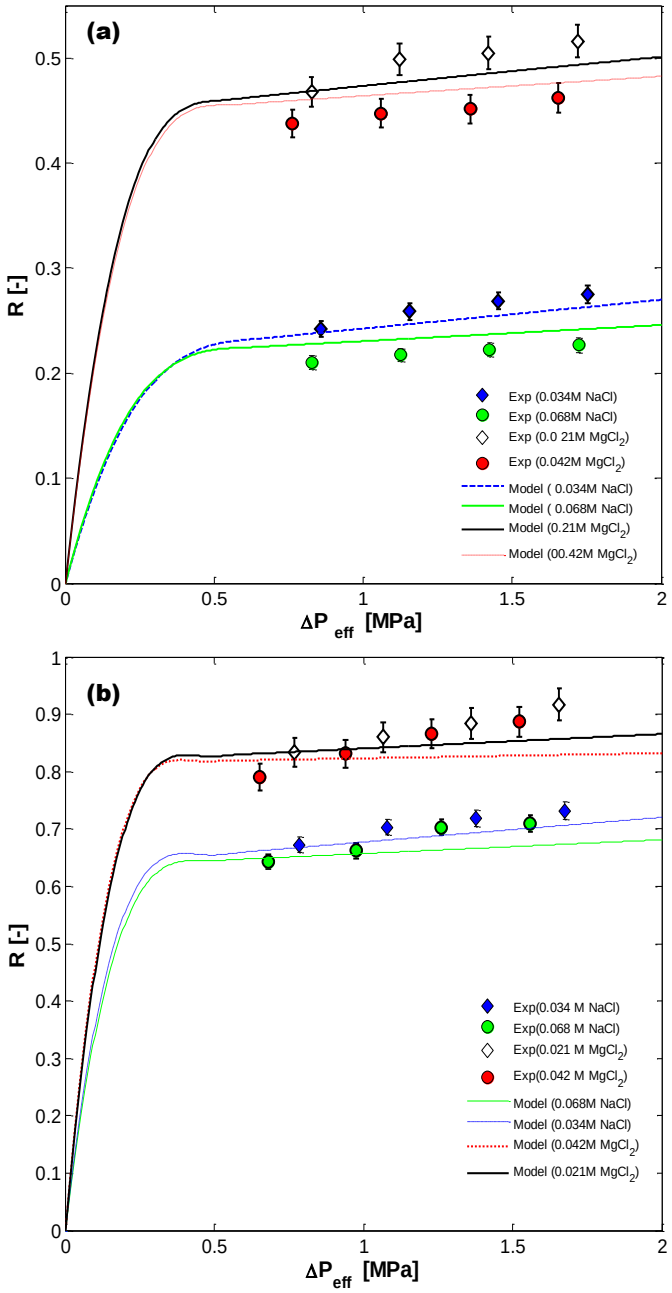

Figure 16: Rejection curves vs. effective applied pressure (ΔP_{eff}) for experimental result ♦: 0.034 M NaCl, ●: 0.068 M NaCl, ◊: 0.021 M $MgCl_2$ and ○: 0.042 M $MgCl_2$) and studied model for NaCl solutions (black dash line: 0.034 M and black solid lines: 0.068 M) and $MgCl_2$ solutions (gray solid line: 0.021 M and black dot line: 0.042 M) for the NF γ-alumina membrane (a) and organosilica (b).

Comparison of Figure 16 (a) and Figure 16 (b) confirms that salt rejection is much higher for the organosilica membrane than for the NF γ-alumina membrane, principally because of the lower pore size of the organosilica membrane. Compared to recent studies by Xu et al [44], the salt rejection by organosilica membrane in our study is lower (around 20% for NaCl and 8% for $MgCl_2$) because of its larger average pore size, though the permeability of our organosilica membrane is higher.

4. Model verification

4.2 Influence of pH on mass transport in mesoporous NF γ-alumina membrane

The NF γ-alumina active layer performance has been studied in a broad pH range (pH values from 5 to 11) for both monovalent (Na^+ and Cl^-) and divalent ions (Ca^{2+} and SO_4^{2-}). The NF γ-alumina membranes are stable in this pH range [109]. The ionic strength of 0.01 M is sufficiently low to permit the development of an electrical double layer in the nanopore (valid until the ionic strength exceeds 0.05 M) and sufficiently high to not be governed just by effective charge density (valid at ionic strength higher than 0.005 M). In contrast to polymeric membranes, the surface charge for inorganic NF membranes can be obtained from measurements unrelated to filtration experiments [123,124]. Therefore, the ζ-potential and surface charge density (σ_d) in the pores has been measured indirectly by measuring ζ-potential and surface charge density for the γ-alumina powder that has been used for the production of the membrane. Operational conditions, such as pressure, temperature and ionic strength, have been held constant, and the impact of the support layer on membrane resistance has been excluded using the resistance-in-series model. The ion rejection by the support layer is ignored due to the large pore size of the support layer (>100 nm). The electroviscous model has been used to simulate the membrane and active layer permeability. Finally, the salt rejection by the active layer has been simulated by using the DSPM model.

Figure 17 presents the ζ-potential as a function of pH for solutions (I = 0.01 M) of NaCl, Na_2SO_4, $CaCl_2$ and $CaSO_4$ and for deionised water (I < 0.1 mM) as a reference. The γ-alumina surface is charged due to the adsorption and desorption of protons, and ion adsorption. Further, the ionic strength lowers the absolute value of the ζ-potential due to electrical double layer reduction.

4. Model verification

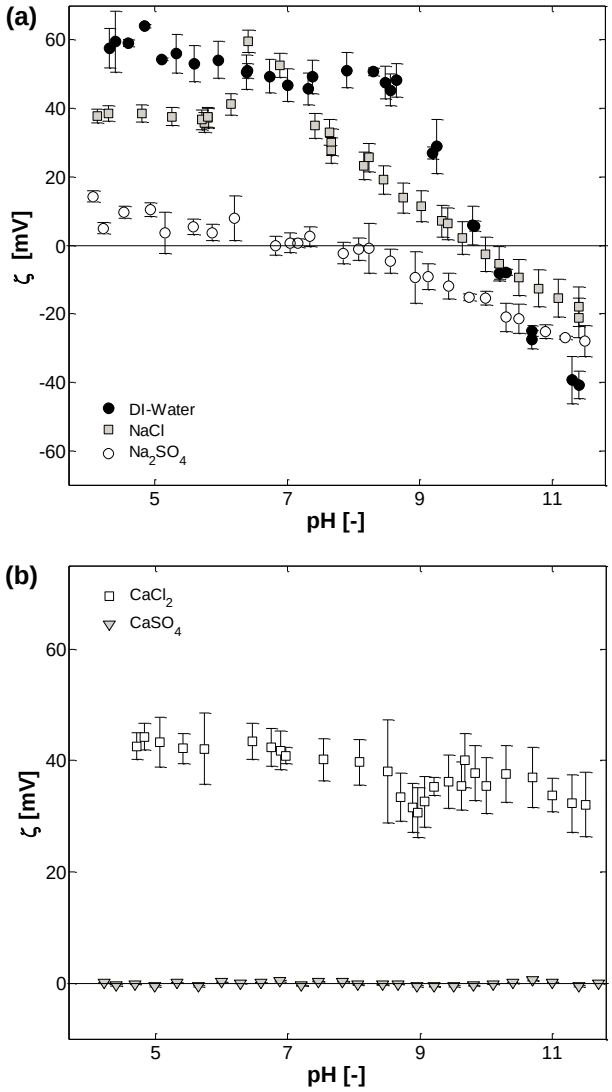

Figure 17: ζ-potential of γ-alumina vs. pH for (a) deionised water, 0.01 M ionic strength NaCl and Na_2SO_4 and (b) 0.01 M ionic strength $CaCl_2$ and $CaSO_4$.

The reference curve (black circles, Figure 17(a)) shows that the γ-alumina pore surface is positively charged at pH values below 9.8 (isoelectric point). The isoelectric point (IEP) of γ-alumina in the presence of deionised water depends on the γ-alumina synthesis method and calcination temperature and varies from pH values of between 7 and 10.Further, γ-alumina is highly charged ($\zeta \sim 60$ mV) below pH=5-6 [109]. The presence of NaCl (I = 0.01 M) lowered the ζ-potential but did not change the IEP (gray squares, Figure 17(a)). This result is not surprising because both Na^+ and Cl^- ions are rarely adsorbed on metal oxide surfaces [123]. Thus, the γ-alumina is still highly charged (ζ-potential ~ 40 mV) at pH 5. Figure 5(a) also shows that Na_2SO_4 (I = 0.01 M) changed both the IEP and absolute value of the ζ-potential. SO_4^{2-} ions are adsorbed on positively charged γ-alumina and reduce the ζ-potential from 60 mV to less than 20 mV and the IEP from pH 9.8 to pH 7.5. The trend of the ζ-potential is the same as NaCl at pH values above the IEP. Studies in the literature have [109,123] reported that SO_4^{2-} ions at

concentrations higher than 0.1 M lowers the IEP and could result in negatively charged γ-alumina above pH 5.

Figure 17 (b) shows that the γ-alumina surface is positively charged in the presence of $CaCl_2$. At pH values lower than 5, γ-alumina is positively charged, which prevents the specific adsorption of Ca^{2+} ions via electrostatic repulsion. Literature [124,125] have reported that the adsorption of Ca^{2+} ions on the γ-alumina surface increases with pH. Therefore, Ca^{2+} is expected to adsorb on the alumina surface and keep it positively charged at higher pH values. Ionic strength has a remarkable effect on the adsorption behavior of alkali earth divalent cations [109,124]. The positively charged γ-alumina above pH 5 is not observed for dilute solutions (ionic strength below 0.001 M) [110]. The absorption of both SO_4^{2-} and Ca^{2+} ions on the γ-alumina surface caused a non-charged γ-alumina surface in the pH range of 5-11 in the presence of the $CaSO_4$ system (Figure 17(b)).

The γ-alumina surface charge density (σ_0) is measured as a function of pH for different electrolytes by using colloidal titration. Figure 18 (a) shows σ_0 for the NaCl solution, which indicates that the γ-alumina IEP is approximately pH 9.5 in the presence of NaCl. This value is lower than the predicted ζ-potential, which could be due to variations in measurements or the presence of additional interacting groups at the γ-alumina surface in the colloidal titration method. The charge density in the diffuse layer (σ_d) has been calculated from the surface charge density (σ_0) using the Gouy-Chapman model (Eq. (27)) and modelled as a function of the ζ-potential using the Grahame model (Eq. (28)). Figure 18 (b) shows a fairly good agreement between the measured and modelled σ_d values determined for NaCl solution. The colloidal titration method can only be used for NaCl solutions due to the interaction between the polymer and divalent ions. Thus, for the ion transport model, the charge density in the diffuse layer (σ_d) for other ions has been calculated by using the Grahame equation (Eq. (28)).

4. Model verification

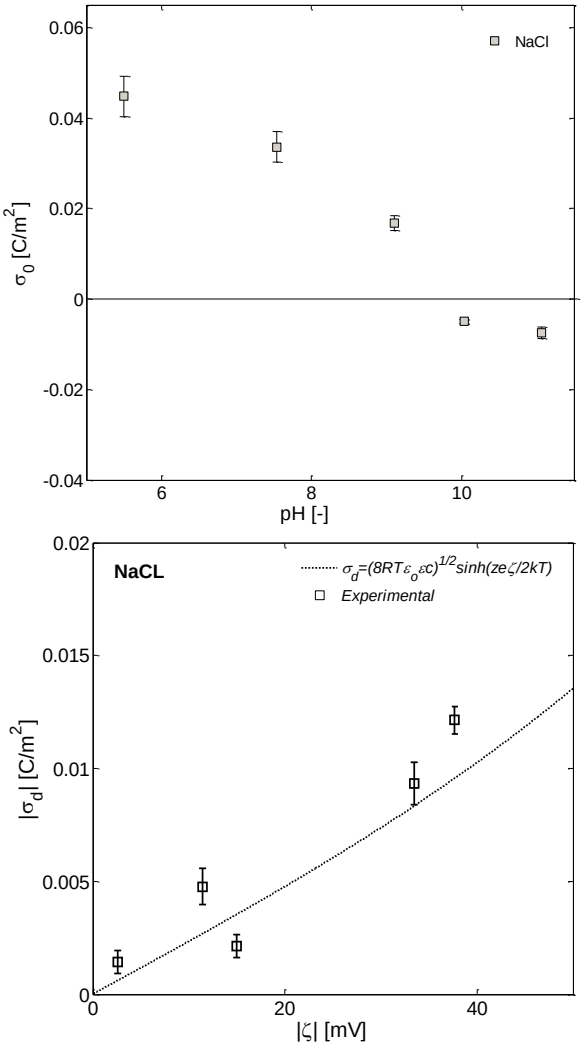

Figure 18: (Top) γ-alumina surface charge measured by the colloidal titration method vs. pH; (Bottom) charge density in the diffuse layer (σ_d) vs. |ζ| experimental (squares) and modelled using the Graham equation (line) for 0.01 M NaCl.

Figure 19 represents experimental and simulated data for both membrane and active layer permeabilities for filtration of NaCl, Na_2SO_4, $CaCl_2$, $CaSO_4$ solution and deionised water. The active layer permeability has been derived from the membrane permeability using the resistance-in-series theory (Eq. (18)). The results showed that the support layer resistance contributes with almost 10% of the total resistance. Figure 19 shows that the γ-alumina permeability is highest at the IEP. The model is in good agreement with the experimental results, considering that the relative error of the model is lower than 9%, with a maximum for the data taken at high ζ-potential.

4. Model verification

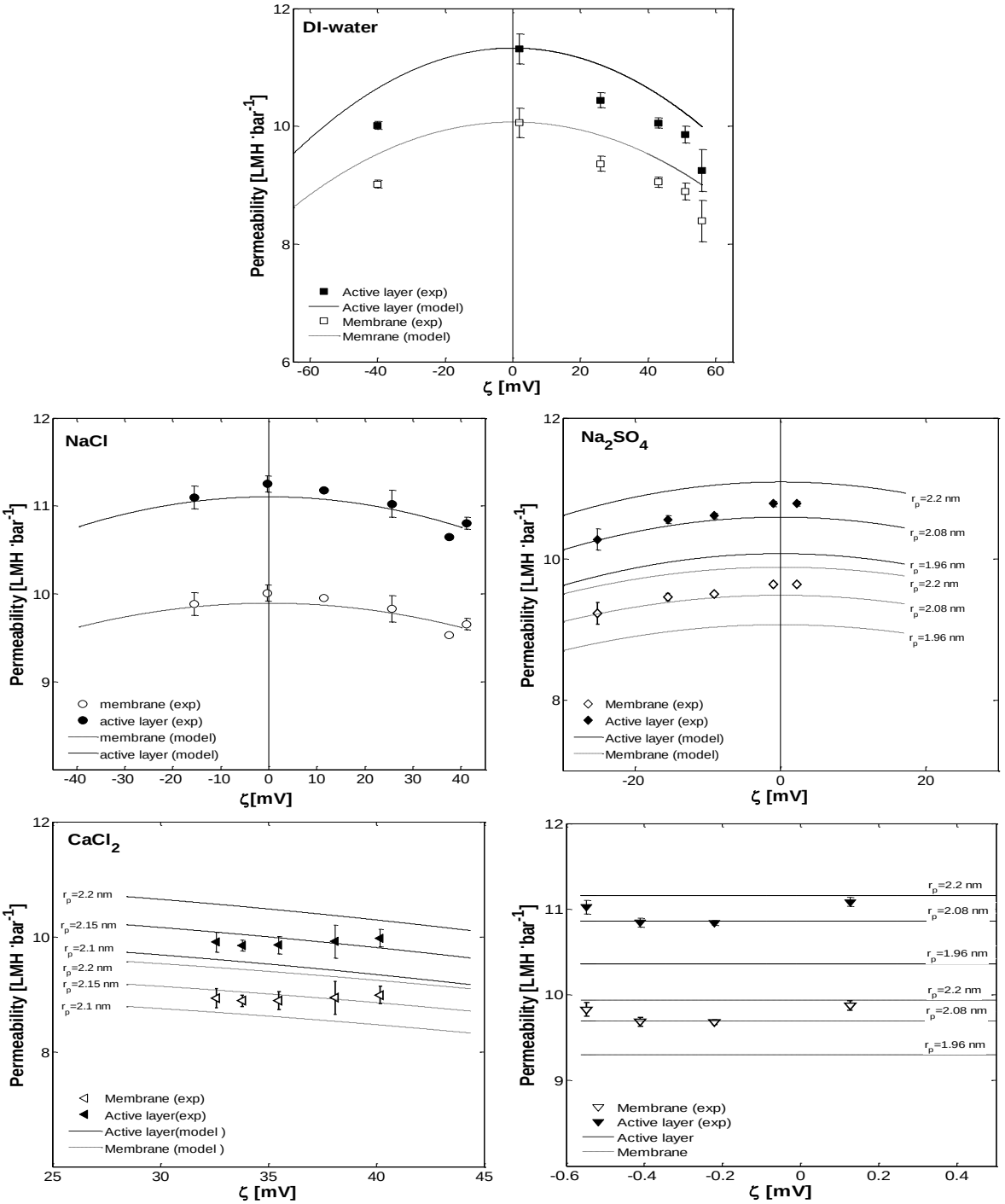

Figure 19: Membrane/active layer permeability vs. ζ for deionised water, NaCl, Na_2SO_4, $CaCl_2$ and $CaSO_4$.

At an ionic strength of 0.01 M (κ^{-1} = 0.87 nm), the electrical double layer covers approximately 40% of the NF γ-alumina pores; therefore, the electroviscous effect should be considered. Setting the pore radius r_p = 2.2 nm for the NF γ-alumina membrane, the model can describe the permeability of NaCl with a maximum relative error of 2%. On the contrary, the model overestimates the permeability of the NF γ-alumina membrane when using the other salt

solutions. Adsorption of SO_4^{2-} and Ca^{2+} ions on the γ-alumina surface might decrease the pore size and subsequently reduce the solvent flux through the membrane. Due to the complex ion adsorption mechanism, it is difficult to determine the amount of membrane pore reduction as results of ion adsorption. Our simulation allowed us to obtain the best fitting suggested by the decrease in membrane pore radius (r_p) to 2.08 nm and 2.15 nm for SO_4^{2-} and Ca^{2+} ions, respectively. These values correspond to a pore reduction, which is twofold smaller than the ionic radius of SO_4^{2-} and Ca^{2+}, which might be explained by asymmetric pore coverage [83]. The new pore size values have been considered for the rejection model.

According to Eq. (4), a combination of diffusion, convection and electromigration govern the ion transport through the NF pores. The charge in the diffuse layer and the solvent flux also influence equilibrium partitioning at the membrane/solution interfaces. Salt rejection is a function of both pore charge density and the ionic strength of the solution. Bowen et al. [3,4] shows that the salt rejection increases with the ratio of effective charge density to the feed concentration ($\chi = X_d/c_b$), because of dielectric interfacial exclusion. For a highly dilute solution (I < 5 mM), the effective charge density governs the rejection mechanism, although the charge effect is decreased by increasing the pore size (Eq. (25)). Hagmeyer and Gimbel [126] showed that for highly dilute solutions (I ~ 2 mM), the effective charge did not have a significantly effect on the rejection for membranes for r_p > 1.9 nm.

The effect of ζ-potential on salt rejection for membranes with different pore sizes has been modeled and presented in Figure 20 for 1:1 electrolytes (e.g., NaCl). The operational conditions, such as ionic strength, temperature and pressure, as well as membrane characterisation, such as porosity, thickness and tortuosity, are considered constant. Ion adsorption on the surface is neglected. For membranes with r_p > 3 nm, ζ-potential increases the rejection due to the higher surface charge, whereas the ζ-potential effect change for membranes with smaller pore sizes. The electroviscous effect is significant in smaller pores, which lowers the solvent flux (convection term) and subsequently the ion rejection. In other words, for membranes with r_p < 3 nm, the ζ-potential lowers the ion passage through the pore because of electrostatic repulsion. An absolute ζ-potential > 20 mV decreases the solvent flux simultaneously and subsequently decreases the rejection due to Eq. (4). The influence of the ζ-potential on membrane permeability is often ignored [3,76]. This assumption may be acceptable for low-charge membranes (e.g., polymeric membranes) or high-ionic-strength electrolytes, i.e., $\kappa^{-1} << r_p$. These opposite effects, ζ-potential increasing the electromigration term and decreasing the convection term, cause an optimum ζ-potential for rejection. The ζ-potential of optimum rejection decreases with increasing r_p and might depend on the nature of the ions and membrane.

4. Model verification

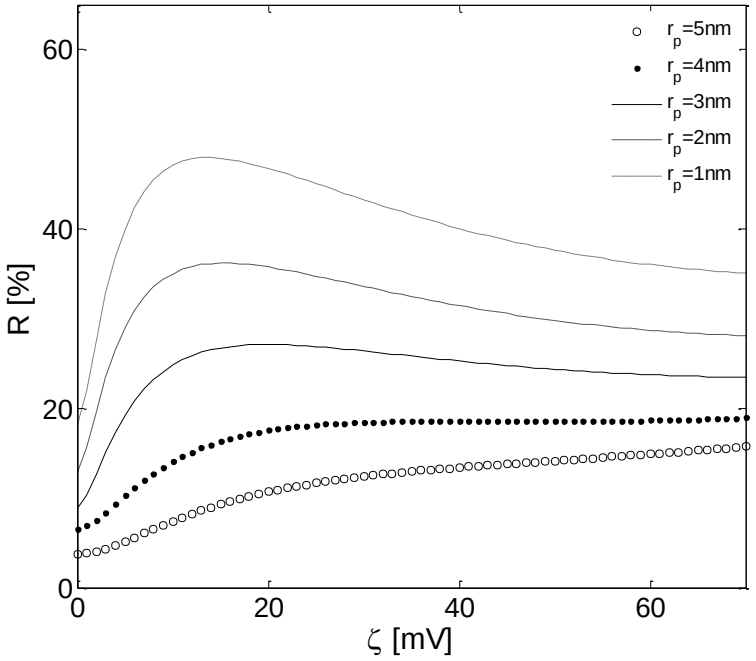

Figure 20: Rejection vs. ζ-potential in different pore ratios for 0.01 M NaCl.

Figure 21 presents salt rejection as a function of the absolute ζ-potential for NaCl, Na_2SO_4, $CaCl_2$ and $CaSO_4$ under a high operating pressure (10 bar). The DSPM was used to predict the rejection, in which the electroviscous model and pore shrinkage due to ion adsorption were considered (Figure 19). The model results for all electrolytes clearly show that the electromigration term governed the rejection solely in the low ζ-potential condition (ζ-potential < 20 mV), whereas the convention term (i.e., permeability) controls the rejection for the ζ-potential condition (ζ-potential > 20 mV). Figure 21 also shows a good agreement between the model and experimental results for high-ζ-potential conditions. The model exhibited errors of less than 10% at $|\zeta| > 20$ mV. The weakness of the model is clear at low ζ-potential. Such low ζ-potential might be caused by ion adsorption, especially for divalent ions (Ca^{2+} and SO_4^{2-}). Rejection because of ion adsorption is not considered in this work. Moreover, the KOH added to increase the pH might influence the membrane surface effect as well because it increases the ionic strength in the feed and change the membrane ζ-potential.

4. Model verification

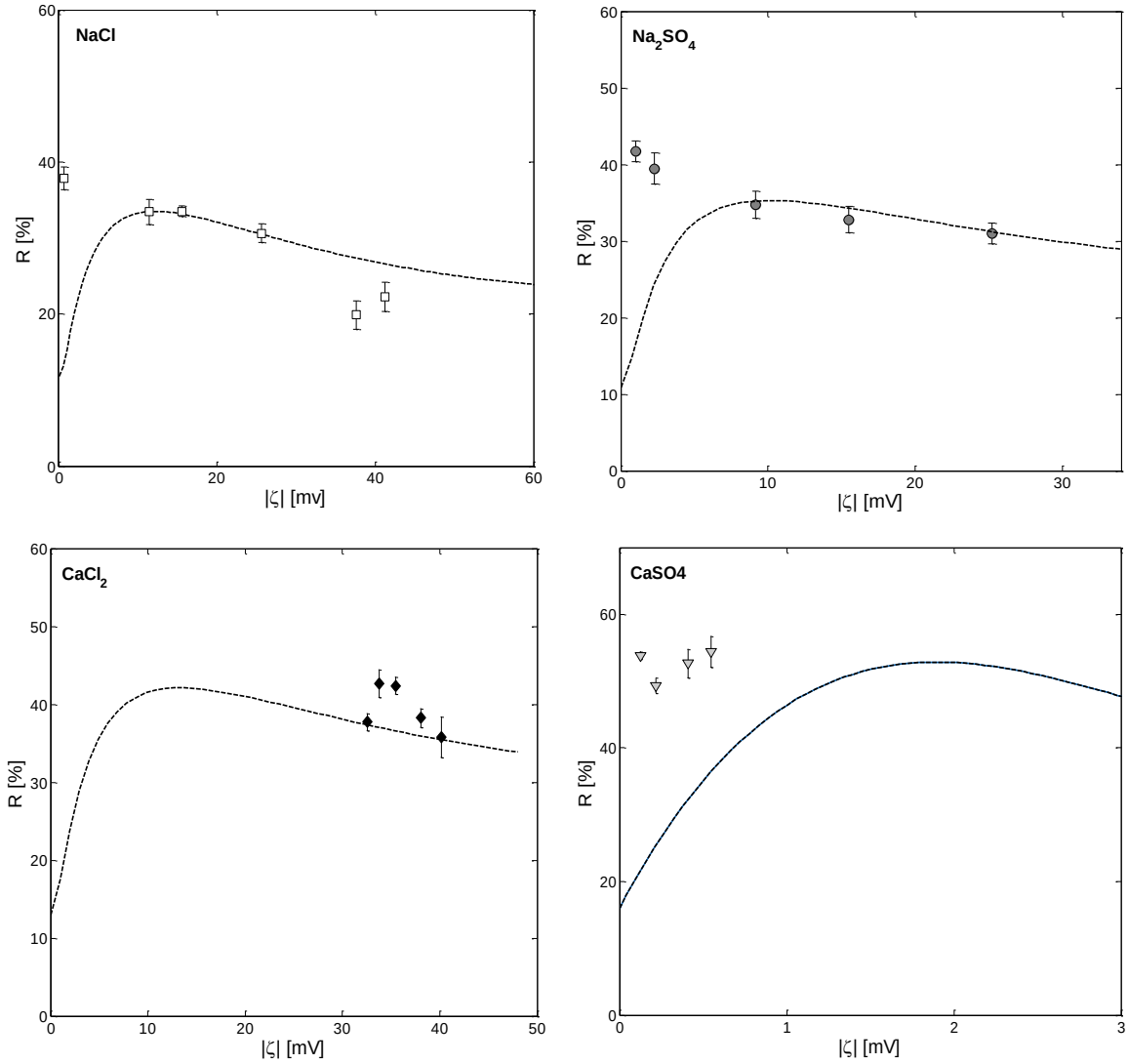

Figure 21: Salt rejection vs. absolute ζ-potential for NaCl, Na_2SO_4, $CaCl_2$ and $CaSO_4$.

5. Inorganic membranes for recovery of effluent from wastewater treatment plants

Different commercial inorganic membranes were studied to test their ability to remove toxic compounds, including aromatic components, humic-like substances, organic micro-pollutants, dissolved inorganic nitrogen compounds and heavy metal ions, from wastewater treatment plant (WWTP) effluent. Existing WWTPs remove organic materials and nutrients (i.e., nitrogen and phosphorus) from the wastewater. However, WWTP effluents often contain toxic compounds, such as organic micropollutants (OMPs), dissolved inorganic nitrogen compounds (DINs) and heavy metal ions [127-130]. OMPs can accumulate in aquatic organisms and adversely affect their growth and reproduction even though their concentrations are typically in the milligram/nanogram per liter range or lower [130]. Based on their functions, the OMPs have been comprised of pharmaceuticals and personal care products, steroid hormones, endocrine-disrupting compounds, surfactants, flame retardants, pesticides, synthetic fragrances, industrial additives, and many other emerging compounds [131,132]. The amounts of these contaminants that have been found in the environment have been increasing, and their extremely low concentrations, as well as their bio-persistence and bio-accumulation, have rendered their measurement and subsequent treatment difficult. Luo et al. [129] provided a comprehensive review of the occurrence data of OMPs in WWTP effluent from recent studies.

DINs exist in fairly high concentrations (typically >5 mg N/L) and in various chemical forms, including ammonium (NH_4^+), nitrate (NO_3^-), and nitrite (NO_2^-) [133,134]. The DINs in WWTP effluent can stimulate bacterial and phytoplankton growth in the receiving waters [135,136]. The DINs can also associate to increase the concentration of hydrogen ions in freshwater ecosystems, resulting in the acidification of the systems and thus inducing the occurrence of toxic algae, which can reach toxic levels that impair the abilities of the aquatic animals to survive, grow and reproduce. Ingested nitrites and nitrates can also be harmful for human health and the economy [137]. Most of the heavy metals in wastewater, such as copper, nickel, chromium, zinc and silver, are harmful and resistant to biodegradation, and they have a propensity for bioaccumulation in living organisms, causing serious health problems [138-140]. Therefore, WWTP effluent must be treated before it is discharged.

Certain advanced physical, chemical, and biological technologies and methods have been investigated to assess their effectiveness for reducing the toxicity of WWTP effluents. These technologies and methods include coagulation-flocculation [141], advanced oxidation processes [142-144], precipitation [145], sorption [146], membrane bioreactor [147], ion exchange [148], sand filtration and activated carbon adsorption [149]. Among these methods, membrane processes, and particularly pressure-driven membrane processes, are promising because no heating or chemical additives are required [150-153]. Previous studies [154,155] have shown that the costs involved in operation of membrane systems in the recovery of WWTP effluents were competitive with conventional treatment processes, such as chlorine and ozone processes [155-157]. In this section, the possibility of using inorganic membrane for the recovery of WWTP effluents is studied. Five inorganic membranes with different pore sizes and different materials were tested. Table 4 lists the support and interlayer structures, the active layer

compositions and the commercial uses for each membrane. These membranes covered a broad range of applications, ranging from MF to NF. MF and UF membranes were expected to have pore sizes that were not sufficiently small for the retention of OMPs and that would render them unsuitable for this application; however, these membranes have been used as supports for the NF membranes and were thus included in this study. The membrane permeabilities and the retention of the colors, UV_{254}-absorbing components (UVAs), conductivities, and DINs were determined for all membranes. There was a correlation between the abatement of various OMPs and the corresponding losses in the UVAs [158-160], as well as between the removal of the total ions and the decrease in the conductivities. The color measurements that were obtained through a spectrophotometric method were a useful index of the dissolved humic-like substances in water [132,158]. Additionally, Wert et al. [132] proposed the reduction of color as a potential method to assess the removal of pharmaceuticals.

The membranes that provided more than 30 L m^{-2} h^{-1} (LMH) of uncolored permeate flux and a 75% retention of UVAs were selected for further investigation. The removal of the toxic compounds and the indicator bacteria by the optimum membrane were investigated using two bioassays that targeted the inhibition of *Daphnia magna* and *Aliivibrio fischeri* and that quantified the indicator bacteria *E.coli* and *Enterococci*.

5.1 Membrane permeability

Figure 22 summarizes the deionised water and WWTP effluent permeabilities as functions of the nominal pore size. The WWTP effluent permeabilities were lower than the deionized water permeabilities for all membranes, with a permeability reduction of 50% for the MF α-alumina membrane, 44% for the UF titania membrane, 47% for the NF γ-alumina membrane, 69% for the NF titania membrane, and 41% for the Hybsi membrane. The decrease in the membrane permeabilities in the WWTP effluent was mainly attributed to the higher viscosities and membrane fouling.

5. Inorganic membranes for recovery of effluent from wastewater treatment plants

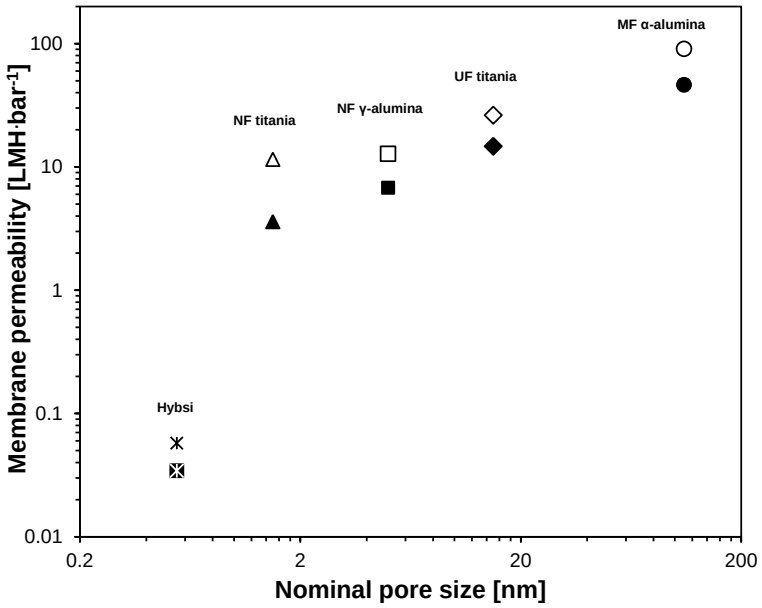

Figure 22: Deionized water (open symbols) and WWTP effluent (filed symbols) permeability of different inorganic membranes (TMP= 6 bar).

To calculate the membrane permeabilities, the osmotic pressure was included in the effective pressure term (ΔP_{eff}) calculating the osmotic pressure by using the Van't Hoff equation. The osmotic pressure of the inorganic ions was less than 5% of the operational pressure (ΔP) and was negligible for the organic and inorganic nitrogen components (<<5 kPa) due to their low concentrations (<< 100 mg/L) and high molecular weights [161]. As expected from Eq. (8), the membrane permeabilities decreased with nominal pore size of the active layer. Interestingly, the NF γ-alumina and NF titania membranes possessed approximately the same permeabilities for the deionized water even though they possessed nominal pore sizes of 5 and 2 nm, respectively. This similarity in permeabilities was mainly attributed to the thickness and tortuosity of the NF γ-alumina active layer. The thickness, porosity and tortuosity of the studied active layers are reported in Table 4. Additionally, according to Eq. 9 and the presence of deionized water ($\kappa^{-1} > r_{\text{p}}$), the electroviscous effect lowered the overall permeability for the NF γ-alumina ($\frac{\eta_{\text{app}}}{\eta_{\text{b}}} = 1.12$), whereas it was negligible for the NF titania membrane ($\frac{\eta_{\text{app}}}{\eta_{\text{b}}} \sim 1$). Sekulic et al. [100] also reported that the NF titania membrane had a higher water permeability compared to the γ-alumina membrane.

The permeability decreased dramatically from the NF titania membrane to the Hybsi membrane (Figure 22). The water permeability of the Hybsi membrane was approximately 200 times less than that of the NF γ-alumina membrane. This result was not surprising considering that the Hybsi active layer consisted of a rather dense material. Water transport through such small pores was hindered by the strong interactions between the water molecules and pore walls, which prevented any practical application in the purification of water.

5.2 Fouling resistance

The active layer resistance for each membrane was calculated using Eqs. (17)-(19). The active layer resistances (R_{ac}) reflected the properties of the active layer and the presence of foulants. The fouling resistance (R_f) can be calculated as follows:

$$R_f = R_{ac,e} - R_{ac,w} \quad (29)$$

where $R_{ac,e}$ and $R_{ac,w}$ were the experimentally determined active layer resistances in the presence of de-ionized water and WWTP effluent, respectively.

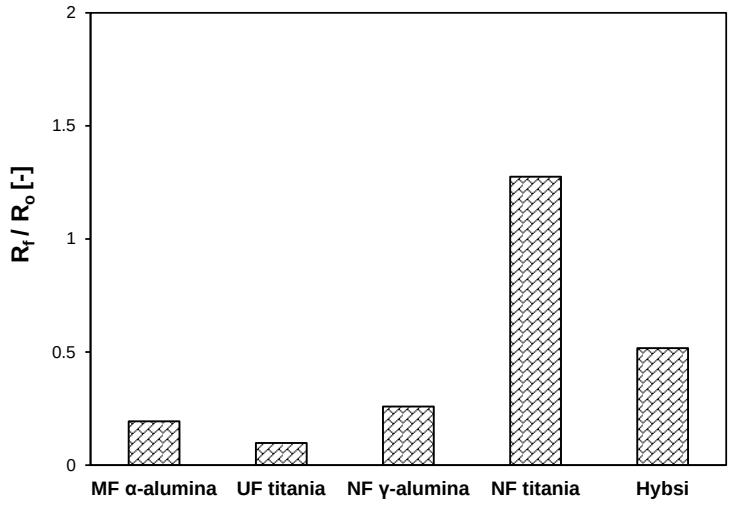

Figure 23. The fouling resistance for different active layers.

Figure 23 represents the ratio of the fouling resistance (R_f) to the membrane resistance in the presence of deionized water (R_o) for the different active layers. The fouling resistance for the MF α-alumina and UF titania was fairly low compared to the membrane resistance of itself, which could be attributed to the pore size and fairly low retention of the organic components. The fouling resistance for the NF titania active layer was greater than the membrane resistance, whereas the fouling resistance for the NF γ-alumina active layer was four-fold lower than its membrane resistance. Due to the equal organic and ion retention for both membranes, the lower fouling resistance for the NF γ-alumina active layer might be explained by the larger ζ-potential. However, the fouling resistance mechanism was also dependent on the feed combination, which was not an objective of the current study.

5.3 Membrane selectivity

Figure 24 represents the membrane selectivities as functions of the membrane permeabilities for different components. Figure 24 (a) shows the UVAs and conductivity rejection as functions of the membrane permeability. As previous studies have reported [158-160], the UVAs mainly consist of aromatic and olefinic compounds. In the absence of suspended solids, the retention of UVAs can yield an estimation of the total organic carbon retention from the WWTP complex mixture. Additionally, the reduction of the conductivity can be used to calculate the total ion rejection. Figure 5 (a) shows that the MF α-alumina membrane (highest permeability) did not reject ions and rejected only 13% of the UVAs. Therefore, the MF α-alumina membrane was not suitable for WWTP effluent recovery. The UF titania, NF γ-alumina and NF titania membranes removed nearly 60%, 75% and 80% of the UVAs, respectively. The conductivities were reduced by 15% when the NF γ-alumina and NF titania membranes were utilized and by 7% when the UF titania membrane was utilized, whereas the amorphous Hybsi membrane possessed a nearly complete rejection of the UVAs and dissolved ions. These results were not surprising considering that the humic-like substances and MOPs typically possess a broad size distribution (6–<1.2 kDa) [162], which explained the continuously increasing rejection of the UVAs when the membranes with lower pore sizes were utilized. In contrast, most of the hydrated ions possessed sizes below 1 nm and were only be retained by the small pores of the Hybsi membrane. The pH values of the WWTP effluent feed and filtration permeate were consistent with these results. The pH of the permeate increased from 7.8 to 8.6 with the decrease in the membrane pore size: WWTP effluent < MF α-alumina < UF titania< NF γ-alumina ~ NF titania. This can be explained by considering that the acidic humic-like substances were rejected by the membrane, whereas the alkaline earth metal ions remained in the permeate.

5. Inorganic membranes for recovery of effluent from wastewater treatment plants

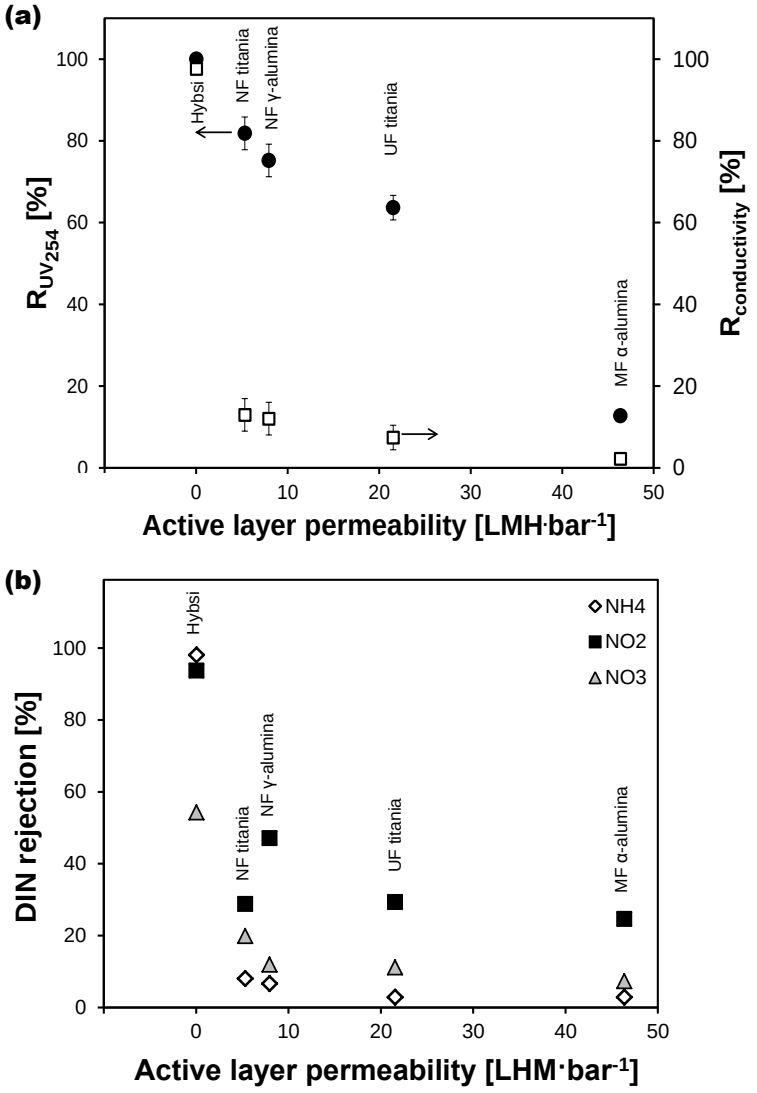

Figure 24: Membrane selectivity vs. active layer permeability: (a) UVAs rejection (circles) and conductivity rejection (squares); (b) DINs rejection.

Figure 24(b) shows the data for the rejection of DINs, ammonium ions (NH_4^+), nitrite ions (NO_2^-) and nitrate ions (NO_3^-) as functions of the membrane overall permeability. Only the Hybsi membrane retained greater than 98% of NH_4^+ components; the retention was less than 10% for the other membranes. Figure 24 (b) also demonstrates that the NO_3^- retention was increased through the utilization of membranes with smaller pore sizes, but a rejection greater than 60% was not obtained, even by the Hybsi membrane. These low rejection rates could be explained by the fact that the solute radii of the DINs was between 0.11 and 0.33 nm, which may make their treatment difficult [134]. Lee and Lueptow [134] showed that a polyamide RO membrane rejected approximately 50%, 85%, 90% and 93% of the urea, sodium nitrite, sodium nitrate and ammonium chloride, respectively. Interestingly, the NF γ-alumina membrane (r_p=2.2

nm) rejected approximately 50% of the NO_2^- compounds, which was nearly 2-fold larger than the rejection rate of the NF titania (r_p=1 nm) membrane. This may be attributed to the adsorption of the nitrite ions onto/into the surface of the membrane. Ma et al. [163] postulated that at room temperature, the water-solvated surface nitrite could be adsorbed by γ-alumina and may be converted to nitrate. The nitrate compounds were also found to be adsorbed on the γ-alumina.

5.4 Membrane selection

Comparison of the membrane selectivities (Figure 24) for the different components and the membrane permeabilities (Figure 22) were considered to select the optimum membrane for the WWTP effluent recovery. Figure 25 schematically represents the selection criteria: a membrane permeate flux lower than 30 LMH was considered as a low-permeability zone, and a retention of the UVAs lower than 75% was considered as a low-selectivity zone. Moreover, the selectivities of other components and the resistance of the membrane to fouling were also considered. The permeate flux of the Hybsi membrane was not sufficiently high (<< 1 LMH) to be considered as a possible solution for the removal of OMPs and toxic compounds from the WWTP effluent even though its selectivity was high. In contrast, the MF α-alumina and UF titania membranes were classified as low-selectivity membranes even though their permeate fluxes were high. As noted above, their permeabilities and selectivities were measured to determine how they affected the system as NF support membranes, as well as in the screening of the WWTP effluent recovery in a wide range of filtration applications.

Figure 25 also shows that although the selectivity value of the NF γ-alumina membrane was comparable to that of the NF titania membrane, its permeate flux was approximately two times higher than that of the NF titania membrane. Both membranes fully removed the color. The NF titania membrane can also be placed in the low-permeability zone for this application. Moreover, the greater fouling resistance of the NF titania membrane may lead to future problems with long-term filtration. Therefore, the bacterial removal, toxicity testing, and specified toxic ion rejection were investigated in detail for the permeate of the NF γ-alumina membrane because this membrane was considered to be the most promising membrane for effluent treatment.

5. Inorganic membranes for recovery of effluent from wastewater treatment plants

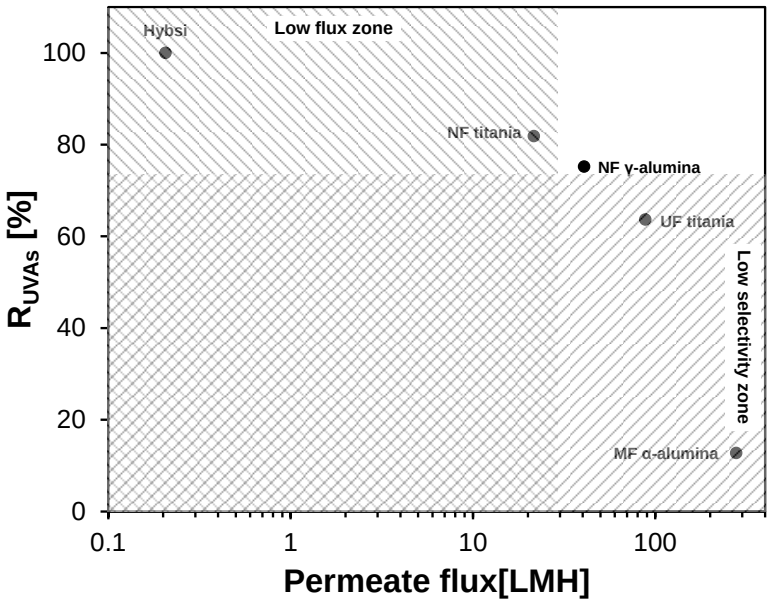

Figure 25: Schematic representation of optimum inorganic membrane for WWTP effluent recovery.

The concentration of a specific toxic ion, copper, was reduced by the NF γ-alumina membrane. The results of these filtration tests are presented in Figure 26. The NF γ-alumina membrane rejected approximately 40% of the CuCl (Cu (I)) and 25% of the $CuSO_4$ (Cu (II)) during the cross filtration of the spiked WWTP effluent whose copper concentration was set at approximately 1±0.1 mg L^{-1}. These results were consistent with results of Chapter 4 and Paper I, which demonstrated that the NF γ-alumina membrane removed approximately 20% of the NaCl and 40% of the $MgCl_2$ from the dilute electrolyte at the same operational conditions.

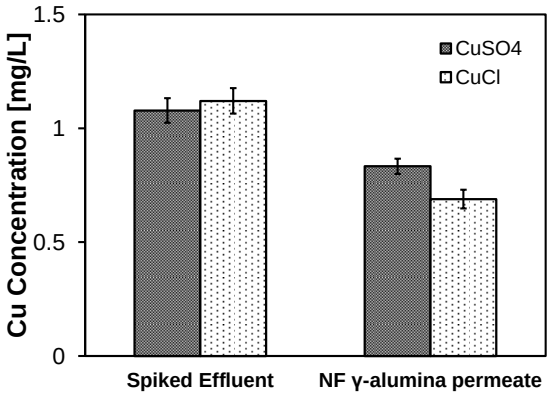

Figure 26: Concentration of toxic Cu in $CuSO_4$ and CuCl spiked WWTP effluent and after NF γ-alumina membrane treatment.

5. Inorganic membranes for recovery of effluent from wastewater treatment plants

The NF γ-alumina membrane dramatically reduced the concentrations of *E. coli* and the intestinal *Enterococci* in the permeate (Figure 27). The reduction in the MPN concentration was comparable with the removal efficiencies of 97.3% and 98.5% for *E. coli* and *Enterococci*, respectively. The removal of the fecal indicator bacteria from the WWTP effluent was relevant because these bacteria are now the guiding parameters in the testing of recreational water quality in many countries [164]. Therefore, the filtration of the WWTP effluent may have contributed to the attenuation of the indicator bacteria concentrations and subsequent compliance with bathing water directives.

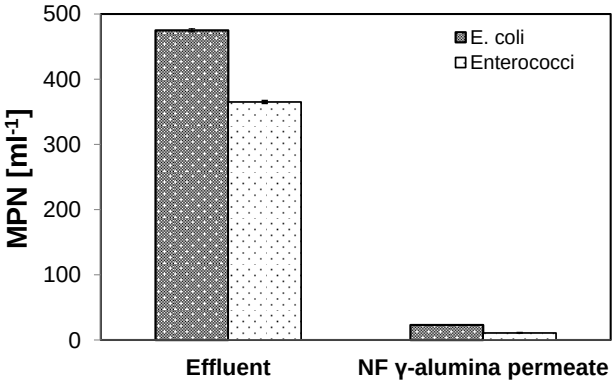

Figure 27: Concentration of E. coli and enterococci in the WWTP effluent and NF γ-alumina permeate.

The toxicity testing of the NF γ-alumina permeate generally showed no apparent acute toxicity to the test organism *D. magna* (Figure 28(a)). Collectively, the results for the *D. magna* and *A. fischeri* organisms suggested EC_{50} values above 50% (v/v), which indicated a low acute toxicity of the NF γ-alumina membrane permeate (Figure 28). The NF γ-alumina membrane treatment was also capable of reducing the toxicity of the WWTP effluent with elevated concentrations of toxic ions (Figure 28(b)). In this case, CuCl was added to the WWTP effluent prior to the NF γ-alumina membrane treatment to increase the background toxicity. The reduction of the toxicity due to the NF γ-alumina membrane treatment increased with the increasing wastewater concentrations, and a maximum reduction of 47-58% was obtained. This attenuation of toxicity was in the same range as the 40% reduction in the CuCl concentration observed in Figure 26.

5. Inorganic membranes for recovery of effluent from wastewater treatment plants

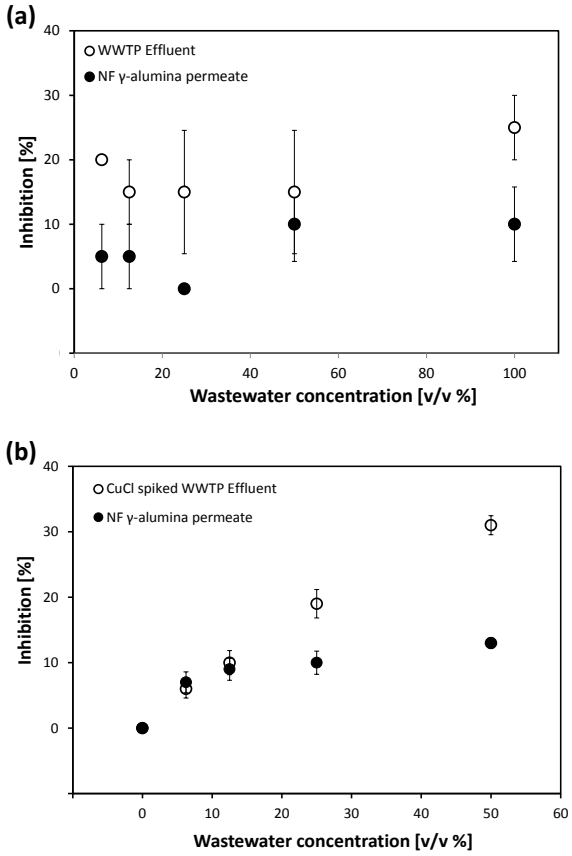

Figure 28: Acute toxicity to D. magna of WWTP effluent and NF γ-alumina permeate (a), and acute toxicity to A. fischeri of CuCl spiked WWTP effluent and NF γ-alumina permeate (b).

The long-term incubation of *A. fischeri* for 3-7 h resulted in a detectable inhibition, but the effect was lower than what was observed for the non-recovered WWTP effluent (Figure 29). The WWTP effluent inhibited *A. fischeri* by 28-38%, whereas the NF γ-alumina membrane reduced the inhibition of *A. fischeri* by 20-35% (Figure 29). These results supported the observations that the toxicity of the effluent was reduced during the NF γ-alumina membrane treatment.

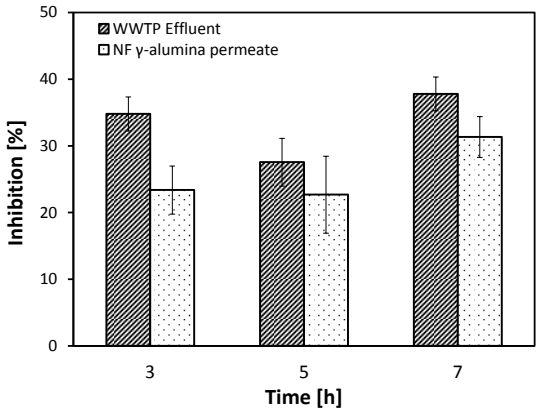

Figure 29: Inhibition of A. fischeri after 3, 5and 7 hours of exposure to WWTP effluent and NF γ-alumina permeate.

6. Designing new materials for nanoporous inorganic membranes for water desalination

As human population increases, water supplies become more limited and water scarcity is a serious global issue. In this context, there is a high demand for energy-efficient technologies for the desalination of seawater and brackish water. In particular, pressure-driven membrane processes provide relatively efficient and convenient means for achieving water desalination [165]. Since the hydrated monovalent and divalent ions have relatively small size (less than 1 nm), pressure-driven membrane technology for water desalination is limited to RO and NF membranes. Both polymeric RO and NF membrane often suffers from polymer swelling, biofouling, scaling and poor thermal and chemical resistance [52-49], which limit their operation time. In reason of that, nanoporous inorganic membranes have been recently proposed as a possible alternative for water desalination [52-49]. Table 5 reports literature results for nanoporous inorganic membranes in water desalination. Among these membranes, MFI-type zeolite (silicalite) membranes showed good salt retention at low applied pressure (4-7 bar). However, they present also low permeability (L_p < 0.1 LMH·bar^{-1}) due to their small pore size and high membrane thickness (2-3 μm). Amorphous silica membrane structure has also been modified by inserting covalent organic bridges into the SiO_2 network. Pore size and thus perm-selectivity of these membranes can be tuned by adjusting the length of these organic bridges [44]. Xu et al. [44] have reported a L_p ~ 0.115 LMH bar^{-1} with R_{NaCl} > 89% for organosilica membrane (l ~ 0.2 μm) in ΔP = 7 bar. Organosilica membranes are typically thinner than zeolite membranes, but they are also denser and have a lower pore fraction, thus they also show low water permeability. Zirconia, titania, and alumina membranes have larger pore size and thus show larger water permeability, but also show low NaCl rejection (R_{NaCl} 52%). By comparing these results with those in Table 2, it is possible that inorganic porous membranes still present lower salt reject compare to polymeric membranes with similar water permeability. It should be stressed that the results in Table 5 were often obtained in strict laboratory condition for dilute NaCl solution (< 0.035M), at low applied pressure (4 < ΔP < 10 bar), and nearly neutral pH (5-7) [52-49].

6. Designing new materials for nanoporous inorganic membranes for water desalination

Table 5: Performance of inorganic NF membranes for water desalination.

Membrane	Top layer	d_p [nm]	l [μm]	ΔP [bar]	T [^oC]	pH	c_{NaCl} [M]	L_p [LMH·bar^{-1}]	R_{NaCl} [%]
MFI Zeolite	Silicalite[42]	0.55	9.8	10	25	7.6	N/A	0.04	47
	Silicalite[43]	0.5-0.6	2	7	25		0.1	0.05	72
	ZSM-5 Si/Al=65[43]	0.5-0.6	2	7	25		0.1	0.02	84
	ZSM-5 Si/Al=50[43]	0.5-0.6	2	7	25		0.1	0.005	88
Organosilica	BTESE_100[44]	0.5	0.2	7	25		0.03	0.11	89
	BTESE_300[44]	0.5	0.2	7	25		0.03	0.06	96
	BTESE[This study]	0.55	0.2	9	25	6-7	0.034	0.18	65
Titania	TiO_2[45]	2	0.1	5		6 -7	0.01	20	10-15
	TiO_2[46]	0.55-2	0.05	6		6-7	0.01	20	38
	TiO_2[47]	4	0.5	7	30	6.2	0.01	8	30
Zirconia	ZrO_2-400[48]	1.8	N/A	6	25	6	0.01	0.3	20
	ZrO_2-350[48]	0.94	N/A	6	25	6	0.01	0.2	22
Alumina	γ-alumina[49]	3.4	N/A	6	25	5.5-6	0.001	2	52
	γ-alumina[34]	8.7	4	6	25	5.5-6	0.001	11	40
	γ-alumina[This study]	4.4	1.2	9	25	5.5-6	0.034	10-12	20

6.1 Potential of nanoporous inorganic membranes in water desalination

The DSPM model was used to investigate the potential of nanoporous inorganic membranes in water desalination, also in comparison with commercial polymeric RO or NF membranes. Figure 30(a) shows the simulation of NaCl rejection (R_{NaCl}) by nanoporous membranes with 0.5 nm < d_p <8 nm and 0 < |ζ| < 50 mV. The bulk feed concentration and applied pressure were considered 10 mM (NaCl ~ 0.6% wt) and 6 bar, respectively. In this concentration, the osmotic pressure differences ($\Delta\pi$) is less than 0.3 bar. The hydration diameters (d_s) of Na^+ and Cl^- were considered 0.37 and 0.24 nm, respectively [3]. As obvious, ion rejection increases by decreasing the pore size, due to steric exclusion at the membrane/solution interfaces. This effect is more evident for non-charged membranes (ζ=0). The ζ-potential increases the volume charge density and electroviscous effect in the pore, simultaneously. The volume charge density increases the ion rejection because of both interfacial exclusion and electromigration (caused by electrical potential gradient); while the electroviscous effect decreases the ion rejection in result of flux

decline. These opposite effects, namely ζ-potential increasing the electromigration term and decreasing the convection term, cause an optimum ζ-potential for salt rejection, which is indicated by R_{max} in Figure 30(a). This maximum is evident for nanoporous membranes with d_p < 6nm. The ζ-potential of optimum rejection decreases with increasing d_p and also depends on the nature of the ions. According to Figure 30(a), R_{NaCl} >85% can be obtained solely by nanoporous membranes with d_p of 0.5 nm or smaller and $|\zeta|$ > 10mV. Rejection of divalent ions, Mg^{2+} (d_s=0.69 nm [3]), Ca^{2+} (d_s=0.62 nm [166]) and SO_4^{2-} (d_s=0.46 nm [3]) is expected to be higher than both Na^+ and Cl^- because of their size. These results are in agreement with reported results for commercial NF membranes (Table 2), which are usually composites of polymer layers with molecular weight cut-off between 200-400 Da, i.e. 0.5 < d_p <1.5 nm. At a ΔP=4.8-7 bar, commercial polymeric NF can remove more than 50% NaCl and 85- 97% divalent salts like $MgSO_4$ and $CaCl_2$, $CaSO_4$.

Figure 30(b) shows the simulation of NaCl rejection and membrane permeability for porous membrane with 0.5 nm < d_p <10nm and 0 < $|\zeta|$ < 60 mV. The membrane thickness (l) was considered to be 1 μm. Effect of membrane thickness on membrane permeability was shown by a black line for 0.2 μm < l < 2 μm. It is worth to mention that depositing and calcining a defect-free nanoporous layer with l < 0.2 μm on a porous carrier is technically challenging with commonly used methods in membrane preparation, like slip casting, tape casting, and dip coating [51]. In this simulation, membrane porosity (ε) was considered 0.5 and we have assumed that the membrane tortuosity (τ) was equal to 3 for all active layers, similar to values reported in the literature [167,168]. Figure 30(b) indicates that membrane permeability increases with pore size and decreases with the ζ-potential. This is consistent with literature data reported in Table 5. For instance, silicalite membranes showed a low NaCl (47-72%) rejection mainly because of low ζ-potential (~ 5 mV at pH=6-7), but Li et al. [42] has increased the ζ-potential of silicalite membrane by increasing the ratio of Si/Al ($|\zeta|$ > 50mV) achieving approximately 90% of NaCl rejection for a membrane with L_p of 0.005 $LMH{\cdot}bar^{-1}$.

In general, the values reported in Figure 30(b) have a good correspondence with the data in Table 5, despite the difference in membrane composition. Figure 30(b) indicates that porous membranes with d > 2nm are not capable to remove more than 45% of NaCl, thus achieving the performances of commercial polymeric NF membranes in applied trans-membrane pressure between 4 and 7 bar (Table 5). Indeed, excluding a few papers [169,170], which have been conducted on unconventional conditions, mesoporous oxide membranes, such as γ-alumina, titania and zirconia with d_p > 2nm, can remove organic molecules, but are not able to remove more than 40% NaCl. Our model also shows that theoretically inorganic porous membranes with pore size of 0.5 nm (e.g. zeolite and organosilica) can achieve the same perm-selectivity of dense polymeric RO membrane for water desalination unless membrane thickness would be technically reduced to be less than 50 nm which is hard to obtain with the current technology. On the other hand, Figure 30(b) suggests that in order to design an inorganic porous membrane to be comparable with commercial polymeric NF membrane, i.e. R_{NaCl} > 50%, the membrane should have a pore size between 1 and 2 nm. In this pore size range, the optimum absolute ζ-potential is between 5 to 20 mV. L_p > 1 $LMH{\cdot}bar^{-1}$ can be obtained with a layer with thickness of 1-2 μm while deposition of a thin layer (e.g. 200 nm) can provide a great L_p > 10 $LMH{\cdot}bar^{-1}$.

6. Designing new materials for nanoporous inorganic membranes for water desalination

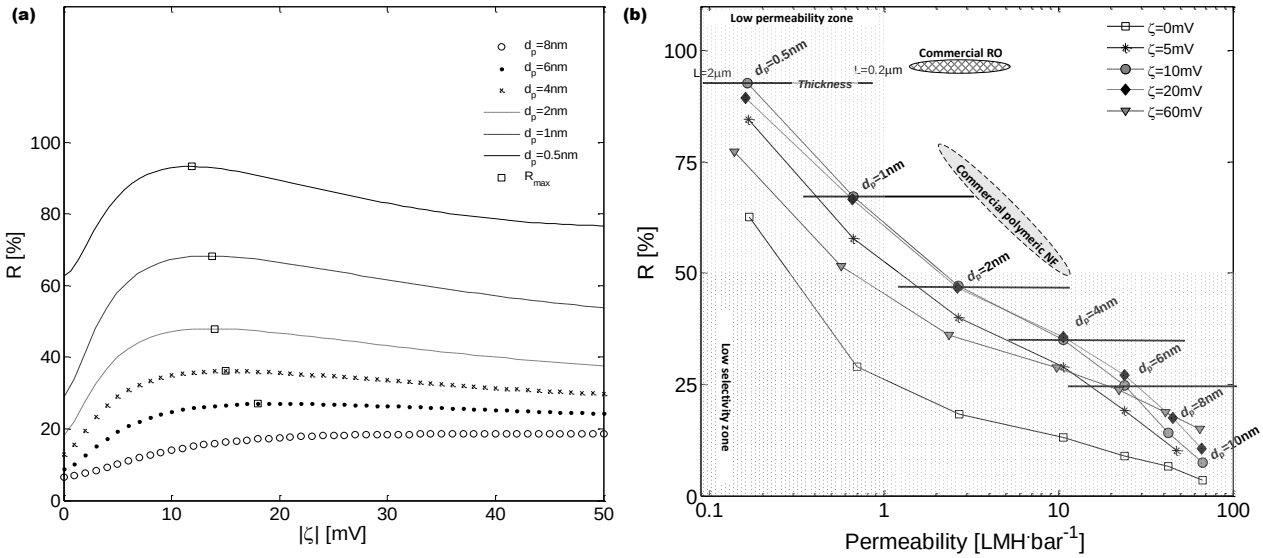

Figure 30: (a) Simulation of NaCl rejection (R) of porous membranes vs. ζ-potential for different pore sizes (d_p); (b) Permeability and NaCl rejection of porous membrane in different pore size and ζ-potential (ΔP = 6 bar, c_{NaCl} = 0.01M, ε = 0.5, τ = 3, l =1μm, T = 25°C, black lines show the effect of membrane thickness on permeability between 2μm and 0.2μm).

6.2 TiO_2 doped silica membrane for water desalination

In this chapter we investigate the potential of a new inorganic NF membrane, namely TiO_2 doped Silica membrane, with in the mentioned pore size and ζ-potential ranges over a broad pH interval. Membrane fabrication and characterization was discussed *in Chapter 3.* Figures 7 and 8 showed TiO_2-doped silica membrane fabricated in this study has the pore size distribution a mean pore size of 1.44 nm with thickness (*l*) of 1.87 μm. This membrane consists of an amorphous silica ion-selective layer coated on a commercial γ-alumina/α-alumina tubular career. Silica surface is known to be negatively charge above pH 2-2.5 [171]. High porosity and pore size in the desired range was attained by means of surfactant micelles as sacrificial template. Cetyltrimethylammonium bromide (CTAB) was used as structural directing agent, because it has been reported to produce 1-2 nm pores in the consolidated membrane layer [170,172,173]. Although membrane stability was not considered in this study, TiO_2 doping was used as it has been reported to increase chemical and hydrothermal stability and hydrophobicity of silica membranes [172,173].

The ζ-potential of the TiO_2-doped silica layer was measured on unsupported membrane particles dispersed in an aqueous NaCl solution (ionic strength 0.01M) over a pH range between 2 and 10. Figure 31 shows that the membrane material is negatively charged when exposed at a solution with pH above 4 and the condition $5 < |\zeta| < 20$mV, i. e. ζ-potential favorable for ion rejection, was verified for the all the range of pH between 5 and 10.

6. Designing new materials for nanoporous inorganic membranes for water desalination

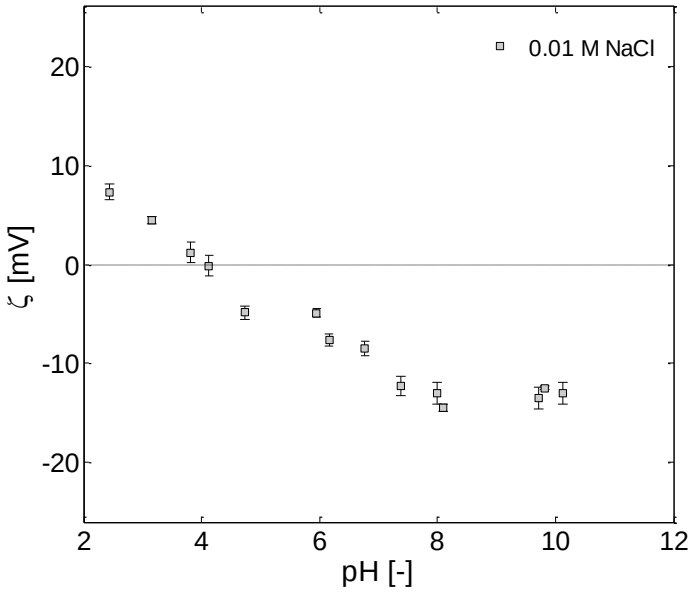

Figure 31: TiO_2-doped silica membrane ζ-potential vs pH (0.01M NaCl).

6.3 TiO_2-doped silica Membrane performance

The desalination performance of TiO_2-doped silica membrane was tested for 0.01M NaCl using a cross-flow filtration apparatus in a pH range between 5 and 10, and at ΔP of 6 bar. As shown in Figure 32, the TiO_2-doped silica membrane was able to remove more than 73% NaCl at pH = 5.5-6. The experimental rejection confirms the model trend. The lowest rejection observed at pH ~ 5.5 where $|\zeta| < 10$mV and the highest rejection was observed at pH~8 where $|\zeta|$ is close to optimum, i.e. 15 mV. Remarkably, the model lower estimates the experimental results for NaCl rejection. This might be partially explained by considering the effect of interlayer, i.e. γ-alumina, in the membrane performance. In *Chapter 4*, we have reported that γ-alumina could remove 10-15% of NaCl in $L_p \sim 1$ LMH·bar^{-1}.

6. Designing new materials for nanoporous inorganic membranes for water desalination

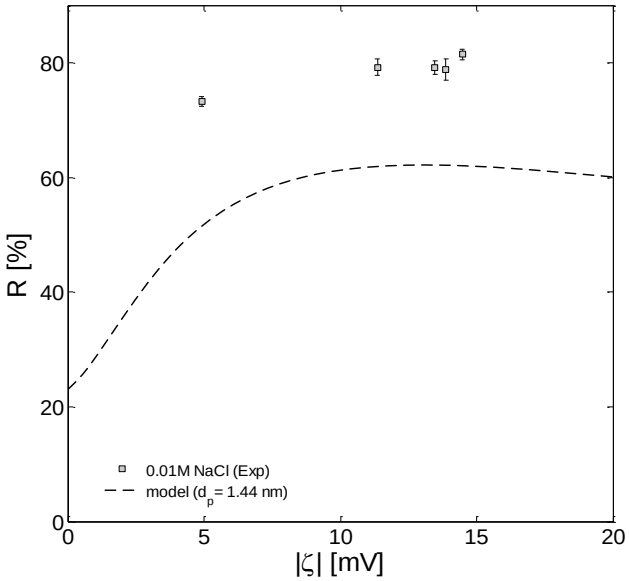

Figure 32: NaCl rejection performance of TiO_2-doped silica membrane vs. pH (ΔP=6 bar, c_{NaCl}=0.01M and T=25°C, dash line shows the model prediction (d_p=1.44nm, l=1.87μm, ε=0.71)).

Salt retention of the TiO_2-doped silica membrane was also tested for Na_2SO_4, $CaCl_2$ and $CaSO_4$ solutions, all in 0.01M ionic strength and ΔP = 6 bar. Figure 33 indicates that the salt rejection of TiO_2-doped silica membrane was almost two times higher than γ- alumina (interlayer of TiO_2-doped silica membrane) and comparable with commercial NF polymeric membranes (Table 2). The ion rejection, caused by steric exclusion in the pore entrance, is higher for the TiO_2-doped silica membrane than for γ-alumina because of the smaller pore size of the TiO_2-doped silica. Moreover, the rejection of $CaSO_4$ was higher than for other salts mainly because of steric exclusion at the pore entrance. Both Ca^{2+} and SO_4^{2-} divalent ions has larger ion hydrated size of than Na^+ and Cl^- monovalent ions. Higher rejection of $CaSO_4$ by γ-alumina membrane (i.e. interlayer) compare to other studied slats was reported in *Chapter 4* due to divalent ion adsorption on the membrane pore, which might decrease the interlayer pore size.

6. Designing new materials for nanoporous inorganic membranes for water desalination

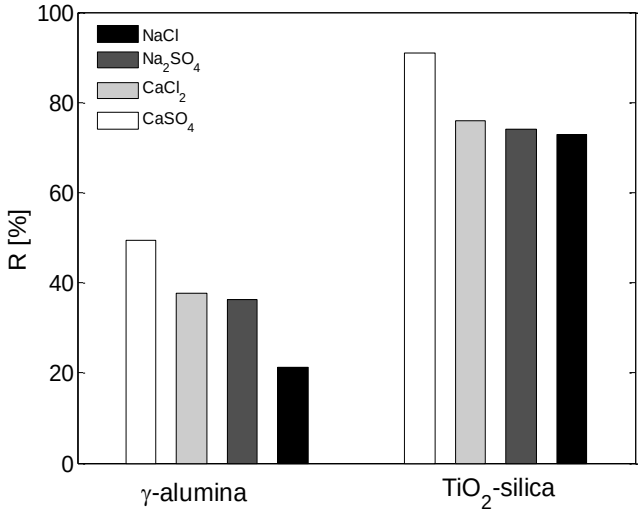

Figure 33: salt rejection performance of TiO_2-doped silica membrane compare with γ-alumina as interlayer (ΔP =6 bar, ionic strength for all solutions was 0.01M and T=25^{o}C).

TiO_2-doped silica membrane showed a L_p=1.24 LMH·bar^{-1}. Figure 34 shows the resistances of inter layer (γ- alumina) and support layer (α- alumina) against the solvent flux. By subtracting the support and interlayer effects on the permeability using the resistance-in-series theory, the active layer permeability (TiO_2-doped silica) was determined to be approximately 1.5 LMH·bar^{-1} which can be expected from a layer with d_p=1.44 nm, l > 1.87 μm , ε = 0.71 and tortuosity (τ) = 6.5. Such tortuosity is consistent with the disordered arrays of nanopores in the silica layer.

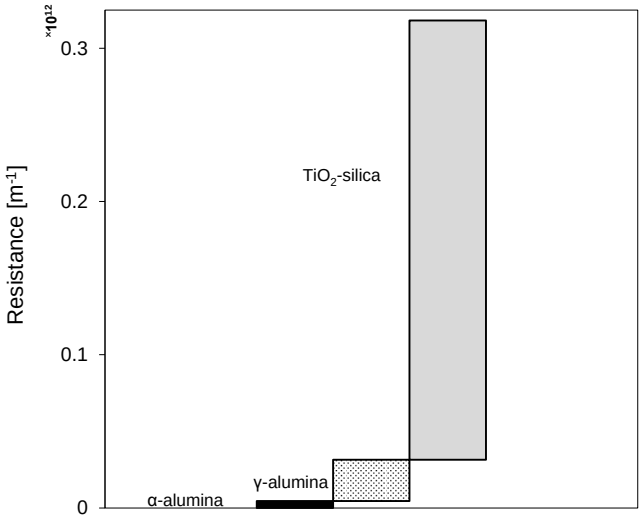

Figure 34: Resistance against water flux of the different membrane layers: as α-alumina (support), γ-alumina (interlayer) and TiO_2-doped silica (top layer).

The perm-selectivity of the TiO_2-doped silica membrane fabricated in this study was compared with commercial polymeric RO and NF membrane and some of the recently reported inorganic membranes (Table 5) for desalination application in Figure 35. Considering rejection of NaCl less than 50 % (i.e. minimum NaCl rejection by commercial polymeric NF) as low selectivity zone, Figure 35 indicates that most of the γ-alumina, titania and zirconia membranes have a salt rejection, which lies in in this zone. On the contrary, the new nanoporous TiO_2-doped silica membrane designed and fabricated in this study was capable to reject NaCl 20-50% more than these inorganic membranes and around 25% more than commercial polymeric NF membranes with 200 < MWCO < 400 Da in operation condition of ΔP = 4-10, T = 20-30^{o}C and pH = 5-7. The TiO_2-doped silica membrane permeability was approximately 1.5 LMH·bar^{-1} which is tenfold more than other silica-based membrane such as silicates and organosilica membranes, which were categorized in the low permeability zone (i.e. L_p < 1 LMH·bar^{-1}). However, the TiO_2-doped silica membrane permeability was still 3-6 fold less than commercial polymeric NF membranes.

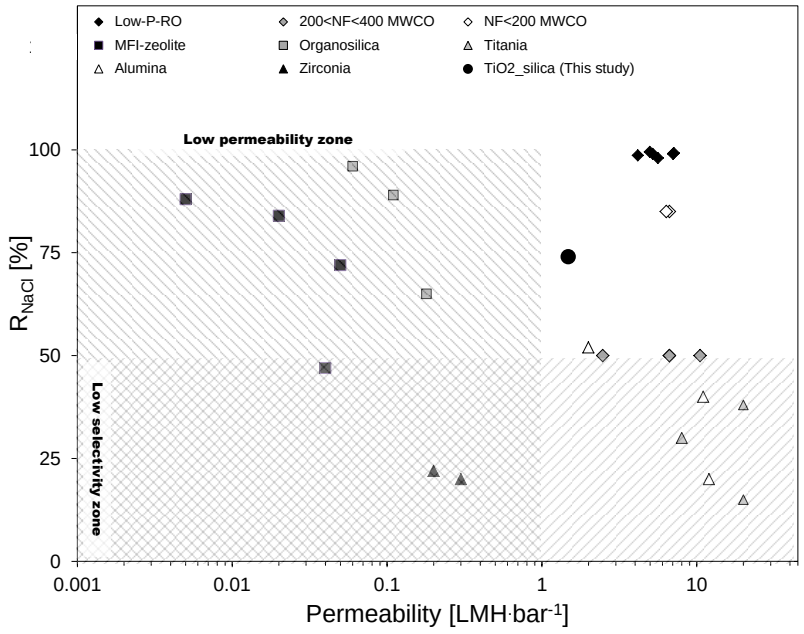

Figure 35: The performance of TiO_2-doped silica membrane fabricated in this study compare to commercial polymeric RO and NF membrane and reported nanoporous inorganic membranes for water desalination (ΔP=4-10bar, T=20-30^{o}C and pH=5-7).

7. Conclusions and perspectives

A new model for simulating solvent flux and salt rejection is proposed for inorganic nanofiltration membranes. The solvent flux is simulated by using a modified Hagen–Poiseuille model where the electroviscosity is used instead of the bulk viscosity. The ion flux and rejection is calculated using the Nernst–Planck model and the Donnan-steric model. The new nanofiltration model were verified by using a mesoporous γ-alumina membrane and a microporous organosilica membranes filtering solutions of NaCl and $MgCl_2$. Compared to previous models, a better flux prediction is observed especially for highly charged NF γ-alumina membrane with low ionic strength solutions, whereas the effect of electroviscosity is negligible for organosilica membrane. In general the electroviscosity effect should be included when modelling membranes with an absolute ζ-potential higher than 20 mV and a pore size below 2-5 times the Debye length.

The modified model has been tested for mesoporous γ-alumina NF membrane over a broad pH range filtering four different salt solutions (NaCl, Na_2SO_4, $CaCl_2$ and $CaSO_4$) with the same ionic strength. The selected ionic strength of 0.01 M was sufficiently low to permit the development of the electrical double layer in the nanopore, and sufficiently high to not be governed solely by the effective charge density. The charge density in the diffuse layer has been calculated by the Gouy-Chapman equation and modelled using the Graham equation. The ζ-potential measurements showed that monovalent ions, such as Na^+ and Cl^- ions, did not adsorb on the γ-alumina surface, whereas divalent ions, such as SO_4^{2-} and Ca^{2+} ions, were highly adsorbed on the γ-alumina surface. Adsorption changes both the membrane ζ-potential value and the isoelectric point. ζ-potentials lowered the membrane permeability, especially for $r_p \leq 3$ nm, absolute ζ-potential > 20 mV and $I \leq 0.01$ M. The nanofiltration model has been modified due to pore shrinkage caused by ion adsorption (Ca^{2+} and SO_4^{2-}). The rejection model shows that for $r_p \leq 3$ nm and ionic strength ≤ 0.01 M, there is an optimum ζ-potential for rejection because of the concurrent effects of the electromigration and convection terms.

Different commercial inorganic membranes, namely, a MF α-alumina membrane, UF titania membrane, NF γ-alumina membrane, NF titania membrane, and Hybsi membrane, has been studied to test their ability to remove toxic compounds, including aromatic components, humic-like substances, OMPs, DINs and heavy metal ions, from WWTP effluent. The permeabilities and selectivities of the membranes have been determined. The NF γ-alumina membrane is the most promising membrane for the recovery of WWTP effluent with regard to its permeate flux and selectivity. The NF γ-alumina membrane removes nearly 75% of the UVAs and 15% of the ions. The membrane rejected 40% of the CuCl and 25% of the $CuSO_4$ from the spiked WWTP effluent. The overall resistance of the NF γ-alumina membrane active layer in the presence of the WWTP effluent is 33×10^{12} m^{-1}. Removal of indicator bacteria and toxic compounds by the NF γ-alumina membrane have tested using bioassays that targeted *E.coli*, *Enterococci*, *D. magna*, and *A. fischeri*. Results from the bioassays indicated that the treatment with the NF γ-alumina membrane reduced the overall bacterial load and environmental toxicity of the treated water. Due to the permeability, selectivity and fouling performance of the NF γ-alumina membrane, this membrane should be considered as a promising alternative in the removal of both toxic organics and OMPs from the effluent of WWTPs.

7. Conclusions and perspectives

Finally, the DSPM model was used to design a pressure-derived inorganic membrane for water desalination in low transmembrane pressure. The model showed that solely a nanoporous inorganic membrane with d_p<0.5 nm and l<50 nm can compete with commercial dense polymeric RO membranes which is technically unachievable with current knowledge. The model suggested that to reduce the NaCl concentration in water sweetening process, the optimized porous membrane should have a mean pore size between 1 and 2 nm with $5 < |\zeta| < 20$ mV. Thus, a TiO_2-doped silica membrane was fabricated with the mean pore size of 1.44 nm on the mesoporous γ- alumina membrane. The membrane removed approximately 73% NaCl at which was significantly higher than reported results for mesoporous inorganic membranes in the same operation conditions. The NaCl rejection of microporous TiO_2-doped silica membrane was also comparable with commercial polymeric NF membranes. The TiO_2-doped silica membrane permeability was approximately 1.5 $LMH \cdot bar^{-1}$, which is tenfold more than modified silica membrane such as silicates and organosilica membranes but still 3-6 fold less than commercial polymeric NF membranes. Further work is needed to decrease the membrane thickness from 1.9 μm to 200 nm to provide more than 11 $LMH \cdot bar^{-1}$, which would make this membrane to have higher selectivity and permeability over the commercially produced polymeric NF membranes with advantages of process applicability such as thermal stability, resistance to solvents and chemicals, mechanical strength.

8. Nomenclature

$L_{p,ac}$ Active layer permeability [l m^{-2} h^{-1} bar^{-1}]

A_{sp} Specific surface area [m^2 kg^{-1}]

c_i Ion concentration [mol m^{-3}]

$c_{i,p}$ Permeate ion concentration [mol m^{-3}]

$c_{i,b}$ Feed bulk ion concentration [mol m^{-3}]

c_{poly} anionic/anionic polymer concentration [kg m^{-3}]

c_{sample} Sample concentration [mol m^{-3}]

c_t Concentration of added titrant [mol m^{-3}]

D Salt diffusion coefficient [m^2 s^{-1}]

$D_{i,\infty}$ Ion bulk diffusion coefficient [m^2 s^{-1}]

F Faraday constant, [96487 C mol^{-1}]

I_0 Zero-order modified Bessel function of the first type [-]

I_1 First order modified Bessel function of the first type [-]

I_p Ionic strength in the pore [mol m^{-3}] Mass transfer coefficient

J_p Solvent flux [m^3 m^{-2} s^{-1}]

$J_{p,ac}$ Solvent fluxin active layer [m^3 m^{-2} s^{-1}]

k Boltzmann constant [1.38066×10^{-23} J K^{-1}]

k_d Mass transfer coefficient

$K_{i,c}$ Hindrance factors for convection [-]

$K_{i,d}$ Hindrance factors for diffusion [-]

l Membrane thickness [m]

R Salt rejection [-]

R_o Overall resistance [m^{-1}]

R_{ac} Active layer resistance [m^{-1}]

R_{cp} Concentration polarisation layer resistance [m^{-1}]

R_{sup} Support layer resistance [m^{-1}]

Re Reynold number [-]

r_i Ion hydrodynamic (Stokes) radius [m]

r_p Membrane average pore size [m]

Sc Schmidt number [-]

8. Nomenclature

Sh Sherwood number [-]

T Absolute Temperature [K]

v_{poly} Anionic/anionic polymer volume [m^3]

v_{sample} Sample volume [m^3]

X_d Effective membrane charge density [mol m^{-3}]

z_i Valence of ion [-]

α Pore geometry factor for surface charge density [-]

β Dimensionless parameter [-]

γ_i Ion activity coefficient in the pore

$\gamma_{i,b}$ Ion activity coefficient in the feed bulk [-]

$\gamma_{i,p}$ Ion activity coefficient in the permeate [-]

$\Delta\pi$ Differential osmotic pressure [Pa]

ΔP_{eff} Effective pressure driving force [Pa]

ΔP Applied pressure [Pa]

ΔW_i Born solvation energy [J]

Δx Membrane thickness [m]

ε Membrane porosity [-]

ε_0 Permittivity of vacuum [8.85419×10^{-12} J^{-1} C^2 m^{-1}]

ε_b Bulk dielectric constant [-]

ε_p Pore dielectric constant [-]

ε^* Dielectric constant reduction coefficient [-]

ζ Surface zeta potential in presence of solution [V]

κ^{-1} Debye length [nm]

λ_i Ratio of ion radius to pore radius [-]

η_b Bulk viscosity [Pa s]

η_{app} Apparent viscosity [Pa s]

σ_b Electrical conductivity of solution in the feed [S m^{-1}]

σ_p Electrical conductivity of solution in the pore [S m^{-1}]

σ_{poly} Anionic/anionic polymer charge density [eq kg^{-1}]

τ Tortuosity [-]

ϕ_i Steric coefficient [-]

8. Nomenclature

ψ Electrical potential gradient [V]

σ_0 Surface charge density [C m^{-2}]

σ_d Charge density in the diffuse layer [C m^{-2}]

9. Bibliography

1. C. K. Diawara, Nanofiltration Process Efficiency in Water Desalination, Separation & Purification Reviews, 37 (2008) 302–324.
2. B. Van der Bruggen, M. Manttari, M. Nystrom, Drawbacks of applying nanofiltration and how to avoid them: a review, Sep. Pur. Techn. 63 (2008) 251–353.
3. W.R. Bowen, J.S. Welfoot, Modelling the performance of membrane nanofiltration—critical assessment and model development, Chem. Eng. Sci. 57 (2002) 1121 – 1137.
4. W. R. Bowen, H. Mukhtar, Characterisation and prediction of separation performance of nanofiltration membranes, J. Membr. Sci. 112 (1996) 353–274.
5. A. I. Cavaco Morao, A. Szymczyk, P. Fievet, A. M. BritesAlves, Modeling the separation by nanofiltration of a multi-ionic solution relevant to an industrial process, J. Membr. Sci. 322 (2008) 320–330.
6. N. Hilal, H. Al-Zoubi, N.A. Darwish, A. W. Mohammad, M. A. Abu Arabi, Comprehensive review of nanofiltration membranes: Treatment, pretreatment, modelling, and atomic force microscopy, Desalination 170 (2004) 281–308.
7. X. L. Wang, T. Tsuru, S. I. Nakao, S. Kimura, The electrostatic and steric-hindrance model for the transport of charged solutes through nanofiltration membranes, J. Membr. Sci.135 (1997)19–32.
8. J. Schaep, B. Van der Bruggen, S. Uytterhoeven, R. Croux, C. Vandecasteele, D. Wilms, E. Van Houtte, F. Vanlerberghe, Removal of hardness from groundwater by nanofiltration, Desalination 119 (1998) 295-302.
9. J.A.M.H. Hofman, E.F. Beerendonk, J.C. Kruithof, J.S. Taylor, Modeling of the rejection of organic micropollutants by nanofiltration and reverse osmosis systems, Proc. - Membr. Technol. Conf. (1995) 733-746.
10. P. Berg, R. Gimbel, Rejection of trace organics by nanofiltration, Membr. Technol. Conf. Proc. (1997) 1147-1153.
11. S. Metsämuuronen, M. Sillanpää, A. Bhatnagard, M. Mänttäri, Natural Organic Matter Removal from Drinking Water by Membrane Technology, Sep. Purif. Rev.43 (2014) 61
12. P. Brandhuber, G. Amy, Alternative methods for membrane filtration of arsenic from drinking water, Desalination 117 (1998) 1-10.
13. T. Urase, J.-I. Ohb, K. Yamamoto, Effect of pH on rejection of different species of arsenic by nanofiltration, Desalination 117 (1998) 11-18.
14. P. Natarajan, State-of-the-art techniques in reverse osmosis, nanofiltration and electrodialysis in drinking-water supply, Water Supply 14 (3/4, 20th International Water Supply Congress and Exhibition, 1995) (1996) 308-310.
15. C. Ratanatamskul, K. Yamamoto, T. Urase, S. Ohgaki, Effect of operating conditions on rejection of anionic pollutants in the water environment by nanofiltration especially in

9. Bibliography

very low pressure range, Water Sci. Technol. 34 (9, Water Quality International '96 art 5) (1996) 149-156.

16. K. Ikeda, S. Kimura, K. Ueyama, Characterization of a nanofiltration membrane used for demineralization of underground brackish water by application of transport equations, Maku 23 (1998) 266-272.
17. MC Garg, H Joshi Optimization and economic analysis of small scale nanofiltration and reverse osmosis brackish water system powered by photovoltaics Desalination, 353(2014) 57–74.
18. N Hilal, V Kochkodan, H Al Abdulgader, D Johnson A combined ion exchange–nanofiltration process for water desalination: II. Membrane selection, Desalination 363 (2014) 51–57.
19. M.B. Hagg, Membranes in chemical processing. A review of applications and novel developments, Sep. Purif. Methods 27 (1998) 51-168.
20. K. Maycock, Z. Twardowski, J. Ulan, A new method to remove sodium sulfate from brine, Mod. Chlor-Alkali Technol. 7 (1998) 214-221
21. R. M. Gould, L. S. White, C. R. Wildemuth, Membrane separation in solvent lube dewaxing, Environ. Prog. 20(2001) 12-16.
22. L. S. White, A. R. Nitsch, Solvent recovery from lube oil filtrates with a polyimide membrane J. Membr. Sci. 179 (2000) 267-274.
23. L. S. White, development of large-scale applications in organic solvent nanofiltration and pervaporation for chemical and refining processes J. Membr. Sci. 286 (2006) 26-35.
24. US Pat., 7 048 846, 2006.
25. M. Kyburz and W. Meindersma, in Nanofiltration. Principles and Applications, ed. A. I. Schafer, A. G. Fane and T. D. White, Elsevier, Oxford, 2005, 13, pp. 329–361.
26. J. T. Rundel, B. K. Paul and V. T. Remcho, Organic solvent nanofiltration for microfluidic purification of poly(amidoamine) dendrimers, J. Chromatogr. A, 1162 (2007) 167-174.
27. J. P. Sheth, Y. Qin, K. K. Sirkar and B. C. Baltzis, Nanofiltration-based Diafiltration Process for Solvent Exchange in Pharmaceutical Manufacturing, J. Membr. Sci. 211 (2003) 251.
28. K.-W. Mok, P.J. Pickering, J.E.V. Broome, Method and apparatus for recovery and purification of lithium from lithium battery waste, PCT WO 9859385, 1998.
29. H.C. van der Horst, J.M.K. Timmer, T. Robbertson, J. Leenders, Use of nanofiltration for concentration and demineralization in the dairy industry: model for mass transport, J. Membr. Sci. 104 (1995) 205-218
30. H.S. Alkhatim, M.I. Alcaina, E. Soriano, M.I. Iborra, J. Lora, J. Arnal, Treatment of whey effluents from dairy industries by nanofiltration membranes, Desalination 119 (1998) 177-184.

9. Bibliography

31. M. Schmidt, D. Paul, K.-V. Peinemann, S. Kattanek, H. Roedicker, Nanofiltration of process solutions highly contaminated with low-molecular organic compounds, F&S Filtr. Sep. 10 (1996) 245-251.
32. S. Wadley, C.J. Brouckaert, L.A.D. Baddock, C.A. Buckley, Modeling of nanofiltration applied to the recovery of salt from waste brine at a sugar decolorization plant, J. Membr. Sci. 102 (1995) 163-75.
33. T. Tsuru, Inorganic porous membranes for liquid phase separation, Sep. Purific. Method. 30 (2001) 191–220.
34. Y. S. Lin, Microporous and dense inorganic membranes: Current status and prospective, Sep. Pur. Techn. 25 (2001) 39–55.
35. K. König, V. Boffa, B. Buchbjerg, A. Farsi, M. L. Christensen, G. Magnacca, Y. Yue, One-step deposition of ultrafiltration SiC membranes on macroporous SiC supports, J. Membr. Sci. 472 (2014) 232–240.
36. M. Facciotti, V. Boffa, G. Magnacca, L. B. Jørgensen, P. K. Kristensen, A. Farsi, K. König, M. L. Christensen, Y. Yue, Deposition of thin ultrafiltration membranes on commercial SiC microfiltration tubes, Ceram. Int. 40 (2014) 3277–3285.
37. W.D. Kingery, H.K. Bowen and D.R. Uhlmann, Introduction to Ceramics, Wiley, New York, 1976, 8, pp.10.
38. J. Burggraaf, K. Keizer and B.A. van Hassel, in L.C. Dufour, Surfaces and Interfaces of Ceramic Materials, Kluwer, Dordrecht, 1989, pp. 705-723.
39. Y.S. Lin, K.J. de Vries and A.J. Burggraaf, Thermal stability and its improvement of the alumina membrane top-layers prepared by sol-gel methods, J. Mater. Sci. 26 (1991) 715.
40. T. Moritz, S. Benfer, P. Arki, G. Tomandl, Influence of the surface charge on the permeate flux in the dead-end filtration with ceramic membranes, Sep. Purif. Technol. 25 (2001) 501–508.
41. Liqtech International A/S, www.liqtech.dk
42. L. Li, N. Liu, B. McPherson, R. Lee, Enhanced Water Permeation of Reverse Osmosis through MFI-Type Zeolite Membranes with High Aluminum Contents, Ind. Eng. Chem. Res. 46 (2007) 1584-1589.
43. B. Zhu, D. T. Myat, J. W. Shin, Y. H. Na, I. S. Moon, G. Connor, S. Maeda , G. Morris, S. Gray, M. Duke, Application of robust MFI-type zeolite membrane for desalination of saline wastewater, J. Membr. Sci. 475 (2015) 167–174
44. R. Xu, J. Wang, M. Kanezashi, T. Yoshioka, T. Tsuru, Reverse Osmosis Performance of Organosilica Membranes and Comparison with the Pervaporation and Gas Permeatio Properties, AICHE 59 (2013) 1298–1307.
45. T. Van Gestel , C. Vandecasteele , A. Buekenhoudt, C. Dotremont, J. Luyten, R. Leysen, B. Van der Bruggen , G. Maes, Salt retention in nanofiltration with multilayer ceramic TiO_2 membranes, J. Membr. Sci. 209 (2002) 379–389.
46. P. Puhlfürß, A. Voigt, R. Weber, M. Morbé, Microporous TiO_2 membranes with a cut off <500 Da, J. Membr. Sci. 174 (2000) 123–133.

9. Bibliography

47. Y. Cai, Y. Wang, X. Chen, M. Qiu, Y. Fan, Modified colloidal sol–gel process for fabrication of titania nanofiltration membranes with organic additives, J. Membr. Sci. 476 (2015) 432–441.
48. H. Qi, G. Zhu, L. Li, N. Xu, Fabrication of a sol–gel derived microporous zirconia membrane for nanofiltration, J. Sol-Gel Sci. Technol. 62(2012) 208–216.
49. J. Schaep, C. Vandecasteele, B. Peeters, J. Luyten, C. Dotremont, D. Roels, Characteristics and retention properties of a mesoporous γ-Al_2O_3 membrane for nanofiltration, J. Membr. Sci. 163 (1999) 229–237.
50. S. Alami-Younssi, A. Larbot, M. Persin, J. Sarrazin, L. Cot Rejection of mineral salts on a gamma alumina nanofiltration membrane, J. Membr. Sci. 102 (1995) 123-129
51. K. Li, Ceramic Membranes for Separation and Reaction, John Wiley & Sons Ltd, 2007, pp.22-28.
52. B. van der Bruggen, J. Geens, Nanofiltration, advanced membrane technology and applications, Edited By N. N. Li, A. G. Fane, W. S. Winston Ho, T. Matsuura, John Wiley & Sons, 2008, pp. 271-295.
53. L. Malaeb, G. M. Ayoub, Reverse osmosis technology for water treatment: State of the art review, Desalination, 267 (2011) 1–8.
54. A. Lhassani, M. Rumeau, D. Benjelloun, M. Pontie, Selective demineralization of water by nanofiltration application to the defluorination of brackish water, Water Research 35 (2001) 3260–3264.
55. FILMTEC™ XLE-2521 Membranes, Form No. 609-00349-0706. www.lenntech.com/Data-sheets/Dow-Filmtec-XLE-2521.pdf.
56. FLUID SYSTEMS® TFC®-ULP® 4" ELEMENT, KOCH membrane system, www.lenntech.com/Data-sheets/Koch-Fluid-Systems-TFC-4040-ULP-L.pdf.
57. Toray Membrane Product, www.toraywater.com/products/ro/pdf/TMG.pdf.
58. Hydranautics Corporate http://www.membranes.com/docs/4inch/ESPA4-4040.pdf.
59. AK Series Low Energy Brackish Water RO Elements, GE water &process technology, http://www.lenntech.com/Data-sheets/GE-Osmonics-AK-series-Low-Energy-Brackish-Water.pdf.
60. FILMTEC™ Membranes, FILMTEC NF270 Nanofiltration Elements for Commercial Systems, Form No. 609-00519-1206, http://www.lenntech.com/Data-sheets/Dow-Filmtec-NF270-2540.pdf.
61. FILMTEC Membranes, Nanofiltration Produces Sparkling Clean Water for Swedish Resort Community, Form No. 609-00379-0503, http://msdssearch.dow.com/PublishedLiteratureDOWCOM/dh_0047/0901b803800478f5.pdf?filepath=liquidseps/pdfs/noreg/609-00379.pdf&fromPage=GetDoc.
62. FILMTEC™ Membranes, FILMTEC NF90-400 Nanofiltration Element, Nanofiltration Elements for Commercial Systems, Form No. 609-00345-0406, http://www.lenntech.com/Data-sheets/Dow-Filmtec-NF90-400.pdf.

9. Bibliography

63. CK Series, Water Softening NF Elements (Cellulose Acetate), GE water &process technology, https://www.gewater.com/kcpguest/salesedge/documents/Fact%20Sheets_Cust/Americas/English/FS1268EN.pdf.
64. Hydranautics Corporate http://www.membranes.com/docs/8inch/ESNA1-LF-LD.pdf.
65. TS80 Nanofiltration Element Series, TriSep Corporation, http://membranes.trisep.com/Asset/8040-TS80-TSA-spec-sheet.pdf.
66. Product Guide for Spiral-Wound RO & NF Elements, CSM, http://www.csmfilter.com/csm/upload/RO_Catalogue/CSM%20RO%20Catalog_Eng_Final_DavidK_11.7.12.pdf.
67. J. Garcia-Aleman, Mathematical Modeling of the Pressure- Driven Performance of McMaster Porefilled Membranes, PhD dessirtation, McMaster University, 2002
68. J.G. Wijmans, R.W. Baker,The solution-diffusion model: a review, J. Membr. Sci. 107 (1995) 1-21.
69. O. Kedem, A. Katchalsky, Thermodynamic analysis of the permeability of biological membrane to nonelectrolytes. Biochim Biophys Acta 27(1958) 229–233
70. K.S. Spiegler, O. Kedem, Thermodynamics of hyperfiltration (reverse osmosis): criteria for coefficient membranes. Desalination 1 (1966) 311–326.
71. H. Lonsdale, U. Merten, R. Riley, Transport properties of cellulose acetate osmotic membranes. J Appl Polym Sci 9 (1965) 13–41
72. D. Bhattacharyya, M.E. Willians, Separation of hazardous organics by low pressure reverse osmosis membranephase II, (1992) Final Report, EPA Report, EPA/600/2-91/045
73. R. Krishna, , J. A.Wesselingh, The Maxwell–Stefan approach to mass transfer. Chem. Eng. Sci. 52,(1997) 861–911.
74. S. Duscher, Ceramic membranes for the filtration of liquids: An actual overview, F & S International Edition No. 14 (2014) 13-21.
75. W.B.S. de Lint, transport of electrolytes through ceramic nanofiltration membranes, PhD thesis, Twenete University, Enschede.
76. S. Deon, P. Dutournie, P. Bourseau, Transfer of monovalent salts through nanofiltration membranes: a model combining transport through pores and the polarization layer, Ind. Eng. Chem. Res.46 (2007) 6752–6761.
77. J. Benavente, V. Silva, P. Pradanos, L. Palacio, A. Hernandez, G. Jonson, Comparison of the volume charge density of nanofiltration membranes obtained from retention and conductivity experiments, Langmuir 35 (2010) 11841–11849.
78. A. Escoda, Y. Lanteri, P. Fievet, S. Deon, A. Szymczyk, Determining the dielectric constant inside pores of nanofiltration membranes from membrane potential measurements, Langmuir 35 (2010) 14628–14635.
79. C. L. Rice, R. Whitehead, Electrokinetic flow in a narrow cylindrical capillary, 69 (1966) 4017–4024.

9. Bibliography

80. M. Sbai, P. Fievet , A. Szymczyka, B. Aoubiza, A. Vidonne, A. Foissy, Streaming potential, electroviscous effect, pore conductivity and membrane potential for the determination of the surface potential of a ceramic ultrafiltration membrane, J. Membr. Sci. 215 (2003) 1-9.

81. I. H. Huismana, G. Trägårdh, C. Trägårdh, A. Pihlajamäki, Determining the zeta-potential of ceramic microfiltration membranes using the electroviscous effect, J. Membr. Sci.147 (1998) 187-194.

82. W. M. Deen, Hindered transport of large molecules in liquid-filled pores, AIChE. 33 (1987) 1409-1425.

83. P. Dechadilok, W. M. Deen, Hindrance Factors for Diffusion and Convection in Pores , Ind. Eng. Chem. Res. 45 (2006) 6953-6959.

84. W. R. Bowen, A. W. Mohammad, N. H., Characterisation of nanofiltration membranes for predictive purposes-use of salts, uncharged solutes and atomic force microscopy, J. Membr. Sci. 126 (1997) 91-105.

85. R. B. McCleskey, Electrical Conductivity of Electrolytes Found In Natural Waters from (5 to 90°C), J. Chem. Eng. Data. 56 (2011) 317-327.

86. J. N. Israelachvili, Intermolecular and surface forces, (2nd ed.) 1991 London: Academic Press.

87. M. Montalvillo, V. Silva, L. Palacio, J. I. Calvo, F. J. Carmona, A. Hernandez, P. Pradanos, Charge and dielectric characterization of nanofiltration membranes by impedance spectroscopy, J. Membr. Sci. 454 (2014) 163–173.

88. S. Senapati, A. Chandra, Dielectric constant of water confined in a nanocavity, J. Phys. Chem. B 105 (2001) 5106–5109.

89. P A Bonnaud, B Coasne, R. J. M Pellenq, Molecular simulation of water confined in nanoporous silica, J. Phys. Condens. Matter 22 (2010) 284110–284125.

90. C. Zhang, F. Gygi, G. Galli, Strongly anisotropic dielectric relaxation of water at the nanoscale, J. Phys. Chem. Lett. 4 (2013) 2477−2481.

91. S. Buyukdagli, M. Manghi, J. Palmeri, Variational approach for electrolyte solutions: From dielectric interfaces to charged nanopores, Phys. Rev. 81 (2010) 041601–041620.

92. S. Deon, A. Escoda, P. Fievet, A transport model considering charge adsorption inside pores to describe salts rejection by nanofiltration membranes, Chem. Eng. Sci. 66 (2011) 2823–2832.

93. S. Deon, P. Dutournie, P. Bourseau, Transfer of monovalent salts through nanofiltration membranes: a model combining transport through pores and the polarization layer, Ind. Eng. Chem. Res.46 (2007) 6752–6761.

94. J. D. Ferry, Statistical evaluation of sieve constants in ultrafiltration. J. Gen. Physiol. 20 (1935) 95–104.

95. R. A. Robinson, R.H. Stokes, Electrolytes Solutions. Butter worths, 1965 London.

96. M. Born, Volumen und hydratationswärme der ionen. Zeit. Phys., 1 (1920) 45–48.

9. Bibliography

97. T. Van Gestel , C. Vandecasteele , A. Buekenhoudt , C. Dotremont , J. Luyten , R. Leysen , B. Van der Bruggen , G. Maes, Alumina and titania multilayer membranes for nanofiltration: preparation, characterization and chemical stability, J. Membr. Sci. 207 (2002) 73–89.

98. K. Keizer, R.J.R. Uhlhorn, R.J. Van Vuren, A.J. Burggraaf, gas separation mechanisms in microporous modified γ-Al2O3 membranes, J. Membr. Sci. 39 (1988) 285–300.

99. M. Kanezashi, M. Asaeda, Hydrogen permeation characteristics and stability of Ni-doped silica membranes in steam at high temperature, J. Membr. Sci. 271 (2006) 86–93.

100. J. Sekulić, J. E. ten Elshof, D. H. A. Blank, A microporous titania membrane for nanofiltration and pervaporation, Adv. Mater. 16 (2004) 1546–1550.

101. S. R. Chowdhury, R. Schmuhl, K. Keizer, J.E. ten Elshof, D. H.A. Blank, Pore size and surfacechemistry effects on the transport of hydrophobic and hydrophilic solvents through mesoporous γ-alumina and silica MCM-48, J. Membr. Sci. 225 (2003) 177–186.

102. X. Ju, P. Huang, N. Xu, J. Shi, Studies on the preparation of mesoporous titania membrane by the reversed micelle method, J. Membr. Sci. 202 (2002) 63–71.

103. J. Sekulic, J.E. Ten Elshof, D.H.A. Blank, Synthesis and Characterization of Microporous Titania Membranes, J. Sol-Gel Sci. Techn. 31 (2004) 201–204.

104. J. H. Schattka, E. H.M. Wong, M. Antonietti, R. A. Caruso, Sol–gel templating of membranes to form thick, porous titania, titania/zirconia and titania/silica films, J. Mater. Chem. 16 (2006) 1414– 1420.

105. I. Agirre , P. L. Arias , H. L. Castricum , M. Creatore , J. E. ten Elshof , G. G. Paradis , P. H.T.Ngamou , H. M. van Veen , J. F. Vente, Hybrid organosilica membranes and processes: Status and outlook, Sep. Pur. Techn. 121 (2014) 2–12

106. M. Kanezashi, K. Yada, T. Yoshioka, T. Tsuru, Organic–inorganic hybrid silica membranes with controlled silica network size: Preparation and gas permeation characteristics, J. Membr. Sci. 348 (2010) 310–318.

107. H. F. Qureshi, A. Nijmeijer, L. Winnubst, Influence of sol-gel process parameters on the microstructure and performance of hybrid silica membranes, J. Membr. Sci. 446 (2013) 19-25.P. Olivier, Modeling physical adsorption on porous and nonporous solids using density functional theory, J. Porous Mater. 2 (1995) 9-17

108. K.S.W. Sing, D.H. Everett, R.A.W. Haul, L. Moscow, R.A. Pierotti, J. Rouquerol, T. Siemieniewska, Reporting physisorption data for gas/solid systems with special reference to the determination of surface area and porosity, Pure Appl. Chem. 57 (1985) 603-619.

109. B. P. Ladewig, Y. H. Tan, C. X. C. Lin , K. Ladewig, J. C. Diniz da Costa, S. Smart Preparation, characterization and performance of templated silica membranes in non-osmotic desalination, Materials 4 (2011) 845-856.

110. B. Kasprzyk-Hordern , Chemistry of alumina, reactions in aqueous solution and its application in water treatment, Adv. Colloid. Interf. Sci. 110 (2004) 19–48.

9. Bibliography

111. V. Gekas, B. Hallström, Mass transfer in the membrane concentration polarization layer under turbulent cross flow: I. Critical literature review and adaptation of existing sherwood correlations to membrane operations, J. Membr. Sci. 30 (1987) 153-180.

112. C.P. Huang, W. Stumm, Specific adsorption of cations on hydrous γ-Al_2O_3, J. Colloid Interface Sci. 43 (1973) 409–420.

113. R. Sprycha, Electrical double layer at alumina/electrolyte interface. I. Surface charge and zeta potential, J. Colloid Interface Sci. 127 (1989) l–11.

114. B.V. Zhmud, A. Meurk, L. Bergstrom, Evaluation of surface ionization parameters from AIM data, J. Colloid Interface Sci. 207 (1998) 332–343.

115. L. H. Mikkelsen, Applications and limitations of the colloid titration method for measuring activated sludge surface charges. Water Res. 37 (2003) 2458–2466.

116. M. L. Christensen, M. Hjorth, K. Keiding, Characterization of pig slurry with reference to flocculation and separation, Water Res. (2009) 773–783.

117. M. Wisniewska, S. Chibowski, T. Urban Adsorption and thermodynamic properties of the alumina–polyacrylic acid solution system, J. Colloid Interface Sci. 334 (2009) 146–152.

118. M. D. Afonso, Surface charge on loose nanofiltration membranes, Desalination 191 (2006) 262–272.

119. ISO 6341 (1997). Water quality - Determination of the inhibition of the mobility of Daphnia magna Straus (Cladocera, Crustacea)–Acute toxicity test. International Standards Organisation. Geneva, Switzerland.

120. ISO 10706 (2000). Water quality - Determination of long term toxicity of substances to Daphnia magna Straus (Cladocera, Crustacea). International Standards Organisation. Geneva, Switzerland.

121. ISO 11348 (part 1 and 2). 2007. Determination of the inhibitory effect of water samples on the light emission of Vibrio fischeri (Luminescent bacteria test). International Organization for Standardization (ISO). Geneva, Switzerland.

122. P. Roslev, A. S. Bukh, L. Iversen, H. Sønderbo, N. Iversen, Application of mussels as biosamplers for characterization of faecal pollution in coastal recreational waters, Water Sci. Techn. 62 (2010), 586-93.

123. W. B. S. de Lint, N. E. Benes, J. Lyklema, H. J. M. Bouwmeester, J. van der Linde, M. Wessling, Ion Adsorption Parameters Determined from Zeta Potential and Titration Data for a γ-Alumina Nanofiltration Membrane, Langmuir. 19 (2003) 5861-5868.

124. C.P. Huang, W. Stumm, Specific adsorption of cations on hydrous γ-Al_2O_3, J. Colloid Interface Sci. 43 (1973) 409–420.

125. Z. Siwy, I. D. Kosinska, A. Fulinski, C. R. Martin, Asymmetric diffusion through synthetic nanopores, Phys. Rev. Lett. 94 (2005) 0481021–0481024.

126. G. Hagmeyer, R. Gimbel, Modelling the rejection of nanofiltration membranes using zeta potential measurements, Sep. Purif. Technol. 15 (1999) 19–30.

9. Bibliography

127. J. A. Camargo, A. Alonso, Ecological and toxicological effects of inorganic nitrogen pollution in aquatic ecosystems: A global assessment, Environ. Int. 32 (2006) 831–849.

128. S. Babel, T. A. Kurniawan, Low-cost adsorbents for heavy metals uptake from contaminated water: a review, J. Hazard. Mater. B 97 (2003) 219–243.

129. Y. Luo, W. Guo, H. H. Ngo, L. D. Nghiem, F. I. b. Hai, J. Zhang, S. Liang, X. C. Wang, A review on the occurrence of micropollutants in the aquatic environment and their fate and removal during wastewater treatment, Sc. Tot. Environ. 473–474 (2014) 619–64.

130. S. Miralles-Cuevas , I. Oller, J.A. Sanchez Perez , S. Malato, Removal of pharmaceuticals from MWTP effluent by nanofiltration and solar photo-Fenton using two different iron complexes at neutral pH, Water Res. 64 (2014) 23-31.

131. W. Yang, H. Zhou, N. Cicek, Treatment of Organic Micropollutants in Water and Wastewater by UV-Based Processes: A Literature Review, Crit. Rev. Env. Sc. Techn. 44 (2014)1443–1476.

132. E. C. Wert, F. L. Rosario-Ortiz, S. A. Snyder, Using Ultraviolet Absorbance and Color To AssessPharmaceutical Oxidation during Ozonation of Wastewater, Environ. Sci. Technol. 43 (2009) 4858- 4863.

133. B. Xu, D. Li, W. Li, S. Xia, Y. Lin, C.Y. Hu, C. Zhang, N. Y. Gao, Measurements of dissolved organic nitrogen (DON) in water samples with nanofiltration pretreatment, Water Res. 44 (2010) 5376 -5384.

134. S. Lee, R.M. Lueptow, Membrane Rejection of Nitrogen Compounds, Environ. Sci. Technol. 35 (2001) 3008-3018.

135. B. Juna, K. Miyanagab, Y. Tanjib, H. Unno, Removal of nitrogenous and carbonaceous substances by a porous carrier–membrane hybrid process for wastewater treatment, Biochem. Eng. J. 14 (2003) 37–44.

136. P.M. Vitousek, J.D. Aber, R.W. Howarth, G.E. Likens, P.A. Matson, D.W. Schindler, Human alteration of the global nitrogen cycle: sources and consequences, Ecol. Appl. 7 (1997) 737–750.

137. National Research Council, Clean coastal waters: understanding and reducing the effects of nutrient pollution National Academic Press, Washington, DC (2000).

138. I. Heidmann, W. Calmano, Removal of Zn(II), Cu(II), Ni(II), Ag(I) and Cr(VI) presenting aqueous solutions by aluminum electrocoagulation, J. Hazard. Mater. 152 (2008) 934–941.

139. N. Adhoum, L. Monser, N. Bellakhal, J.E. Belgaied, Treatment of electroplating wastewater containing Cu^{2+}, Zn^{2+} and Cr(VI) by electrocoagulation, J. Hazard. Mater. 112 (2004) 207–213.

140. Agency for Toxic Substances and Disease Registry, Copper, September 2004. www.atsdr.cdc.gov/

141. Marmagne, C.Coste, Color removal from textile plant effluents, Am. Dyest. Rep. (1996) 15–21.

9. Bibliography

142. V. Fontanier, S. Baig, J. Albet, J. Molinier, Comparison of conventional and catalytic ozonation for the treatment of pulp mill wastewater, Environ. Eng. Sci. 22 (2005) 127–137.

143. A. B.C. Alvares, C. Diaper, S.A. Parsons, Partial oxidation by ozone to remove recalcitrance from wastewaters – a review, Environ. Technol. 22 (2001) 409–427.

144. N. Merayo, D. Hermosilla, L. Blanco, L. Cortijo, A. Blanco, Assessing the application of advanced oxidation processes, and their combination with biological treatment, to effluents from pulp and paper industry, J. Hazard. Mat. 262 (2013) 420– 427.

145. L.D. Benefield, J. M. Morgan, Chemical precipitation, in: R.D. Letterman (Ed.), Water Quality and Treatment, McGraw-Hill Inc. NY (1999) pp. 10.1–10.57.

146. T.A. Kurniawan, G.Y.S. Chan, W.H.Lo, S. Babel, Comparisons of low-cost adsorbents for treating wastewaters laden with heavy metals, Sci. Total Environ. 366 (2006) 409 – 426.

147. C. Kappel, A. J. B.Kemperman , H. Temmink, A. Zwijnenburg, H. H. M. Rijnaarts, K. Nijmeijer, Impacts of NF concentrate recirculation on membrane performance in an integrated MBR and NF membrane process for wastewater treatment, J. Membr. Sci. 453 (2014) 359–368.

148. E. Alvarez-Ayuso, A. Garcia-Sanchez, X. Querol, Purification of metal electroplating wastewaters using zeolites, Water Res. 37 (2003) 4855–4862.

149. L.S. Berry, P.F. Lafayette, F.E. Woodard, Sand filtration and activated carbon treatment of poultry process water, J. Water Pollut. Cont. Fed. 48 (1976) 2394-2405.

150. V. Yangali-Quintanilla, A. Sadmani, M. McConville, M. Kennedy, G. Amy, Rejection of pharmaceutically active compounds and endocrine disrupting compounds by clean and fouled nanofiltration membranes, Water Res. 43 (2009) 2349–2362.

151. B. Van der Bruggen, C. Vandecasteele, Removal of pollutants from surface water and groundwater by nanofiltration: overview of possible applications in the drinking water industry, Environ. Pollut. 122 (2003) 435–445.

152. K. Madireddi, R.W. Babcock, B. Levine, T.L. Huo, E. Khan, Q.F. Ye, J.B. Neethling, I. H. Suffet, M.K. Stenstrom, Wastewater reclamation at Lake Arrowhead, California: an overview, Water Environ. Res. 69 (1997) 350–362.

153. C. V. Gherasim, P. Mikulášek, Influence of operating variables on the removal of heavy metal ions from aqueous solutions by nanofiltration, Desalination 343 (2014) 67–74.

154. G. Owen, M. Bandia, J.A. Howella, S.J. Churchouse, Economic assessment of membrane processes for water and waste water treatment, J. Membr. Sci.102 (1995) 77-91.

155. K. D. Pickering, M.R. Wiesner, Cost model for low-pressure membrane filtration, J. Environ. Eng. 119 (1993) 772–797.

9. Bibliography

156. P. Xu, C. Bellona, J. E. Drewes, Fouling of nanofiltration and reverse osmosis membranes during municipal wastewater reclamation: Membrane autopsy results from pilot-scale investigations, J. Membr. Sci. 353 (2010) 111–121.

157. L. Nghiem, A. Schafer, M. Elimelech, Pharmaceutical Retention Mechanisms by Nanofiltration Membranes, Environ. Sci. Technol. 39 (2005) 7698–7705.

158. M. Neamţu , D. Grandjean, A. Sienkiewicz, S. L. Faucheur, V. Slaveykova, J. J. V. Colmenares, C. Pulgarín, L. F. de Alencastro, Degradation of eight relevant micropollutants in different water matrices by neutral photo-Fenton process under UV254 and simulated solar light irradiation–A comparative study, App. Cat. B: Environ. 158–159 (2014) 30–37.

159. Y. Pi, J. Schumacher, M. Jekel, Decomposition of aqueous ozone in the presence of aromatic organic solutes. Water Res. 39 (2005) 83–88.

160. P. Westerhoff, G. Aiken, G. Amy, J. Debroux, Relationships between the structure of natural organic matter and its reactivity towards molecular ozone and hydroxyl radicals. Water Res. 33 (1999) 2265–2276.

161. S. Navalon, M. Alvaro, H. Garcia, Analysis of organic compounds in an urban wastewater treatment plant effluent, Envir. Techn. 32 (2011) 295–306.

162. D. Bhatiaa, I. Bourven, S. Simon, F. Bordas, E. D. van Hullebusch, S. Rossano, P. N. L. Lens, G. Guibaud, Fluorescence detection to determine proteins and humic-like substances fingerprints of exopolymeric substances (EPS) from biological sludges performed by size exclusion chromatography (SEC), Bioresource Techn. 131(2013) 159–165.

163. D. Faust, O.M. Aly Chemistry of water treatment (2nd ed) Lewis Publishers, Boca Raton, London, New York, Washington, DC (1999).

164. EU (2006). Directive 2006/7/EC of the European Parliament and of the Council of 15 February 2006 concerning the management of bathing water quality. Official Journal of the European Union, 64, 37–51.

165. E. Drioli, F. Laganh, A. Crlscuoh, G. Barbieri, Integrated membrane operations in desalination processes. Desalination, 122(1999) 141–145.

166. B. E. Conway, Ionic Hydration in Chemistry and Biophysics, Elsevier Scientific Pub.

167. W.B. S. de Lint, N. E. Benes, Separation properties of γ-alumina nanofiltration membranes compared to charge regulation model predictions, J. Membr. Sci. 248 (2005) 149–159.

168. G. Aryanpour, M. H. Abbasi, Computer simulation of ordinary gas transfer in tubes, J. Porous Media 8 (2005) 379–391.

169. T. Kuzniatsova, M. L. Mottern, K. Shqau, D. Yu, H. Verweij, Micro-structural optimization of supported γ-alumina membranes J. Membr. Sci. 316 (2008) 80–88.

170. Y. T. Chua, C. X. C. Lin, F. Kleitz, X. S. Zhao, S. Smart, Nanoporous organosilica membrane for water desalination, Chem. Commun. 49 (2013) 4534-4536.

9. Bibliography

171. E. Chibowski, A. Szcześ, L. Hołysz, Changes of zeta potential and particles size of silica caused by DPPC adsorption and enzyme phospholipase A2 presence, Adsorption 16 (2010) 305-312.

172. Boffa, J.E. ten Wehner Elshof, D.H.A. Blank, Preparation of templated mesoporous silica membranes on macroporous α-alumina supports via direct coating of thixotropic polymeric sols, Microporous Mesoporous Mater. 100 (2007) 173–182.

173. V. Boffa, G. Magnacca, L. B. Jørgensen, A. Wehner, A. Dörnhöfer, Y. Yue, Toward the effective design of steam-stable silica-based membranes, Microporous Mesoporous Mater. 179 (2013) 242-249.

174. Y.F. Gu, S.T. Oyama, Permeation properties and hydrothermal stability of silica–titania membranes supported on porous alumina substrates, J. Membr. Sci. 345 (2009) 267–275.

ISSN (online): 2246-1248
ISBN (online): 978-87-7112-273-2

AALBORG UNIVERSITY PRESS